INTERNATIONAL SCHOOL for ADVANCED STUDIES

CONDENSED MATTER THEORY SECTOR

Non Equilibrium Dynamics in Strongly Correlated Systems

Thesis submitted for the Degree of *Doctor Phylosophiæ*

Advisor:
Prof. Michele Fabrizio

Candidate:
Marco Schiró

Academic Year 2009/2010

Contents

Part I

Introduction

Chapter 1

In and Out of Equilibrium

Non equilibrium phenomena are ubiquitous in Nature and they appear under very different flavours. At the same time, as a result of a huge phenomenology, a simple definition of this concept is clearly a delicate issue, which necerssarily requires further clarifications. What non-equilibrium *stands for, at least from the perspective of the present work, is the first question we address in this introductory chapter.*

The concept of thermodynamic equilibrium is one of the building block of modern statistical physics. It deals with properties of macroscopic systems which are isolated or weakly coupled to an environment and can be summarized as follows:

> A macroscopic system is said to be in thermal equilibrium when (i) its state (physical properties) is defined in terms of a unique set of **intensive** and **extensive** variables which do not change with time and (ii) no currents of charges associated to conserved quantities (particles, energy, ...) flow through it.

If one think for a moment about this definition then he immediately realizes that such a concept is more an exception than a rule in every day life. Indeed, non equilibrium effects are extremely common in many different physical situations of the greatest simplicity, the flow of electric current through a metallic conductor being just a trivial example. This is even more true if we think that the very basic idea of performing experiments on materials and compounds amounts to act with some external field on an otherwise equilibrium system and to monitor its response to the applied perturbation. As a result one could be tempted to ask why, inspite of the restrictiveness of the above definition, the assumption of thermal equilibrium has been (and actually still is) so powerful and useful to describe physical properties of macroscopic systems. A possible answer to this question should be based on two observations.

From one side, as often happens in physics, what matters are the orders of magnitude of tipical time scales a system need to reach a quasi-equilibrium state compared to the time scales on which observation takes place. As a consequence, with a good degree of approximation, a macroscopic system can be considered as in thermal equilibrium if all fast processes have taken place while the slowest one still have to occur. Clearly the distinction between *fast* and *slow* depends on the observation time that is considered [111, 114, 56].

A second key observation comes from a basic result in the statistical theory of many particle systems which goes under the apparently innocuous name of linear response theory. It simply states that a small external perturbation can only probe small fluctuations around equilibrium. Hence, as long as applied fields are weak enough, the system can be considered as in thermal equilibrium for all practically purposes. This major result is of paramount importance in connecting theory to experiments, since it provides a way to compute experimental relevant quantities such as susceptibilities in terms of equilibrium correlation functions, which are the natural quantities in terms of which the many body problem is formulated.

There are however physical situations in which the relevant effects cannot be accounted for by assuming that the system is close to an equilibrium state. We will refer to two main classes of non equilibrium phenomena throughout this work. The first one can be realized by attaching the system of interest to external sources which allow it to sustain stationary currents providing a dissipation mechanism which prevent indefinite heating. In this case, after some transient, the system will reach a stationary state where physical properties do show time-translational invariant. However, due to the external forcing a finite current flows across the systems and the steady state is not an equilibrium state.

A second class of non equilibrium phenomena concerns explicitly time dependent situations. These can be realized, for example, by exposing the system to time dependent external fields or to time dependent variation of its Hamiltonian parameters. The simplest example one can imagine within this class concerns the relaxation of an highly excited state toward equilibrium.

In the next two chapter we will present experimental and theoretical motivations to address these phenomena in the context of strongly correlated electron systems.

Chapter 2

Non Equilibrium Physics in Strongly Correlated Systems

Recent years have seen an enourmous progress in preparing, controlling and probing quantum systems in non-equilibrium regime. Experimental breakthroughs in the field of nanoscale transport, ultra cold atomic gases and time resolved pump probe spectroscopies on solid state materials triggered a huge interest on the field of strongly correlated systems out of equilibrium. In this chapter we will briefly review some of these recent achievements which provide the main experimental motivation for this work.

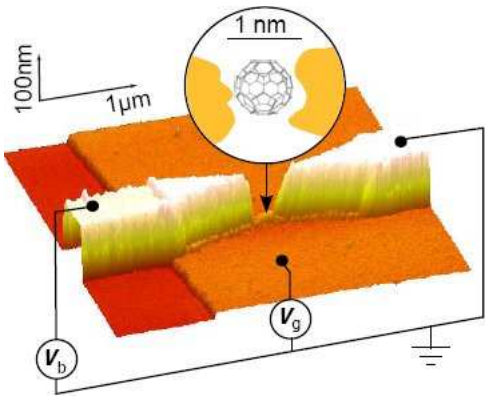

Figure 2.1: Single Molecule Transistor built with C_{60} molecule using electromigration technique. AFM image from [152].

2.1 Quantum Transport at Nanoscale

Recent advances in nanotechnology have made it possible to contact microscopic quantum objects to large metallic reservoirs [179, 37]. Single molecules or even artificial atoms, so called quantum dots, have been contacted, opening a route towards promising nanoelectronic devices. Beside their obvious relevance for technological applications, in view of building a molecular-based electronics overcoming the famous Moore's Law, these experimental breakthroughs have triggered an enormous scientific interest around the field of *quantum transport*. Many questions that up to recent years seem to be purely speculative (if not completely meaningless) such as *measuring the conductance of a single atom*, may be now experimentally addressed in a more of less controlled setup [172].

From an experimental point of view, many different techniques can be employed depending whether the object to contact is a lithographically designed quantum dot, a magnetic adatom on a metallic surface or a single molecule bridging two metallic electrodes. In the first case the coupling between the reservoirs and the artificial atom obtained by quantum confinement of the two dimensional electron gas, is through tunneling barriers. In the latter two cases the usual setup typically involves respectively scanning tunneling microscope (STM) techniques, for magnetic adatoms, and breakjunction/electromigration techniques for single molecule transistors.

From a more theoretical perspective, contacting microscopic objects to large metallic reservoirs is particularly intriguing since allows to probe trans-

port phenomena in a completely different regime with respect to conventional solid-state materials [129]. While electron-electron interactions in bulk macroscopic conductors are in general efficiently screened and other physical mechanisms are responsible for the relaxation processes, the behavior of those *strongly-correlated* nanodevices is greatly affected by a large (unscreened) Coulomb repulsion experienced by localized electrons sitting on the dot/molecule. Notice that despite the discrete set of levels of the isolated quantum system, which would suggest an exact treatment, hybridization to the reservoirs makes the problem extremely challenging. In addition, due to the size of the tunneling rate which may become comparable or even lower with respect to *local* energy scales (such as the electron-electron repulsion or the energy of atomic displacements) at sufficiently low temperatures non trivial many body phenomena can emerge.

In this respect the experimental observation of the Kondo Effect, one of the hallmark of strong correlation phenomena, in a quantum dot coupled to a metallic lead [72, 36] created huge excitement. Many theoretical and experimental investigations followed, which have made the field of transport through correlated nanostructures a privileged arena where strong correlation phenomena can be experimentally probed with an high degree of tunability and, more interestingly, in novel physical regimes. In particular, inducing non equilibrium effects in these nano-devices is rather natural, once the difficult task of contacting the molecule has been accomplished. The simplest example one can think of is to apply a dc-bias voltage between source and drain electrodes to induce a current flowing across the contact. This drives the system through a transient regime, toward a steady state which although being stationary - hence time-translational invariant- features a finite amount of current through it. Such an highly excited state of the coupled system (molecule+electrodes) is referred to as a non-equilibrium steady state (NeqSS). It is worth noticing that, by measuring the $I-V$ characteristic or the differential conductance $\partial I/\partial V$, experiments can directly probe physical properties of such non equilibrium state.

In the following we briefly sketch some recent experimental results that are particularly relevant for the subject of this work, since they highlight beautiful interplay between correlations and non equilibrium effects. The reader has to be careful however, since many other interesting non equilibrium phenomena can be investigated in those systems. Indeed beside the case of dc transport, which is the likely simplest one can imagine and practically realize, the high degree of control offered by these nano-devices allows one to engineer many different protocols (and correspondingly probes) to induce out of equilibrium effects. In this respect we note that experiments are

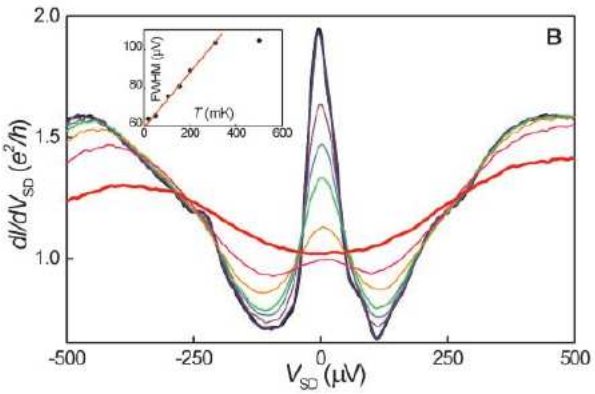

Figure 2.2: Experimental data for transport through a semiconductor quantum dot, from [182]. Differential conductance as a function of the source-drain voltage V_{sd} for different temperatures ranging from $T = 15mK$ (thick black) to $T = 900mK$ (thick red). Notice the Kondo anomaly at low bias, where the unitarity limit is almost approached.

rapidly moving in the direction of time-resolved techniques to detect charge transport by counting individual electrons while tunneling across correlated nanostructures such as semiconducting quantum dots [184, 165, 78].

Coulomb Blockade and Kondo Effect Out of Equilibrium

Signatures of electron-electron correlations in transport through nano-devices clearly appear in the $I(V)$ characteristic and in the differential conductance $G(V) = \partial I/\partial V$, which are very sensitive probes of local many body physics [119]. The simplest example is the Coulomb Blockade effect, which has been observed in a number of experiments with quantum dots or single molecule transistors, see [138]. It results from the large charging energy E_C one has to pay to add an extra electron on the dot/molecule, due to Coulomb repulsion. It tipically appears as sharp peaks in the zero bias conductance as a function of the gate voltage or equivalently as a gap in the $I(V)$ curve, meaning that a finite bias voltage of order E_C is needed to make charge transport possible. The most striking effect of many body correlations occurs at low enough temperatures and for gate voltages such that the dot accommodates an odd number of electrons. Then, upon decreasing the applied bias voltage, the conductance crosses over from the low-conductance Coulomb blockade regime to the high-conductance Kondo regime, as shown in figure 2.2. Such a zero-bias anomaly eventually reaches the unitary limit [182] as the tem-

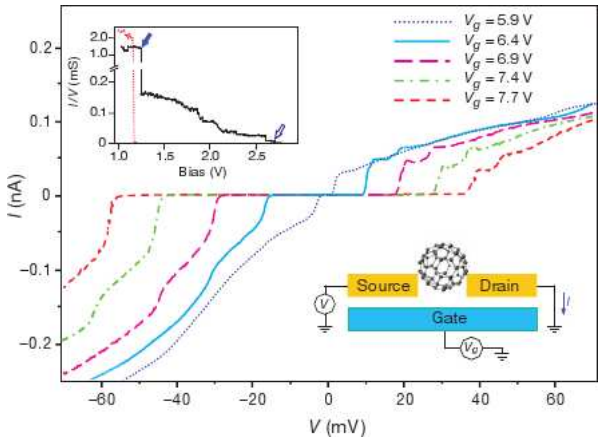

Figure 2.3: Experimental data for transport through single C_{60} molecule, from [137]. The current-voltage curve show at low bias the characteristic Coulomb Blockade plateau. At larger bias signatures of excitations of molecular phonons are visible as steps at regularly displaced voltages.

perature goes to zero, reflecting the complete screening of the local moment by the conduction electrons of the nearby Fermi Sea. While the effect of temperature on this many-body state is well known since the early experiments on metallic alloys, its competition with an external source drain bias is a genuine non-equilibrium effect which has been possible to measure only much more recently thanks to nano-scale devices [182, 76].

Phonons Effects in Molecular Transistors

A relevant issue in transport through devices that are built with single molecules is the role played by the internal vibrational degrees of freedom during the transport process. Indeed due to the current flowing across the system, electrons are repeatedly added and removed from the molecule, a process which may result into novel physical effects, such as a change of shape or position of the molecule itself with respect to the leads. In addition, due to the finite bias applied across the junction the internal vibrational degrees of freedom can be also driven out of equilibrium due to their coupling with electronic degrees of freedom.

In this respect pioneering transport measurements on vibrating single molecule transistors have been performed [137] where the conductance of a molecular junction made by a C_{60} molecule connected to gold electrodes has been measured. Beside the Coulomb blockade plateau, the $I-V$ curve

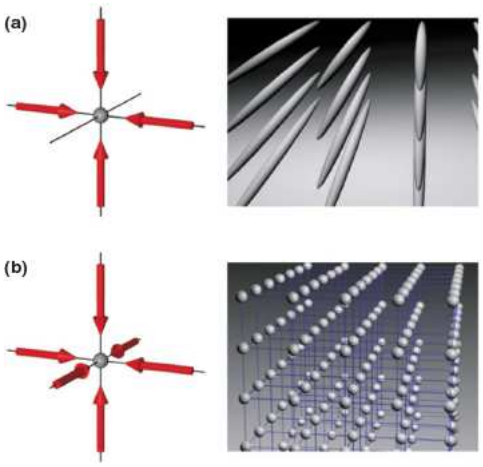

Figure 2.4: A cartoon picture of two dimensional (top) and three dimensional (bottom) optical lattices. From [17].

shows characteristic steps at regularly displaced voltages due to excitations of molecular phonons, a peculiar non equilibrium effect.

2.2 Ultra-Cold Atomic Gases in Optical Lattices

Recent advances in the field of ultra cold atoms have allowed to engineer macroscopic quantum many-body systems with tunable interactions and almost perfect isolation from the environment [17]. This has been possible thanks to a series of experimental breakthroughs which start with the realization of novel cooling mechanisms, allowing to observe dilute gases made by bosonic and fermionic atoms at extremely low temperatures[1]. Here genuine quantum effects due to spin-statistics become relevant and phenomena such as Bose-Einstein condensation [7, 21, 40] or Fermi Degeneracy [42, 169, 180] have been observed.

These results triggered a large body of research which mainly focused on macroscopic quantum coherence phenomena which characterize both bosonic and fermionic condensates. However, due to the very diluted regime ($n \simeq 10^{14} cm^{-3}$), effective interactions in these systems are often weak enough that an effective single particle description is sufficient and interesting many body effects are missed. Therefore an huge excitement has been generated by the experimental achievement of two major steps in the direction toward a

[1] Temperatures as low as $T \simeq 100\mu K$ with laser cooling techniques and $T \simeq 100nK$ with evaporative cooling have been reached.

strong-interaction regime in ultracold quantum gases. The first one was the development of Fesbach resonance techniques [35, 93] to tune the interaction strength of individual atoms by means of an external magnetic field. This allowed to increase the effective scattering length far beyond the average interparticle spacing, thus turning a weakly interacting diluted gas into a strongly interacting one.

A second important step was the possibility to confine cold atoms into configurations of reduced dimensionality or to load them in periodical lattices built with laser light fields, known as optical lattices [74]. Here dipolar forces localize the atoms in the minima (or maxima) of the stationary and monochromatic electromagnetic potential, thus generating situations in which the effects of the interactions are enhanced. Interestingly the parameters of the light field directly affect the properties of the lattice, the half wavelength being the lattice spacing while the intensity of the radiation field controlling the depth of the potential, hence the hopping strength and the value of two particle interactions.

The resulting set-up may be seen as an idealized version of a conventional solid state system where spin-full electrons, here fermionic atoms with different hyperfine states, feel the periodic potential of ionic lattice. Equivalently, ultracold atoms in optical lattices can be considered as the simplest experimental realization of popular lattice models of interacting quantum particles. The combination of these experimental results largely extended the range of physics which is accessible with ultra cold atoms, opening the way to study strongly correlated systems in a completely tunable set-up. An important step in this direction has been the experimental realization of a Mott Insulator made by bosonic [74] and fermionic atoms [96, 167]. It is worth noticing, however, that the major bottleneck toward the experimental achievement of exotic many body phases is still represented by the issue of cooling mechanisms. Indeed the energy scales controlling the physics of those systems are so small that reaching temperature for the onset of antiferromagnetism or superconductivity has been so far elusive. This is particularly true for fermions, which are more difficult to cool down due to Pauli principle which largely reduces their scattering amplitude in the s-wave channel.

2.2.1 Non Equilibrium Experiments

One of the main feature of experiments with cold atomic gases, which largely differ from conventional solid-state setup, is the possibility to change dynamically - i.e. in the time domain - any microscopic parameters, such as the interaction between atoms or the external trapping potential. In addition,

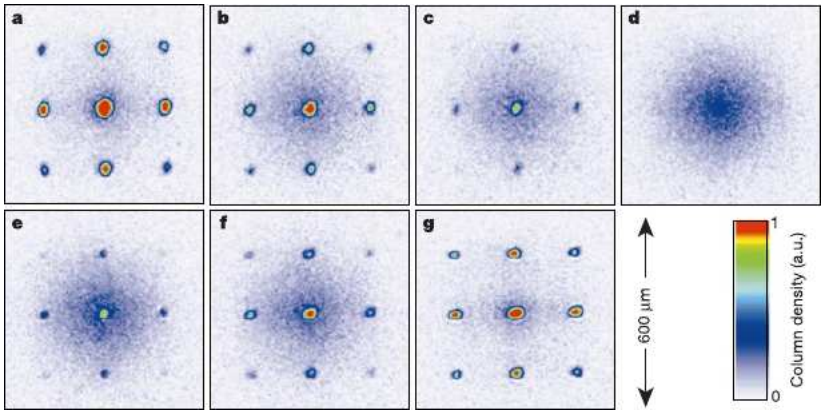

Figure 2.5: Time of flight measurements [75] of the momentum distribution of ultra-cold *Rb* bosonic atoms, taken at different times t after the change of the potential depth. From left to right: (a) 0μs, (b) 100μs, (c) 150 μs, (d) 250 μs, (e) 350 μs, (f) 400 μs, (g) 550 μs. Notice the collapse and revival of the superfluid coherence peak.

the aforementioned low energy scales in these systems (typically $\sim$ kHz) and the almost perfect isolation from the environment result into relatively long time scales compared to solid state materials (see next section). This makes those systems the natural laboratory where the unitary quantum dynamics following an external perturbation can be probed in real-time. In the following we will briefly survey some keynote recent experiments that triggered an enormous interest on the field of non equilibrium dynamics of isolated many body systems.

Collapse and Revival Oscillations

The first seminal experiment probing the non equilibrium dynamics of ultra-cold bosonic atoms in optical lattices has been realized in [75]. Here a sudden change of the strength of the lattice depth has been performed, driving the system from a weakly interacting superfluid regime to the Mott Insulator. Hence the system is hold with the final value of lattice depth for a variable time t, after which time of flights measurements are taken to probe the evolution of momentum distribution, see figure 2.5.

As we can see from panel a), the initial state shows coherent peaks in the interference pattern which are characteristic features of the superfluid phase. After some transient time those peaks get washed out and the systems show no more signatures of phase coherence, see panel d. Surprisingly

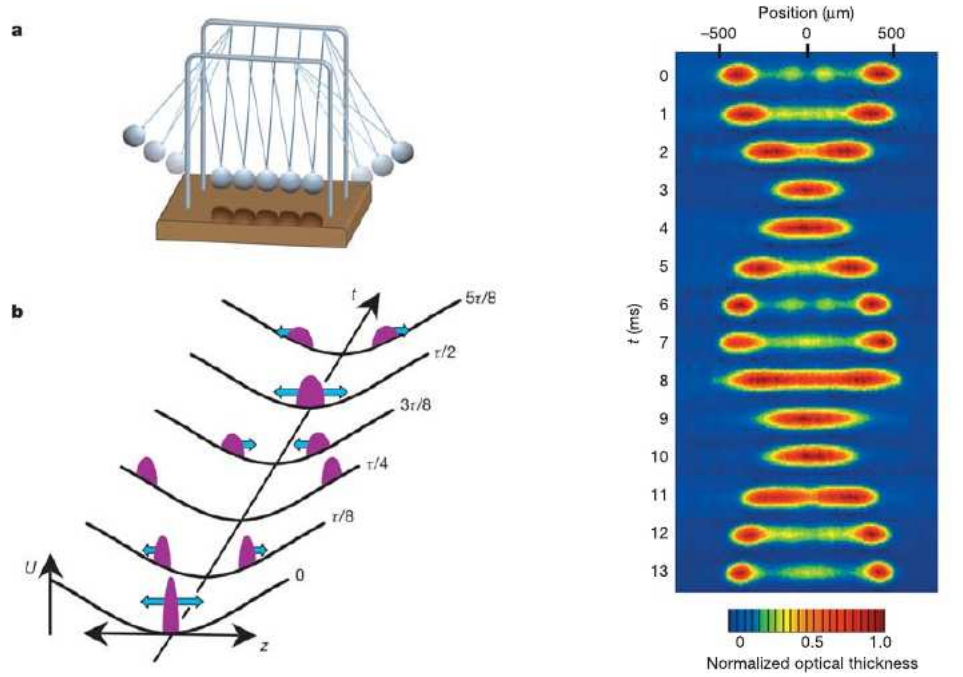

Figure 2.6: Left Panel: cartoon picture of the classical Newton's cradle and its quantum analogue. The initial BEC is splitted in two wavepackets which oscillate out of phase with period τ. Right Panel: Absorption images during the first oscillation cycle. From [106].

enough, however, after waiting further time the coherence is restored as clearly shown in the last panel g. Actually, the non equilibrium dynamics of the system shows a full series of collapse and revival oscillations of the superfluid phase coherence, which eventually fade out at longer time scales. While a qualitative explanation of the observed periodic pattern has been given in terms of simple mean field arguments [197] a full understanding of the non equilibrium dynamics in interacting bosonic (and fermionic) systems is still a subject of intense research activity.

Quantum Newton's Cradle

A second ground-breaking experiment probing the dynamics of bosonic atoms has been performed more recently [106]. Here a BEC of *Rb* atoms was confined by means of a strong two dimensional optical lattice into an effectively one-dimensional geometry. Then, by applying along the axial direction a pulse signal with wave vector k and frequency ω_0, the zero-momentum state

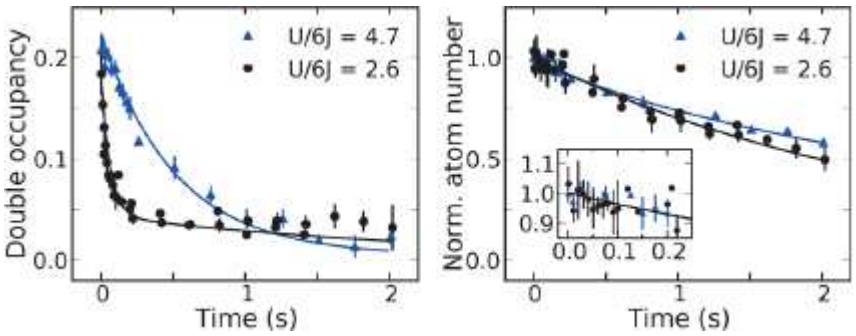

Figure 2.7: Experimental data from [177] showing time evolution of doubly occupied sites in a strongly correlated system made by ultra cold $40K$ fermionic atoms.

is splitted in two coherent wave-packets with momentum $\pm 2\hbar k$ that recollide periodically after a time $t_{col} \sim \pi/\omega_0$, see cartoon in figure 2.6. The remarkable experimental observation was that even after several hundred of oscillations the initial non-equilibrium momentum distribution did not relax to a new equilibrium one consistent with given macroscopic constraints such as energy and particle conservation.

This experimental result triggered many theoretical investigations on the non equilibrium dynamics of integrable and non-integrable interacting quantum systems.

Lifetime of Doublons

Non equilibrium experiment involving ultra cold fermionic atoms in the strongly correlated regime have been reported only much more recently. A recent work addresses the decay of doubly occupied lattice sites (doublons) in the fermionic single band Hubbard model. In order to prepare a largely out of equilibrium initial state the system was exposed to lattice modulation which created an excess of doublons. After the modulation the system is let evolve freely at the initial lattice depth and interaction strength for up to 4s. As shown in figure 2.7 the experimental results show an elastic decay of doublons spanning two-order of magnitude. The decay rate of this highly excited state is found to be, within a good agreement, exponentially large in the ratio U/J, where U is the Hubbard repulsion and J the hopping integral. This result confirms what firstly noticed in [155]. Indeed the decay of highly excited states on a lattice with bandwidth D is inhibited by energy conservation. In order to dissipate a huge energy $E \gg D$ a n-particle scattering

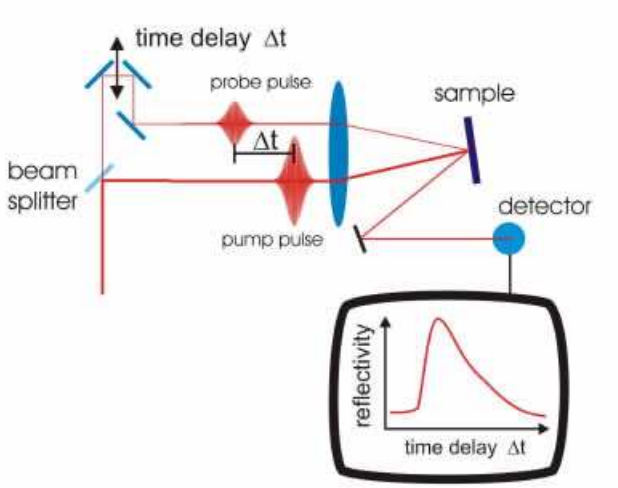

Figure 2.8: Schematic set-up of a time resolved pump probe experiment. In this approach, an ultrashort laser pulse is split into two portions, a stronger beam (pump) is used to excite the sample generating a non-equilibrium state, while a weaker beam (probe) is used to monitor the pump-induced changes in physical properties of the system.

process is required, with $n \sim E/D$. In a system with two-body interactions such a process is expected to have an exponentially small rate, thus to be long-lived.

2.3 Time-Resolved Spectroscopies on Correlated Materials

In the previous sections we have described artificially engineered systems in which electron-electron interactions can have dramatic effects on the observed physical properties. This is not only true in artificial systems but also, and perhaps more interestingly, in real solid state materials.

In this respect relevant examples are provided by a certain class of transition-metal oxides with partially filled d-shells, or by many molecular solids with large separations between neighboring molecules. Here the energy gain due to electron wavefunction delocalization can be lower than the energy associated to the local electron-electron Coulomb repulsion. When this is the case the coherent electronic motion can become energetically unfavourable with respect to charge localization around atomic or molecular

sites and the system is a so called Mott Insulator (MI). Such a *strongly correlated* state of matter represents a remarkable example of the failure of conventional band theory. According to it, due to the partially filled band, a Mott Insulator should indeed behave like a metal, while it features charge gapped excitations due to the large Coulomb repulsion. This is typically missed in standard electronic structures calculations which account for interactions only at mean field level.

From the physical point of view it is worth noticing that many non trivial phenomena are known to occur in strongly correlated materials which are on the verge of becoming Mott insulators, high-temperature superconductivity being one of the most striking example [112] . It is hence not surprising that many different experimental techniques have been developed, since the early discovery of superconductivity in copper-based oxides [128], to characterize physical properties of these materials with an increasing resolution either in energy [38] or in real-space [139].

Recently a large interest has been generated by the possibility to investigate correlated materials using modern time-resolved spectroscopies with femtosecond resolution, techniques which have been mainly borrowed from the realm of atoms and molecules [196].

Pump-probe spectroscopy is the simplest experimental technique used to study ultrafast dynamics in solids and molecules. In such experiments, one first shoots an ultrafast (typically 10-100 fs) *pumping* pulse on the sample to drive its electronic system out of the equilibrium state. Then after a brief time delay (Δt) of typically tens of femtoseconds to tens of picoseconds, a *probing* pulse of either photons or electrons is sent in to probe the sample transient state. By varying Δt, one can study the process by which the system relaxes back to the equilibrium state, thus acquiring the related dynamic information. Most conventional set-ups use optical probes to measure, for example, the changes in the optical constants (such as reflectivity or transmission) as a function of time delay between the arrival of pump and probe pulses. This yields information about the relaxation of electronic states in the sample [67].

It is worth mentioning that the very idea of recording transient phenomena by shining short pulses followed by a second one at fixed delay was developed long-time ago, already before the end of XIX century [109]. Although the conceptual framework for pump-probe spectroscopy was settled, it takes the whole century to develop proper techniques to generates and detect fast enough pulses. In this respect the resolution in the time domain was limited by nanosecond duration of incoherent light sources for almost fifty years. Then the development of broadband lasers and non-linear op-

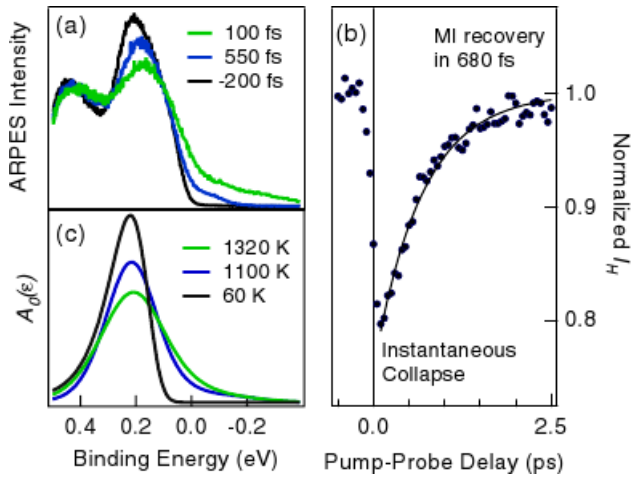

Figure 2.9: Time-Resolved ARPES measurements [141] of the evolution of electronic structure of 1T-TaS2 after an infrared optical excitation. Right panel shows the instantaneous collapse of the intensity of the Hubbard band and the slower subsequent recovery. Left panel shows the dynamics of the spectral function which firstly shows a transfer of spectral weight from the Hubbard band to the Fermi level and then a slower depletion.

tical techniques pushes the resolution power of pump-probe techniques six order of magnitude up, from nanosecond to femtosecond regime. This largely widens the range of physical processes that can be addressed by means of these techniques. In addition, since it is now possible to generate and detect femtosecond pulses across the whole electromagnetic spectrum, novel time-resolved spectroscopic techniques have been proposed in addition to more conventional optical probes. Among them we mention ultrafast electron diffraction [29] and photoemission spectroscopy [141]. As we briefly mentioned, a common feature of these dynamical techniques is that the system investigated is no longer in strict thermodynamic equilibrium. The material under study may be either in an excited state whose decay into other degrees of freedom is being probed, yielding information unavailable to conventional time-averaged frequency domain spectroscopies, or in a metastable state with fundamentally different physical properties. Many interesting experiments have been recently performed on correlated materials using time-resolved spectroscopies, see for example [66, 34] for interesting works on cuprate high-Tc superconductors. In the next paragraph we briefly sketch one among them, that we found of particular interest for the present work.

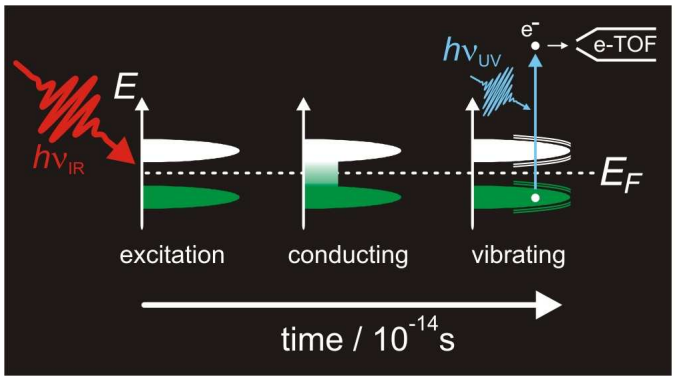

Figure 2.10: Cartoon picture of the transient dynamics of electronic structure of 1T-TaS2 after photo-induced excitation.

2.3.1 Time Evolution of the Electronic Structure across an Insulator to Metal transition

Differently from metallic compounds, Mott insulators features a large gap in the spectrum of single particle excitations. Chemical doping is a possible and widely used route to induce an insulator to metal transition. An alternative path is offered by the so called photo-doping as it has been shown in [141].

Here an infrared femtosecond laser pulse excites the insulating phase of 1T-TaS2, a material which shows a Mott transition driven by electronic correlations. Hence the transient electronic structure is measured directly with time-resolved photoelectron spectroscopy by photoemitting valence electrons by a time-delayed ultra-violet laser pulse. In figure 2.9 we report ARPES data at different time delays. The results show that the optical excitation induces an ultrafast transformation to a semi-conducting transient phase.

This is shown by the instantaneous collapse of the electronic band gap (right panel) and by the major transfer of spectral weight from the Hubbard band to the originally gapped region close to the Fermi level. This process occurs on a rather short time scale, $t < 100fs$. Then the hot electron distribution decays rapidly within a few hundred femtosecond and the band gap is subsequently re-established. Notice however that the peak of the Hubbard band is slightly shifted toward the Fermi level due to photoinduced doping. In addition, the hot electrons launch a nuclear motion of the lattice atoms which vibrate coherently after the instantaneous excitation. Since these vibrations do not alter the band gap, the material remains insulating. Nevertheless the breathing of the lattice structure modifies the binding energy of electronic states by electron-phonon coupling.

Chapter 3

Theoretical Challenges in Correlated Systems Out of Equilibrium

The experimental advances we have described in previous chapter offer the chance to probe strongly correlated systems in a completely novel regime, where the combination of interactions and non equilibrium effects may result in many non trivial phenomena. A theoretical description of this new regime poses serious challenges, both from a conceptual and a methodological point of view. In this chapter we briefly review the main theoretical issues behind the study of strongly correlated systems out of equilibrium.

3.1 A Glimpse on Many Body Theory of Non Equilibrium States

Strongly correlated electron systems and their rich physical properties represent a major challenge for theoretical condensed matter physics since last thirty years. They usually escape any single particle description and are often associated to intrinsically non perturbative effects. The main goal of the theoretical research has been so far mainly focused on understanding low temperature equilibrium properties of these systems, which is the regime typically probed in condensed matter experiments. Here ground state correlations and low-lying excited states completely dominate the physics. This effort resulted into a large variety of analytical and numerical methods able to cope with electron-electron interaction beyond perturbation theory.

However, as experiments start probing physical properties far beyond the linear response regime, the interest on correlated phenomena in out of equilibrium rapidly starts to grow.

In its original formulation the many body theory of non equilibrium states dates back to early works by Schwinger [170], Keldysh [105], Kadanoff and Baym [97] in the mid sixties. In their seminal contributions these authors settled the proper theoretical framework to describe systems which are evolved under the action of external fields or which are driven into non equilibrium steady states by external forcing. Without entering in too much details, for which we refer the reader to existing monographs [147, 98], we can try to point out the main difference between equilibrium (zero temperature) many body theory and its non-equilibrium counterpart. It lies in the fact that, once the systems is pushed out of equilibrium, the nature of the quantum state on which physical properties are computed is not defined *a priori*, but is determined by the dynamics itself. This point is central in the whole formulation and reflects the fact that we would like to describe phenomena such as the flow of currents where the system, even if stationary, could not be in its ground state but in an arbitrarily excited state. This is at the opposite of standard many body theory based on the so called Gell-Mann Low theorem [64], which assume that, provided the interaction is switched on adiabatically in the infinite past, the system will remain in its ground state even after infinite time. While this statement is generally true for ground states it can be violated for arbitrary states [110], which evolve after infinite time into a combination of excited states. From a different perspective we could say that while in thermal equilibrium the general goal is to solve the Hamiltonian and find its spectrum, out of equilibrium also the distribution function have to be determined by solving appropriate kinetic equations.

Although extremely valuable and general, this approach as it stands cannot provide too much insights into the strongly interacting regime where perturbative approaches usually fail. This is even more true for what concerns the real-time dynamics. Indeed it is well known [13] that bare perturbation theory in real-time is usually plagued by *secular terms* which make the limit of long-times/small-interactions tricky to handle. Partial summations of certain class of diagrams are not sufficient to ensure a stable long-time limit and one has to resort to more sophisticated approaches, see for example [68, 63] Among them we mention in particular the flow equation approach [81, 82] which provides a reliable analytical tool to study the non equilibrium real-time dynamics in the weak coupling regime.

This has motivated a huge effort for developing methods that treat strong correlations and non equilibrium effects on equal footing. This effort has been triggered by few main theoretical issues which we will briefly review here, since they have a special interest from the perspective of the present work.

3.2 Non Equilibrium Physics in Quantum Impurity Models

Several intriguing theoretical questions arise from the possibility to couple small interacting quantum systems to external reservoirs and to drive them out of equilibrium by applying a forcing field, such as a dc voltage bias. As a result a strongly correlated non equilibrium steady state (NeqSS) is reached, after waiting some transient time, with a finite current flowing across the system. A natural question concerns how to describe such a state when interactions are not weak and in particular what is the effect of decoherence and dissipation - two genuine non equilibrium effects - on the physical properties of the system. Also, an interesting question concerns the typical time scales which control the onset of a NeqSS.

Quantum Impurity (QI) models represent the natural framework to study quantum transport through nanocontacts. These consist of a small quantum system with few interacting degrees of freedom, the impurity, tunnel coupled to a reservoir of fermionic excitations. Worthily, while the equilibrium physics of these nutshell strongly correlated systems can be studied with a wide range of powerful numerical and analitical tools, their non equilibrium dynamics is still challenging. The reason for this gap is mainly due to the fact that most of the theoretical tools which has been developed in the last thirty years to solve quantum impurity models in equilibrium, most notably Numerical Renormalization Group [192, 23] (NRG), can not be directly ap-

plied to the out of equilibrium case. This has triggered a large amount of theoretical works. Many interesting issues have been addressed in the context of quantum impurities in non equilibrium steady states. Without sake of completeness, we briefly summarize some of them here.

3.2.1 Anderson Impurity Out of Equilibrium

A theoretical paradigm for correlated quantum transport is provided by the so called Anderson Impurity model firstly introduced in [8] to explain the low temperature behaviour of magnetic impurities embedded in metallic hosts. It contains the basic physics of the Kondo effect [192, 133], namely the complete screening of the impurity spin by conduction electrons as the temperature is lowered to zero, and it was later recognized [131, 69, 2] to be responsible for the zero bias anomaly observed in the low temperature conductance of semiconducting quantum dots.

Non equilibrium effects on this correlated local many body state have been studied theoretically very intensively in last years, due to their direct relevance to experiments on nanodevices.

In particular, the effect of a dc voltage bias has been firstly addressed using (weak-coupling) perturbative renormalization group methods, see for example [99, 100, 153, 103, 44, 59], that provide a sensible approximation in the regime $eV \gg T_K$. The general outcome of these studies is that the flow of the current across the impurity induces decoherence thus cutting-off the characteristic logarithmic singularities associated with Kondo effect. Also the role of a magnetic field has been addressed in the same regime [154, 60, 168]. Moreover, the behaviour of differential conductance at low bias voltage $eV \ll T_K$ has been also obtained using Fermi Liquid Theory [100, 135].

However, as these works focus mainly on the asymptotic regimes of low and high voltages, the theoretical description of the whole bias-induced crossover from low conductance up to the unitary limit is still a challenging open problem. In addition many characteristic non equilibrium features due to the bias voltage, such as for example its effect on the impurity spectral function, has not been yet fully clarified. Finally, we also mention that theoretical approaches able to deal with more complicated impurity models (such as those with more impurities or orbitals) would be highly desirable.

Recently a new interest has been triggered by the developments of non perturbative methods for quantum impurities out of equilibrium. We mention here, in particular, the extension of Bethe-Ansatz [118, 20] and many interesting numerically exact methods. Among those that have been recently

applied to study quantum transport through a correlated Anderson Impurity in the non linear regime we mention the scattering state extension of NRG [3], the time-dependent Density Matrix Renormalization Group [107, 88] (DMRG), and the ISPI method [186, 46]. In addition, a novel numerical method based on Diagrammatic Monte Carlo [183] has been recently proposed by a number of authors [127, 162, 191]. This will be the main subject of the first part of this thesis and we refer the reader to chapters 4 and 5.

3.2.2 Vibrational effects in non equilibrium transport

Theoretical investigations of vibrational effects in quantum transport through single molecules, starting with the pioneering works [70, 193], keep attracting a large interest in the community [122, 61]. The interplay between electronic and vibronic degrees of freedom in molecular conductors and the large number of energy scales that are involved result in non trivial behaviors that are generally difficult to grasp within a unified theoretical framework. Several interesting issues have been recently addressed.

One concerns, for example, the possible signatures of electron-vibron coupling in transport properties such as differential conductance [51], shot noise [87] and more generally full counting statistics [166, 10]. These may appear as so called voltage-induced singularities [53], arising when bias voltage hits the vibrational frequency of the molecule, or as side bands in the finite bias differential conductance [57].

A relevant issue in the process where electrons flow across the molecule is the role played by phonon distribution function which may be or not thermalized with the fermionic reservoirs [54, 122]. In the latter case we could expect the bias to play the role of effective temperature for the vibrionic excitations.

More recently also the transient non equilibrium dynamics has been studied, using lowest order Keldysh perturbation theory and a mean-field strong coupling approach [151]. It is worth noticing that the dynamical behaviour of these single molecule devices may display intriguing effects especially in the strong electron-vibron coupling regime where the junction may be on the verge of a bistable behaviour [121]. In this respect a proper treatment of quantum fluctuations is also crucial to correctly reproduce the physics [122, 123].

3.2.3 Real-Time Dynamics after Local Quantum Quench

Beside their interest for steady state non equilibrium transport quantum impurity models also offer a clean setup to study real-time dynamics after a

sudden perturbation, a so called *quantum quench*.

In the context of impurity models this problem has a long history that goes back to the seminal works by Nozières and De Dominicis on the X-ray edge singularity [134], passing through the famous Anderson and Yuval approach to the Kondo model [195].

More recently, this problem stimulated new interest [132, 113, 5], due to the experimental progresses in nanotechnology, which made it possible to contact microscopic quantum objects with metallic electrodes, thus realizing quantum impurity models in a fully tunable set-up [71].

Two kinds of quenches can be considered in this context, depending on the amount of energy that is injected into the system, also referred as the work done during the quench. Global quantum quenches are particularly relevant for transport through correlated nanostructures, where a net current flow is forced by suddenly switching on e.g. a dc bias voltage. Since the switched perturbation is extensive, the system is driven into a non-equilibrium steady state at long times [44]. Conversely, local quantum quenches amount to suddenly change the impurity Hamiltonian. These kinds of quenches can be realized in an optical absorption experiment, as suggested in [181] and more recently in [90], and the resulting non-equilibrium dynamics can be tracked in real-time using pump-probe techniques or, in real-frequencies, measuring the absorption lineshape. Furthermore, local quenches are interesting as they are the simplest examples of non-equilibrium processes whose statistics may show non trivial fluctuations [171].

In the context of the Anderson Impurity Model the real-time dynamics has been studied using td-NRG [5]. This study reveals the presence of separate time scales for charge and spin excitations, the first being controlled by the hybridization width while the latter being long lived and controlled by the Kondo temperature T_K. We will come back on this problem in next chapters.

In the context of Kondo Model many theoretical works addressed the real-time dynamics after a local perturbation using analytical and numerical approaches [6, 143, 102].

An intriguing problem, which will be partially addressed in next chapters, is related to the interplay between the quench and the low energy spectral properties of the bath. Indeed, as it is well known, the equilibrium fixed point structure of the AIM is very sensitive to the low energy properties of the bath [194, 73] and this may result in non trivial behaviors for what concerns the non equilibrium dynamics. This point has some connection with a recent investigation of the dynamics in ferromagnetic Kondo model [83], made with td-NRG and flow equation approach.

3.3 Non Equilibrium Dynamics of Correlated Bulk Systems

A second main line of theoretical research on strongly correlated physics out of equilibrium has been triggered by the opportunity to probe relaxation dynamics of highly excited states in macroscopic quantum systems. This is offered by recent developments in ultra cold atoms and pump-probe spectroscopies on correlated materials that we have briefly reviewed in chapter 2.

As opposite to previous cases of quantum impurities where most of the interest was triggered by the existence of a strongly correlated non-equilibrium steady state due to the reservoirs, here the main focus is on the relaxation dynamics after the excitation, hence on *transient dynamical phenomena*. As a consequence of their rich equilibrium low temperature phase diagram, featuring many competing phases all very close in energy, strongly correlated electrons are expected to display intriguing dynamical behaviors when an external perturbation drive them away from thermal equilibrium. This may include, for example, the trapping into long-lived metastable states which may differ completely from their low energy equilibrium counterpart [155].

It is worth mentioning that a theoretical modeling of non equilibrium experiments we have described in chapter 2, both for what concerns ultra cold atoms and particularly strongly correlated materials, may be very difficult. For this reason theoretical investigations mostly focused on prototypical non equilibrium problems with the idea of gaining further insights on the physics of time dependent strongly correlated phenomena.

3.3.1 Global Quantum Quenches

From a theoretical point of view the simplest way to push the system out of equilibrium is through a so called quantum quench [25]. Here the system is firstly (i) prepared in the many-body ground state $|\Psi_i\rangle$ of some initial Hamiltonian H_i which is then (ii) *suddenly* changed to $H_f \neq H_i$. As a consequence of this instantaneous change the initial state $|\Psi_i\rangle$ turns to be an highly excited state of the final Hamiltonian, which will drive the dynamics for later times. It is worth to notice that the perturbation induced by the change of Hamiltonian is in general *extensive*. We can therefore say that quantum quenches provide the simplest protocol to induce a global excitation into the system and to monitor how the energy is distributed among different degrees of freedom and correlations. Naturally, many non trivial questions arise concerning the real-time evolution after the quantum quench.

These primarily address the onset of thermalization at long time scales or the possible realization of non thermal steady states.

Before we proceed a word is in order to further clarify the meaning of the so called thermalization debate [27, 126, 124].

Since the quantum dynamical evolution of isolated systems is *unitary*, no entropy production is ultimately possible. Hence a pure state, such that $\mathrm{Tr}[\rho_i^2] = 1$, will never relax strictly speaking toward a thermal state, which is by construction a mixed one $\mathrm{Tr}[\rho_{therm}^2] < 1$. However, as long as suitable observables are considered, their quantum dynamics can reach long-time steady states which (i) are robust against changes in the initial conditions and (ii) whose properties resemble those obtained within a finite temperature Gibbs ensemble at the same intensive energy and particle density. From a broader perspective, we notice that the issue of thermalization in interacting quantum systems has been firstly addressed in contexts which are far from condensed matter physics. In particular, in connection with quantum chaos roughly a decade ago [43, 176] and with high-energy physics and cosmology, more recently [14, 15, 68]. In this respect, the experimental developments with ultra cold gases have brought fresh new ideas and triggered the attention of the condensed matter community [149].

The recent literature on quantum quenches in interacting bosonic and fermionic systems is by now very broad, see for example the recent topical reviews [50, 12, 31]

An interesting issue which has been widely discussed and is still matter of scientific debate is the role played by integrability in the issue of thermalization. The general expectation is that integrable systems fail to thermalize due to the extensive number of conserved quantities which forbid loosing memory of the initial condition. While these expectations have been generally confirmed [30, 94, 47, 150, 148], the specific mechanisms for such a lack of thermalization is still under debate [16, 156, 157].

For generic non integrable systems the physical expectation is that relaxation to thermal equilibrium will take place after some (eventually large) transient time scale. However few results are available in this case, since the problem of solving real-time dynamics of non-integrable interacting quantum systems is extremely challenging. This leaves still open the question whether and in which way relaxation to a thermal steady state takes place.

For lattice one dimensional systems results have been obtained mainly using time-dependent DMRG and Lanczos algorithm. In the bosonic case [108, 158] the numerical results show that while for small interaction quenches correlations functions do actually thermalize, the same it is no more true for large quenches. Here a long lived quasi steady-state different from the

thermal one was reached, thus making difficult to conclude whether thermalization occurs on a much longer time scale or not. Even more surprisingly, the results for one dimensional spinless lattice fermions [116] both in the integrable and non-integrable case show that up to the longest accessible time scale the dynamics relax to a stationary state which differs from the thermal one.

For strongly correlated electrons in more than one dimension only few results are available concerning the dynamics after an interaction quench in the Fermionic Hubbard Model. In the following we will discuss in more details these works which will play an important role from the point of view of this work.

3.3.2 Quench Dynamics in the Fermionic Hubbard Model

The single band Hubbard model [91, 79, 101] represent one of the simplest yet non trivial models encoding the physics of strong correlations, namely the competition between electronic wave function delocalization due to hopping t and charge localization due to large Coulomb repulsion U. Out of this competition, on the verge of a Mott metal-insulator transition, many non trivial phenomena may arise. While theoretical investigations on its ground state properties continue since thirty years, the non equilibrium dynamics of this paradigm strongly correlated model has been started only much more recently. The dynamics of Fermi system after a sudden switch-on of the Hubbard interaction has been studied firstly in [125, 126] using the flow-equation approach.

The resulting evolution, evaluated up to second order in the interaction, shows a full a sequence of transient regimes. For short time scales[1], $0 < t \ll 1/U^2$, one observes a fast reduction of Fermi surface discontinuity Z which can be understood as formation of quasiparticles from the initial non interacting state. At time scales of order $t_1 \simeq 1/U^2$ the quasiparticle distribution function has relaxed to a quasi steady state which makes the system resembling a zero-temperature Fermi Liquid but with a characteristic mismatch in the quasiparticle weight $1-Z_{NEQ} = 2(1-Z_{EQ})$. Notice that such a *prethermal* regime is stable for time scales $1/U^2 < t < 1/U^4$. In this time window excitation energy is already relaxed to equilibrium, hence from an energetic point of view the system can be considered as thermal, while the distribution function is trapped into a metastable configuration. This has been attributed to phase space constraints characteristic of interacting

[1] Hereafter we fix the unit of energies and times by setting the non-interacting density of states at the Fermi level, ρ_F, equal to one.

Fermi systems. Full thermalization eventually occurs on a much longer time scales, $t_2 \simeq 1/U^4$, due to residual quasiparticle interactions. This has been described phenomenologically within a quantum Boltzmann equation. The two stage relaxation that has been described within flow equation approach is strictly speaking restricted to small interaction quenches. For larger values of the interaction one may expect the two time scales t_1, t_2 to still be present, although less separated.

This has been indeed confirmed by solving the quench dynamics for the Hubbard model using non-equilibrium extension [58] of Dynamical Mean Field Theory [65] (DMFT). DMFT has emerged in the last decades as a very powerful non-perturbative approach to strongly correlated electron systems in thermal equilibrium. This method maps the full lattice model of interacting fermions onto a Quantum Impurity model coupled to a self-consistently determined external bath. In a general non equilibrium situation, where one is interested in studying relaxation dynamics in real-time, the bath cannot be assumed to be in thermal equilibrium. Using a recently developed real-time Diagrammatic Monte Carlo algorithm [191] the dynamics after an interaction quench starting from a zero temperature Fermi sea was investigated [48]. The results show that both for weak and strong interaction quenches the system is trapped into quasi-stationary states on intermediate times which delay thermalization to much longer time scales, far beyond the longest time so far accessible with real-time QMC. The weak coupling prethermal regime is consistent with flow equation analysis and appears as a plateau in the dynamics of quasiparticle weight. As opposite the strong coupling prethermal regime originates from the exponentially long-time scales associated to the decay of double occupations [155] and results in a characteristic pattern of collapse and revival oscillations.

In addition, DMFT results show evidence for a fast thermalization occurring at a special value of the final interaction, in correspondence of which the quasiparticle weight relaxes to zero consistently with the relatively high-temperature $T_\star$ fixed by the initial energy. As later analysis has confirmed that not only one-time observables but also correlations function are thermal for this special value of quench [49].

The appearance of such a sharp crossover at U_c^{dyn} in the dynamical behavior is surprising if thought in terms of the equilibrium phase diagram of Hubbard Model within DMFT. Indeed this would appear at a much higher temperature $T_\star$ than the critical Mott ending point. Its ultimate origin and its relation with the equilibrium Mott metal-insulator transition has not been yet fully understood.

3.4 Plan of the Thesis

In light of previous discussions we can conclude that understanding the physics of interacting quantum systems out of thermal equilibrium represents one of the most intriguing open problem in modern condensed matter physics.

In this perspective, the aim of present thesis is to address some of the issues arising in this field by means of novel analytical and numerical methods able to deal with strong electron-electron correlations and non equilibrium effects.

In the first part of this work we consider quantum impurity models as paradigmatic examples of strongly correlated nanodevices. We develop a general approach to deal with their real-time non equilibrium quantum dynamics and apply this Real-Time Diagrammatic Monte Carlo method to two relevant physical examples. This part of the thesis is organized as follows. In chapter 4 we introduce the method, which is based on a Diagrammatic Monte Carlo sampling of the real-time perturbation theory in the hybridization between the impurity and the bath. In chapter 5 we present two applications, namely we study dynamics after a local quantum quench in the Anderson Impurity Model and non linear transport through a simple Holstein model of molecular conductor.

In the second part we move our attention to bulk macroscopic systems and to the non equilibrium dynamics induced by global quantum quench. In this context we propose a non perturbative approach to quantum dynamics of strongly correlated electron systems based on a time dependent extension of the Gutzwiller wave function. In chapter 6 we present a general formulation of the time dependent variational method and consider as a relevant application the dynamics induced by an interaction quench in the single band fermionic Hubbard model.

Part II

Dynamics in Quantum Impurity Models

Chapter 4

Diagrammatic Monte Carlo on the Keldysh Contour

In this chapter we introduce the Real-Time Diagrammatic Monte Carlo method we have proposed to study non equilibrium dynamics in correlated quantum impurity models. We formulate the problem on the full three branches Kadanoff-Baym-Keldysh contour which allows us to deal with an arbitrary, even interacting, initial density matrix. We discuss two main non equilibrium set up, namely quantum transport in dc bias and local quantum quenches.

4.1 Non Equilibrium Dynamics in Quantum Impurity Models

The aim of this section is to set-up the proper framework to study non equilibrium real-time dynamics in quantum impurity (QI) models. To this purpose, we consider a set of discrete electronic levels, the "impurity", with creation operator $c_a^\dagger$ labeled by an integer $a = 1, \dots \mathcal{N}$ which may include both spin and orbital degrees of freedom. These levels are coupled to one or more baths of free fermions with momentum $\mathbf{k}$ and creation operator $f_{\mathbf{k}\,a}^\dagger$. The generic Hamiltonian of a QI model reads

$$\begin{aligned} \mathcal{H}_- &= \sum_{\mathbf{k}\,a} \varepsilon_{\mathbf{k}}^- \, f_{\mathbf{k}\,a}^\dagger \, f_{\mathbf{k}\,a} + \mathcal{H}_{loc}^- \left[c_a^\dagger, c_a \right] \\ &\quad + \sum_{\mathbf{k}\,a} \left(V_{\mathbf{k}\,a}^- \, f_{\mathbf{k}\,a}^\dagger \, c_a + h.c. \right) , \end{aligned} \tag{4.1}$$

where the first term describes the continuum of fermionic excitations, the local Hamiltonian $\mathcal{H}_{loc}^- \left[c_a^\dagger, c_a \right]$ generally contains many-body interactions for electrons on the impurity, while the last term is the hybridization which couples the impurity and the bath and it is assumed here, for the sake of simplicity, to be diagonal in the a index.

Since we are interested in studying non equilibrium dynamics of model (4.1), we have to specify an initial condition as well as a protocol to drive this system out of equilibrium. Following general ideas of non equilibrium many body theory [147, 97], we imagine to prepare the system at $t = 0$ in a thermal state of $\mathcal{H}_-$, namely we choose the Boltzmann distribution as initial density matrix

$$\rho(t = 0) = \rho_{eq} \equiv \frac{e^{-\beta \mathcal{H}_-}}{Z} , \qquad Z = \mathrm{Tr}\, e^{-\beta \mathcal{H}_-} , \tag{4.2}$$

and then, for $t > 0$, let the system evolve under the action of a new Hamiltonian

$$\mathcal{H}(t) = \mathcal{H}_- + \mathcal{V}(t) , \qquad t > 0 \tag{4.3}$$

Choosing the initial density matrix as the thermal one gives access to the response of a *correlated* quantum impurity model to external fields. For what concerns the driving protocol, namely the nature of the external perturbation, there are actually several ways to push a quantum impurity model out of equilibrium. In this work we shall focus on the simplest one, namely a quantum quench experiment, but the method allows to address even more general *time dependent* out of equilibrium problems. In a quantum quench, one imagines to prepare the system, at $t = 0$, in a given state of some initial

Hamiltonian ($\mathcal{H}_-$ in the case of our interest) and then, for $t > 0$, to suddenly change some of its parameters letting evolve the system under the unitary action of a new Hamiltonian $\mathcal{H}_+$. Such a protocol therefore represents the simplest example of time-dependent problem where the variation in time is step-like

$$\mathcal{H}(t) = \mathcal{H}_- + \theta(t)\,\delta\mathcal{H}\,, \qquad \delta\mathcal{H} = \mathcal{H}_+ - \mathcal{H}_-\,. \tag{4.4}$$

The sudden quench injects energy into the system and leads to a relaxation dynamics towards a new steady state, provided the perturbation $\delta\mathcal{H}$ is not a conserved quantity of $\mathcal{H}_-$. The main task is therefore to compute quantum averages with the full density matrix $\rho(t)$ evolved in real-time

$$\langle O(t)\rangle = Tr\,[\rho(t)\,\mathcal{O}] = Tr\,\left[\rho_{eq}\,U^\dagger(t)\,\mathcal{O}\,U(t)\right]\,. \tag{4.5}$$

where the trace has to be taken over the bath and the impurity degrees of freedom, while $U(t)$ and $U^\dagger(t)$ are, respectively, the unitary operator generating the dynamics and its hermitian conjugate. In the specific case of a time independent Hamiltonian, as we have for $t > 0$ see Eq. (4.4), these operators read

$$U(t) = e^{-i\,\mathcal{H}_+\,t} \qquad U^\dagger(t) = e^{i\,\mathcal{H}_+\,t}\,. \tag{4.6}$$

To proceed further, it is convenient to specify the nature of the perturbation $\delta\mathcal{H}$ induced by the quantum quench. To keep the discussion as general as possible we write the Hamiltonian of the system for $t > 0$ as

$$\begin{aligned}\mathcal{H}_+ \;=\; & \sum_{\mathbf{k}\,a} \varepsilon^+_{\mathbf{k}}\, f^\dagger_{\mathbf{k}\,a}\, f_{\mathbf{k}\,a} + \mathcal{H}^+_{loc}\left[c^\dagger_a, c_a\right] \\ & + \sum_{\mathbf{k}\,a}\left(V^+_{\mathbf{k}\,a}\, f^\dagger_{\mathbf{k}\,a}\, c_a + h.c.\right)\,,\end{aligned} \tag{4.7}$$

namely we allow for an abrupt change of all the parameters entering in the Hamiltonian (4.1), in such a way that different kind of non equilibrium phenomena can be treated within the present approach. Throughout this chapter we will mainly refer to two different set up.

In a first protocol the impurity is prepared in equilibrium with the bath then a dynamics is induced by a sudden change of any impurity energy scales. These can be, for example, the local electron-electron interaction or the position of the impurity energy level. Alternatively, one can imagine to act on the impurity-bath hybridization, namely to start from a decoupled impurity and suddenly switch-on the coupling with the reservoir. Interestingly enough, this latter set up can be used to study transient currents flowing through the quantum impurity, provided two reservoirs held at different chemical potential are coupled to the impurity at time $t > 0$ via hybridization. In figure 4.1

we plot a cartoon of the different non equilibrium protocols we are mostly interested in. Once we have specified the structure of the Hamiltonian after

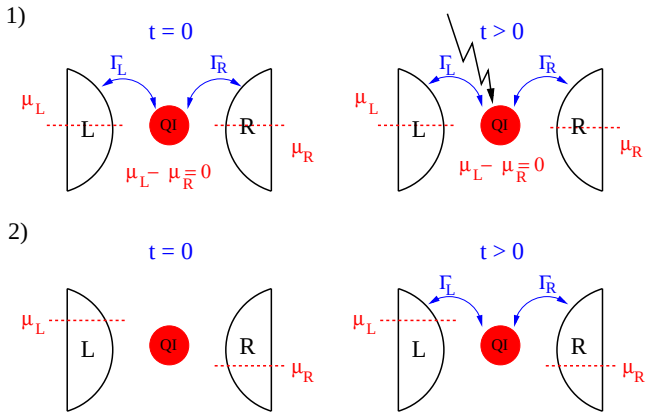

Figure 4.1: The two non equilibrium set-up we will consider to study real-time dynamics in the Quantum Impurity Models. In set-up 1 we prepare at time $t = 0$ the impurity in equilibrium with the baths at temperature T and chemical potentials $\mu_L = \mu_R$. Then at time $t > 0$ some energy scale entering the impurity Hamiltonian is suddenly changed. In set-up 2 we prepare at time $t = 0$ the impurity decoupled from the leads which are in equilibrium at temperature T and chemical potentials $\mu_L \neq \mu_R$. Then at time $t > 0$ the couplings Γ_α between then impurity and then leads are suddenly switched on.

the quench, we can perform the hybridization expansion in formal analogy to what has been done previously in the equilibrium imaginary-time case [187], with however important differences reflecting the genuine non-equilibrium nature of the problem. This is will be described in detail in the next few sections.

4.2 Hybridization Expansion on the Kadanoff-Baym-Keldysh Contour

In order to study the non equilibrium real-time dynamics of quantum impurity models starting from a generic initial density matrix, we formulate the diagrammatic monte carlo algorithm (diagMC), in its hybridization expansion version, on the Kadanoff-Baym-Keldysh contour made by the usual imaginary time axis and the real-time Keldysh contour. As we are going to show, this structure naturally emerges from the definition of real-time

quantum averages given in equation (4.5). To proceed further, we introduce a *dynamical* time-dependent partition function for the QI model which is defined as

$$\mathcal{Z}(t,\beta) \equiv \mathrm{Tr}\left[e^{-\beta\mathcal{H}_0}\, U^\dagger(t)\, U(t)\right] . \tag{4.8}$$

We note that this quantity does not actually depend on time t since, by construction, the evolution is unitary, nevertheless it represents the natural quantity to derive the hybridization expansion. As it will appear more clearly later on, $\mathcal{Z}(t,\beta)$ can be seen a dynamical generating functional of the Monte Carlo weights needed to compute any quantum average in real-time. The basis of any continuous-time diagMC algorithm is the expression of evolution operators as time-ordered exponentials. For the real-time operator and its hermitian conjugate we get

$$U(t) = \mathrm{T}\,\exp\left(-i\int_0^t dt\,\mathcal{H}_+(t)\right) \tag{4.9}$$

$$U^\dagger(t) = \bar{\mathrm{T}}\,\exp\left(i\int_0^t dt\,\mathcal{H}_+(t)\right) \tag{4.10}$$

where T ($\bar{\mathrm{T}}$) is the time ordering (anti-time ordering) operator, whose action is order a string of real-time fermionic operators according to their time arguments, placing to the left the operators at later (earlier) times, with an overall plus or minus sign according, respectively, to the parity of the number of fermionic exchanges needed to move the string from the original to the final ordering. Using the well known properties of the equilibrium density matrix (4.2) we can write also the Boltzmann weight as an imaginary time evolution along the path $[-i\beta, 0]$

$$\begin{aligned} e^{-\beta\mathcal{H}_-} &= \mathrm{T}\,\exp\left(-\int_0^\beta d\tau\,\mathcal{H}_-(-i\tau)\right) \\ &= \mathrm{T}_\urcorner\,\exp\left(-i\int_0^{-i\beta} dt\,\mathcal{H}_-(t)\right) = U(-i\beta)\ , \end{aligned} \tag{4.11}$$

where $\mathrm{T}_\urcorner$ is an imaginary-time-ordering operator defined in complete analogy with T.

Inserting these expressions in the dynamical partition function previously introduced, we get

$$\begin{aligned} \mathcal{Z}(t) &= \mathrm{Tr}\left[\mathrm{T}_\urcorner\, e^{i\int_{-i\beta}^0 dt\,\mathcal{H}_-(t)}\ \bar{\mathrm{T}}\, e^{i\int_0^t dt\,\mathcal{H}_+(t)}\ \mathrm{T}\, e^{i\int_t^0 dt\,\mathcal{H}_+(t)}\right] \\ &= \mathrm{Tr}\left[\mathrm{T}_C\, e^{i\int_C dt\,\mathcal{H}(t)}\right] \end{aligned} \tag{4.12}$$

where, in the second line, C is the Kadanoff-Baym-Keldysh contour plotted in figure 4.2, which is made of three branches $\mathcal{B}_i$, $i = 1, 2, 3$, being respectively

the upper real-time branch, the lower one and the imaginary-time branch. Hereafter the time argument t in Eq. (4.12) is assumed to live on such a contour, unless differently specified. Time ordering along C, enforced by operator T_C, acts similarly to the standard Keldysh time-ordering, placing operators with later time on the left, namely

$$T_C\left(A\left(t_1\right)A\left(t_2\right)\right)=\begin{cases} A\left(t_1\right)A\left(t_2\right) & t_1 \overset{C}{>} t_2 \\ -A\left(t_2\right)A\left(t_1\right) & t_1 \overset{C}{<} t_2 \end{cases}, \tag{4.13}$$

where $\overset{C}{>}$ ($\overset{C}{<}$) means greater (lesser) on the contour C. By the definition of the partition function $\mathcal{Z}\left(t\right)$, it follows that

$$\mathrm{T}_C=\mathrm{T}_{\urcorner}\otimes\bar{\mathrm{T}}\otimes\mathrm{T}\,. \tag{4.14}$$

The integral along the contour is defined as

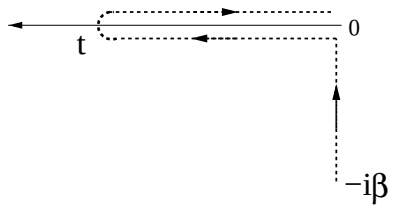

Figure 4.2: Kadanoff-Baym-Keldysh contour which starts at time 0 on the first branch, runs up to time $t=t_*$ then back from t_* to $t=0$ and finally along the imaginary axis from $t=0$ to $t=-i\beta$.

$$\int_C dt=\int_{-i\beta}^{0}dt+\int_0^t dt+\int_t^0 dt\,, \tag{4.15}$$

while, along the contour, the Hamiltonian entering in Eq. (4.12) is

$$\mathcal{H}\left(t\right)=\begin{cases} t\in\mathcal{B}_1,\mathcal{B}_2 & \mathcal{H}_+ \\ t\in\mathcal{B}_3 & \mathcal{H}_- \end{cases} \tag{4.16}$$

Once we have written the partition function $\mathcal{Z}\left(t,\beta\right)$ as a time ordered exponential, we can treat different terms in the contour Hamiltonian as c-numbers. Therefore we can write Eq.(4.12) as

$$\mathcal{Z}\left(t,\beta\right)=\mathrm{Tr}\left[\mathrm{T}_C\,e^{i\int_C dt\,\mathcal{H}_0(t)+\mathcal{H}_{hyb}(t)}\right] \tag{4.17}$$

where we have explicitly indicated the hybridization Hamiltonian $\mathcal{H}_{hyb}(t)$, defined as

$$\mathcal{H}_{hyb}(t) = \sum_{\mathbf{k}\,a} \left(V_{\mathbf{k}\,a}(t)\; f^{\dagger}_{\mathbf{k}\,a}(t)\; c_a(t) + h.c. \right) \tag{4.18}$$

with a time dependent hybridization $V_{\mathbf{k}\,a}(t) = V^{\pm}_{\mathbf{k}\,a}$ depending on the position of time t along the contour C. To proceed further, it is convenient to introduce the bath operators at the impurity site, defined as

$$f^{\dagger}_{a}(t) = \sum_{\mathbf{k}} V_{\mathbf{k}\,a}(t)\; f^{\dagger}_{\mathbf{k}\,a}(t) \tag{4.19}$$

which enter the hybridization Hamiltonian Eq.(4.18). Then we formally expand $\mathcal{Z}(t,\beta)$ in power of the hybridization Hamiltonian (4.18) and trace out, at any order in the expansion, separately the bath and the impurity degrees of freedom which are completely decoupled in the absence of $\mathcal{H}_{hyb}$. Let us define n_{ab} ($\tilde{n}_{ab}$) as the number of creation(annihilation) impurity operators, in the following also called kinks, with flavour a and in branch b. These integers run in general between zero and infinity, the only constraint is that the total number of creation and annihilation kinks for each flavour a, say k_a and $\tilde{k}_a$, have to be equal due to total particles conservation. This introduces the following constraint

$$\tilde{k}_a \equiv \sum_{b} \tilde{n}_{ab} \equiv k_a \equiv \sum_{b} n_{ab} \qquad a = 1, \ldots, \mathcal{N}$$

The resulting expansion for the partition function reads

$$\begin{aligned} \mathcal{Z}(t,\beta) \;=\; & \prod_{a=1}^{\mathcal{N}} \prod_{b=1}^{3} \sum_{\tilde{n}_{ab}, n_{ab}} \mathrm{s}(\tilde{n}_{ab}, n_{ab}) \prod_{i}^{k_a} \int dt^a_i \int d\tilde{t}^a_i \;\times \\ & \prod_{a} \langle\, T_C\, f(t^a_1)\, f^{\dagger}(\tilde{t}^a_1) \ldots f(t^a_{k_a})\, f^{\dagger}(\tilde{t}^a_{k_a}) \rangle_{bath} \;\times \\ & \langle\, T_C \prod_{a} \left(c^{\dagger}(t^a_1)\, c(\tilde{t}^a_1) \ldots c^{\dagger}(t^a_{k_a})\, c(\tilde{t}^a_{k_a}) \right) \rangle_{local}\,, \end{aligned} \tag{4.20}$$

where the contour integrals must be constrained to the time ordered regions

$$t^a_1 \overset{C}{>} t^a_2 \overset{C}{>} \ldots \overset{C}{>} t^a_{k_a} \qquad , \qquad \tilde{t}^a_1 \overset{C}{>} \tilde{t}^a_2 \overset{C}{>} \ldots \overset{C}{>} \tilde{t}^a_{k_a}\,, \tag{4.21}$$

while $\mathrm{s}(\tilde{n}_{ab}, n_{ab})$ includes all the signs(phases) coming from the real-time evolution operators as well as from the integration along the imaginary time axis

$$\mathrm{s}(\tilde{n}_{ab}, n_{ab}) = (-i)^{\tilde{n}_{a3}+n_{a3}}\, i^{\tilde{n}_{a2}+n_{a2}}\, (-i)^{\tilde{n}_{1a}+n_{1a}}\,. \tag{4.22}$$

By using our definition of the total number of kinks k we can write these factors as

$$\mathrm{s}(\tilde{n}_{ab}, n_{ab}) = (-1)^{k_a} \, (-1)^{\tilde{n}_{a2}+n_{a2}} \, (-i)^{\tilde{n}_{a3}+n_{a3}} \, . \tag{4.23}$$

Concerning the trace over the bath degrees of freedom with flavour a, this can be written by using Wick's theorem as the determinant of a $k_a \times k_a$ matrix $\mathbf{\Delta}^a$

$$\langle T_C \, f\left(t_1^a\right) f^\dagger\left(\tilde{t}_1^a\right) \ldots f\left(t_{k_a}^a\right) f^\dagger\left(\tilde{t}_{k_a}^a\right) \rangle_{bath} = \det \mathbf{\Delta}^a \tag{4.24}$$

whose entries Δ_{ij}^a are the contour-ordered hybridization functions defined as

$$\begin{aligned} \Delta_{ij}^a &\equiv i\Delta_C\left(t_i^a, \tilde{t}_j^a\right) = \\ &= \sum_{\mathbf{k}} V_{\mathbf{k}\,a}\left(t_i^a\right) \, \langle T_C \, f_{\mathbf{k}}\left(t_i^a\right) f_{\mathbf{k}}^\dagger\left(\tilde{t}_j^a\right) \rangle \, V_{\mathbf{k}\,a}\left(\tilde{t}_j^a\right) \end{aligned} \tag{4.25}$$

the average being taken over the bath degrees of freedom. This function is defined along the Kadanoff-Baym-Keldysh contour and therefore naturally acquires the structure of a 3×3 matrix in the branch space[185], as we discuss in the appendix A.

Unlike what happens for the bath, the trace over the local hilbert space cannot be written in terms of single particle contractions since in general Wick's theorem does not hold for an interacting impurity. This consideration holds regardless of the specific form of the local Hamiltonian $\mathcal{H}_{loc}$ and it is also true in equilibrium. It is therefore clear that the evaluation of the local term in Eq. (4.20) for a given configuration of kinks is the computational bottleneck of the algorithm, especially in the case where multi-orbital interactions are considered. We note that such a kind of expressions arise also in NCA-kind of approaches to QI models[104]. To efficiently evaluate this local term we follow[188, 86] and take advantage of the reduced hilbert space of the impurity to write the multi-point correlation function of Eq. (4.20) in the basis of the local eigenstates. The trace then reduces to multiplying matrices sandwiched by local evolution operators. If we define a global time ordering along the contour such that

$$t_1 > t_2 > \ldots > t_{2N} \, ,$$

where $N = \sum_a k_a = \sum_a \tilde{k}_a$, then the local trace can be written as

$$\begin{aligned} &\langle T_C \, \textstyle\prod_a \left(c^\dagger\left(t_1^a\right) c\left(\tilde{t}_1^a\right) \ldots c^\dagger\left(t_{k_a}^a\right) c\left(\tilde{t}_{k_a}^a\right)\right) \rangle_{local} = \\ &\qquad s_{T_C} \, \mathrm{Tr}\left[\rho_{loc} \, X_1\left(t_1\right) \, X_2\left(t_1\right) \ldots \, X_N\left(t_N\right)\right] \end{aligned} \quad , \tag{4.26}$$

where we have introduced an extra sign s_{T_C} due to time ordering. In the previous equation the X's are creation or annihilation operators (depending on the time ordering) evolved in time with the local Hamiltonian

$$X_l(t_l) = e^{i\mathcal{H}_{loc}t_l} X_l e^{-i\mathcal{H}_{loc}t_l} \qquad l = 1, \ldots, 2N, \tag{4.27}$$

Combining all the above results, we write the hybridization expansion for the dynamical partition function as

$$\begin{aligned} \mathcal{Z}(t,\beta) &= \prod_{a=1}^{\mathcal{N}} \prod_{b=1}^{3} \sum_{\tilde{n}_{ab}, n_{ab}} \mathrm{s}(\tilde{n}_{ab}, n_{ab}) \prod_{i}^{k_a} \int' dt_i^a \int' d\tilde{t}_i^a \times \\ &\prod_a \mathrm{Det}\left[\mathbf{\Delta}^a\right] s_{T_C} \mathrm{Tr}\left[\rho_{loc} X_1(t_1) \ \ldots \ X_{2N}(t_{2N})\right] \end{aligned} \tag{4.28}$$

It is worth noticing that this expression represents an exact result for the partition function of the original quantum impurity model. As we are going to show in the next section, the goal of the Diagrammatic Monte Carlo method is to sum up *stochastically* the hybridization expansion using a Metropolis algorithm.

4.2.1 Role of the Imaginary-Time Axis

The formulation of the problem on the the full three-branches Kadanoff-Baym-Keldysh contour allows us to deal with the most generic non equilibrium set-up, namely an *interacting* quantum impurity model described at time $t = 0$ by some thermal density matrix, driven out of equilibrium for time $t > 0$ by a generic, possibly time dependent, perturbation.

There are however situations of interest in which the imaginary-time axis is actually not required. This can be the case when the initial density matrix for the impurity and the bath is of special form, either the one of a Resonant Level Model (RLM) with no many body interactions on the impurity or when the impurity and the reservoirs are initially decoupled, such as in figure 4.1. In those cases the method can be formulated directly at zero temperature and on the conventional two branches Keldysh contour, as it has been done in the first place [127, 162, 191]. It is easy to show that the expansion we have derived in previous section reduces to the one on Keldysh contour when the hybridization term in the initial Hamiltonian 4.1 vanishes.

From a physical point of view, as long as the focus is on steady state properties either in or out of equilibrium, the specific choice of the initial density matrix is not expected to play any role. However this may be not the case for the non equilibrium dynamics which may displays different relaxation

behaviors. This has triggered the effort to extend the method in order to deal with a correlated initial density matrix [161, 190].

As a by product, we obtain a general real-time solver for quantum impurity models which can be therefore used for Non Equilibrium Dynamical Mean Field Theory. Even in this context, the possibility of studying the non equilibrium real-time dynamics starting from interacting initial states look particularly intriguing in the light of first DMFT results on quantum quenches in the Hubbard model[48, 49] which focus so far on quenches starting from a non interacting initial state.

4.2.2 Effective Action Formulation

An important outcome of the previous calculation has been to obtain an exact and closed expression for the dynamical partition function $\mathcal{Z}(t,\beta)$ of the quantum impurity model, written as a *functional* of the contour-ordered hybridization $\Delta_C(t,t')$. This result holds in general. Indeed, right the same expression for $\mathcal{Z}(t,\beta)$ is recovered within a path integral formulation of the problem. Following Kamenev[98], we define the dynamical partition function $\mathcal{Z}(t)$ as a path integral over the fermionic coherent states $c(t), \bar{c}(t)$ defined along the three branch contour

$$\mathcal{Z}(t) = \int \prod_a \mathcal{D}\bar{c}_a \, \mathcal{D}c_a \; e^{i\mathcal{S}_{eff}[c_a,\bar{c}_a]} \tag{4.29}$$

The effective action describing the real-time dynamics of the impurity model can be written generally as

$$i\,\mathcal{S}_{eff} = i\,\mathcal{S}_{loc} + \int_C dt \int_C dt' \sum_a c_a(t')\, i\Delta_C^a(t,t')\, \bar{c}_a(t) \tag{4.30}$$

where $\mathcal{S}_{loc}$ is the local-in-time impurity action while the quadratic part is defined in terms of the contour-ordered hybridization function $i\Delta_C(t,t')$ which takes into account the coupling to the bath. It is worth noticing here that, by construction, time arguments lie along the three-branch contour $\mathcal{C}$, while the integrals are defined as in Eq. (4.15). As a consequence, the contour-ordered hybridization function naturally acquires a 3×3 matrix structure in the Keldysh-Matsubara space,

$$i\Delta_C(t,t') \rightarrow i\Delta_{\alpha\beta}(t,t') \qquad \alpha,\beta = 1,2,3 \tag{4.31}$$

where the 2×2 block with $\alpha,\beta \neq 3$ is the Keldysh subspace, the last diagonal element $\alpha=\beta=3$ is the Matsubara sector while the remaining off-diagonal terms are mixed hybridization functions describing the effect of the initial

condition. We want to show now how is possible within this framework to recover the result for hybridization expansion we previously derived. The idea is to formally expand the effective action in power of the contour-ordered hybridization $i\Delta_C$ and use the definition of path-integral as the contour time-ordered average of field-operators[98] to get for the partition function $\mathcal{Z}(t)$ the following expansion

$$\begin{aligned}\mathcal{Z}(t) &= \prod_a \sum_{k_a} \frac{(-1)^{k_a}}{k_a!} \int_{\mathcal{C}} dt_1^a \, d\tilde{t}_1^a \ldots \int_C dt_{k_a}^a \, d\tilde{t}_{k_a} \; i\Delta_C^a(t_1^a, \tilde{t}_1^a) \ldots \times \\ & i\Delta_C^a(t_{k_a}^a, \tilde{t}_{k_a}^a) \langle T_C \prod_a \left(c^\dagger\left(t_1^a\right) c\left(\tilde{t}_1^a\right) \ldots c^\dagger\left(t_{k_a}^a\right) c\left(\tilde{t}_{k_a}^a\right)\right) \end{aligned} \tag{4.32}$$

where the average is taken over the initial local density matrix. To proceed, we symmetrize the integrand with respect to the $k_a!$ permutations of creation times $\left\{t_1^a, t_2^a, \ldots, t_{k_a}^a\right\}$ resulting into an extra $1/k_a!$ and a determinantal combination of the k_a hybridization functions, where the correct signs to build the determinant are provided by the contour time ordered local trace. The k_a-th order term in the expansion therefore reads

$$\begin{aligned}&\textstyle\prod_a \frac{(-1)^{k_a}}{(k_a!)^2} \int_{\mathcal{C}} dt_1^a \, d\tilde{t}_1^a \ldots \int_C dt_{k_a}^a \, d\tilde{t}_{k_a} \, \mathrm{Det}\left[\boldsymbol{\Delta}^a\right] \times \\ &\times \langle T_C \textstyle\prod_a \left(c^\dagger\left(t_1^a\right) c\left(\tilde{t}_1^a\right) \ldots c^\dagger\left(t_{k_a}^a\right) c\left(\tilde{t}_{k_a}^a\right)\right) \, . \end{aligned} \tag{4.33}$$

Now the integrand is fully symmetric under permutations and we can take advantage of this fact to reduce the size of the integration domain, namely we choose among the $k_a!$ possible contour time-orderings for the creation and annihilation times with flavour a the following ones

$$t_1^a \overset{C}{>} t_2^a \overset{C}{>} \ldots \overset{C}{>} t_{k_a}^a \qquad , \qquad \tilde{t}_1^a \overset{C}{>} \tilde{t}_2^a \overset{C}{>} \ldots \overset{C}{>} \tilde{t}_{k_a}^a \, . \tag{4.34}$$

As anticipated, the final result we get for the dynamical partition function $\mathcal{Z}(t)$ coincides with the one quoted in Eq. (4.28).

These considerations are relevant for studying quantum quenches and real-time dynamics of correlated lattice models within Dynamical Mean Field Theory (DMFT). In this case, as one can show explicitly, the full non equilibrium many body problem is mapped, in the limit of infinite lattice coordination, onto a quantum impurity model coupled to a *non-equilibrium* bath and subject to a self-consistency condition. The dynamical partition function of this effective non equilibrium problem acquires exactly the same form as in Eq. (4.29), with an unknown contour ordered hybridization function $i\Delta_C(t, t')$, which generally lacks time translational invariance. This fact makes ineffective most of the conventional impurity solvers used in equilibrium DMFT, which rely on a time independent Hamiltonian formulation of

the effective problem, thus suggesting diagrammatic Monte Carlo method as a natural candidate to solve Non-Equilibrium Dynamical Mean Field equations.

4.3 Diagrammatic Monte Carlo

Diagrammatic Monte Carlo (diagMC) is a numerical algorithm for sampling infinite series of multiple integrals, such as those arising in any perturbative expansion [146]. As it is well known in many body theory, these expansions often admit a diagrammatic representation[1], even in out-of-equilibrium situations. This is true also for the hybridization expansion of section 4.2, as we are now going to show, which is obtained by a proper extension of the graphical representation introduced by Werner and coworkers [187, 188] in the context of the imaginary-time diagMC algorithm.

As it can be immediately read out from Eq. (4.28), the dynamical partition function can be written as a weighted sum over configurations $\mathcal{C}$ made by diagrams on the Kadanoff-Baym-Keldysh contour

$$\mathcal{Z}(t,\beta) = \sum_{\mathcal{C}} W(\mathcal{C}) \,. \tag{4.35}$$

A given configuration contains, for each channel $a = 1, \dots N$, a total of $2k_a$ vertices occurring at times $\{t_i^a, \tilde{t}_i^a\}$ on the contour, with $i = 1, \dots k_a$. Half of these vertices represent an impurity creation operator $c_a^\dagger(t_i^a)$ while the other half stems for an impurity annihilation operator $c_a(t_i^a)$, both of them being evolved in time with the local Hamiltonian $\mathcal{H}_{loc}$. All together we have $2\sum_a k_a$ impurity operators which we store in such a way to always preserve global time ordering along the contour. In summary a typical configuration reads

$$\mathcal{C} = \begin{cases} a = 1, 2, \cdots, \mathcal{N} \\ k_a = 0, \dots \infty \\ t_1^a \overset{C}{>} t_2^a \overset{C}{>} \dots \overset{C}{>} t_{k_a}^a \\ \tilde{t}_1^a \overset{C}{>} \tilde{t}_2^a \overset{C}{>} \dots \overset{C}{>} \tilde{t}_{k_a}^a \,. \end{cases} \tag{4.36}$$

An example of such a configuration is shown in figure 4.3. The weight $W(\mathcal{C})$ associated to each configuration $\mathcal{C}$ can be read directly from the hybridization expansion, see Eq. (4.28). For later convenience we define it as

$$W(\mathcal{C}) = \mathrm{Det}[\mathcal{C}] \; \mathrm{sign}[\mathcal{C}] \; \mathrm{Tr}_{loc}[\mathcal{C}] \,, \tag{4.37}$$

where $\mathrm{sign}[\mathcal{C}]$ includes all the signs(phases) coming from the evolution as well as from the time ordering, while the trace over the configuration reads

$$\mathrm{Tr}_{loc}[\mathcal{C}] = \mathrm{Tr}\left[\rho_{loc} X_1(t_1) \; X_2(t_2) \; \dots \; X_{2N}(t_{2N})\right] , \tag{4.38}$$

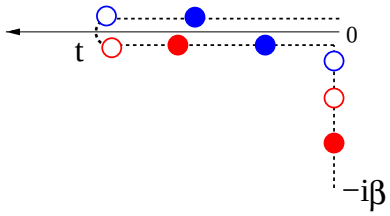

Figure 4.3: An example of configuration $\mathcal{C}$ sampled by diagMC algorithm.

so that by definition we get for $\mathcal{Z}(t)$

$$\mathcal{Z}(t) = \sum_{\mathcal{C}} W(\mathcal{C}) \,. \tag{4.39}$$

The same weights $W(\mathcal{C})$ are also required for evaluating the average of any local operator O acting on the impurity Hilber space. Indeed, if consider the definition of quantum averages given in Eq. (4.5), namely

$$\langle O(t) \rangle = Tr \left[\rho_{eq} U^{\dagger}(t) \, \mathcal{O} \, U(t) \right] , \tag{4.40}$$

and perform the hybridization expansion of the previous section, we find that

$$\langle O(t) \rangle = \frac{\sum_{\mathcal{C}} \mathcal{O}(\mathcal{C}) W(\mathcal{C})}{\sum_{\mathcal{C}} W(\mathcal{C})} , \tag{4.41}$$

where the estimator of local operator has been defined as

$$O(\mathcal{C}) = \frac{\mathrm{Tr}\left[\rho_{loc} X_1(t_1) \ \ldots \mathcal{O} \ldots \ X_{2N}(t_{2N})\right]}{\mathrm{Tr}\left[\rho_{loc} X_1(t_1) \ \ldots \ X_{2N}(t_{2N})\right]} . \tag{4.42}$$

Once the real-time average of a local operator is written as in Eq. (4.41), it would be natural natural to sample it using a Monte Carlo method, namely generating a random walk in the configuration space which visit configurations $\mathcal{C}$ with probability $P(\mathcal{C}) = W(\mathcal{C}) / \sum_{\mathcal{C}'} W(\mathcal{C}')$.

When trying to implement this idea in the context of real-time quantum dynamics the problem one have to face is that the weight $W(\mathcal{C})$ is in general a complex number. In the specific case of interest this is not only due to the explicit "i-factors" coming from the real-time evolution and entering sign$[C]$ but also to the fact that the contour ordered bath, defined in Eq (4.25) and entering the determinants, is indeed a complex function of its time arguments (see Appendix A). The simplest way to circumvent this problem is to sample the absolute value of the weight, $|W(\mathcal{C})|$, while including the phase $\eta(\mathcal{C})$, defined as

$$\eta(\mathcal{C}) = \frac{W(\mathcal{C})}{|W(\mathcal{C})|} , \tag{4.43}$$

in the Monte Carlo estimator. While this approach allows for a straightforward implementation, it becomes problematic when the average phase goes to zero. In this respect, we note that more refined but computationally expensive techniques, based on sampling blocks of configurations at fixed sign, has been developed in recent years to cope with this dynamical sign problem[52]. Therefore a possible future direction could be to merge them with present implementations of diagMC method to see if a compromise between efficiency and accuracy can be found. For the time being we avoid this route, sampling directly the absolute value of the weight.

4.3.1 Metropolis Algorithm

The standard technique to generate configurations with a given probability (in the case of our interest $P_\infty(\mathcal{C}) \equiv |W(\mathcal{C})| / \sum_{\mathcal{C}'} |W(\mathcal{C}')|$) is to build up a Markov chain, namely a stochastic process which describes the evolution of the probability to visit configuration $\mathcal{C}$ after n steps.

$$P(\mathcal{C}, n) = Proba(\mathcal{C}(n) = \mathcal{C}) \tag{4.44}$$

This Markov chain is fully determined once we assign the conditional probability $\mathcal{S}[\mathcal{C}'|\mathcal{C}]$ to be in $\mathcal{C}'$ at step $n+1$ being in $\mathcal{C}$ at step n. Indeed, this is the quantity entering the master equation

$$P(\mathcal{C}', n+1) = \sum_{\mathcal{C}} \mathcal{S}[\mathcal{C}'|\mathcal{C}] \; P(\mathcal{C}, n) \; . \tag{4.45}$$

Sufficient conditions for this master equation to reach, after waiting a proper *equilibration* time, the desired probability $P_\infty(\mathcal{C})$ is that the matrix $\mathcal{S}[\mathcal{C}'|\mathcal{C}]$ is *ergodic* and satisfies the so called detailed balance condition. Ergodicity means that it has to be possible to reach any configuration $\mathcal{C}$ from any other configuration $\mathcal{C}'$ in a finite number of steps, while detailed balance means that for any couple of configuration $\mathcal{C}$ and $\mathcal{C}'$ the following relation has to hold

$$\mathcal{S}[\mathcal{C}'|\mathcal{C}] \, P_\infty(\mathcal{C}) = \mathcal{S}[\mathcal{C}|\mathcal{C}'] \, P_\infty(\mathcal{C}') \; , \tag{4.46}$$

where P_∞ is the probability distribution we want to sample through the Markov chain.

A simple algorithm to generate configurations so to satisfy detailed balance was introduced by Metropolis[120]. The idea is to start from a given initial configuration $\mathcal{C}$ and to propose to visit a new configuration $\mathcal{C}'$ with a certain transition probability $T(\mathcal{C}'|\mathcal{C})$. Then this new configuration is accepted or rejected according to the probability $A(\mathcal{C}'|\mathcal{C})$ so that the full

conditional probability to move toward $\mathcal{C}'$ starting from $\mathcal{C}$ is given by

$$\mathcal{S}\left[\mathcal{C}'|\,\mathcal{C}\right] = T\left(\mathcal{C}'|\,\mathcal{C}\right)\; A\left(\mathcal{C}'|\,\mathcal{C}\right)\;. \tag{4.47}$$

The Metropolis choice for the acceptance probability $\mathcal{A}\left(\mathcal{C}'|\mathcal{C}\right)$ reads

$$\mathcal{A}\left(\mathcal{C}'|\mathcal{C}\right) = min\left\{1, \frac{P_\infty\left(\mathcal{C}'\right)\, T\left(\mathcal{C}|\mathcal{C}'\right)}{P_\infty\left(\mathcal{C}\right)\, T\left(\mathcal{C}'|\mathcal{C}\right)}\right\}\;. \tag{4.48}$$

It is easy to show that such a choice satisfies the detailed balance condition in Eq. (4.46). While this algorithm is completely standard and model independent, two main issues have to be taken into account with reference to the problem at hand, since they can strongly affect the performance or even the reliability of the Monte Carlo simulations.

The first one concerns the choice of the transition probability $T\left(\mathcal{C}'|\,\mathcal{C}\right)$. In the case of interest, we implement two main classes of local moves, in which the number of kinks in a given channel a is changed by unity, $\Delta k_a = \pm 1$. These moves amount to add or remove one creation and one annihilation fermionic operator in the a channel at randomly chosen times along the contour and are required for the ergodicity of the matrix $\mathcal{S}$. Indeed it is evident that, using these two basic updates any configuration can be reached, in principle, after a finite number of steps[1]. Therefore using these two classes of moves and the Metropolis acceptance Eq. (4.48) we can guarantee that the sampling process visits configurations according to probability $P_\infty\left(\mathcal{C}\right)$. A second issue, which is different from the ergodicity one, concerns the efficiency and the speed-up of the Monte Carlo sampling (for example the number of steps which one has to wait before reaching the desired probability distribution). For this purpose, additional kind of updates may enhance the sampling procedure. In the present algorithm, following standard practice in diagMC, we also implement moves that connect configurations at fixed number of kinks ($\Delta k_a = 0$) such as for example shifting an annihilation operator. We also note that other kind of moves, in which more than two operators are added/removed/shifted, may become relevant when dealing with off-diagonal baths. Similarly global moves, in which a whole set of operators is changed, has proven to be fundamental in the case of multiorbital models[144]. We note that, as it happens for the imaginary time algorithm[187], a major issue in the implementation of these Monte Carlo

[1] One can imagine, given a configuration $\mathcal{C}$ with $2k$ kinks, to remove all kinks and then add $2k$ new kinks at different times to obtain a new configuration $\mathcal{C}'$. Whether such a series of updates is likely to occur during typical simulation time is a different matter. Additional updates may be useful to speed-up the process. This point is enlightened in [77].

moves is to properly take into account the structure of the impurity hilbert space to avoid, when it is possible, moves toward configurations which have zero weight. In the case of impurity models without exchange or hopping terms, these zero-weight configurations can be immediately read out since, for each channel a, creation and annihilation operators have to occur in alternated order along the contour, to have a finite local trace in Eq. (4.37). This leads to a very convenient segment picture[187].

A further point which requires some comment concerns the evaluation of the acceptance ratio in Eq. (4.48). As can be seen from the expression of the weight $W(C)$ in Eq. (4.37), this amounts to evaluate the ratio of two determinants as well as the ratio between two local traces. While for the former fast update routines are available, which makes this operation rather efficient, dealing with the ratio among local traces is the most time-consuming part of the algorithm, at least in the general case of a multi-orbital quantum impurity model. In such a case, indeed, one have to evaluate from scratch the whole chain of fermionic operators. Several tricks have been proposed to implement this evaluation[86] in an efficient way and we have used most of them in our algorithm. In particular, we write the fermionic operators entering in Eq. (4.38) in the basis of local eigenstates and store the whole chain of matrix products from left to right (and viceversa), so that the evaluation of trial moves is reduced to few matrix multiplications.

4.4 Performance of the diagMC algorithm

To test the algorithm, in this section we study the non-equilibrium dynamics in the Anderson Impurity Model[8] after a local quantum quench. This model, which serves as a fundamental paradigm for strong correlation physics, describes a single interacting fermionic orbital coupled to a an equilibrium bath of free conduction electrons. The local Hamiltonian before and after the quench reads

$$\mathcal{H}^{\pm}_{loc}\left[c^{\dagger}_{\sigma}, c_{\sigma}\right] = \frac{U_{\pm}}{2}\left(n-1\right)^{2} + \varepsilon_{d\pm}\, n \qquad n = \sum_{\sigma} c^{\dagger}_{\sigma} c_{\sigma}\,. \tag{4.49}$$

The conduction electrons are assumed to be non interacting, hence the coupling to the impurity occurs via an energy-dependent hybridization function $\Gamma(\varepsilon)$, which is defined in terms of the conduction density of states (DoS) $\rho(\varepsilon)$ as

$$\Gamma(\varepsilon) = \pi \sum_{\mathbf{k}} |V_{\mathbf{k}}|^{2}\, \delta(\varepsilon - \varepsilon_{\mathbf{k}}) = \pi\, V^{2}\, \rho(\varepsilon)\ , \tag{4.50}$$

where we have assumed for simplicity $V_{\mathbf{k}}$ independent of momentum. As a model for the DoS we start considering a flat band of width $2W$

$$\rho(\varepsilon) = \rho_0 \, \theta(W - |\varepsilon|) \, , \tag{4.51}$$

which encodes the main physics of a metallic conduction bath, namely a finite weight at the Fermi level ($\rho_0 = 1/2W$ at $\varepsilon = 0$) and a finite bandwidth. In this case the basic energy scale describing the coupling between the impurity and the bath is the hybridization strength $\Gamma = \pi V^2 \rho_0$. In all calculations we take Γ as our unit of energy and choose $W = 10\Gamma$.

This section is structured as follows. We first discuss some aspect of the algorithm (statistics of kinks and average sign) in the specific case of the Anderson Impurity Model and then present the results for its charge and spin real-time dynamics after a local quantum quench.

In order to analyze the performances of the diagMC algorithm on the Kadanoff-Baym-Keldysh contour we will consider two main quantities, namely the probability distribution of perturbative orders in the diagrammatic expansion and the average sign of the Monte Carlo weight, both being sensitive measures to establish the efficiency of the method. In the specific case of the single impurity Anderson Model, with reference to the notation introduced in section 4.2, we have only $\mathcal{N} = 2$ channels, corresponding to spin $\sigma = \uparrow, \downarrow$.

Statistics of Kinks

As we have shown in section 4.3, diagMC amounts to stochastically sample the expansion for $\mathcal{Z}(t)$ in powers of the hybridization, by performing a random walk in the space of diagrams. It is therefore quite natural to monitor during the simulation the statistics of different perturbative orders (number of kinks), namely the probability to visit a Monte Carlo configuration $\mathcal{C}$ featuring k creation vertices (and $\tilde{k}$ annihilation vertices) in the spin sector σ. We define this quantity as

$$P_\sigma(k) = \frac{\sum_{\mathcal{C}} |W(\mathcal{C})| \, \delta(k(\mathcal{C}_\sigma) - k)}{\sum_{\mathcal{C}} |W(\mathcal{C})|} \, , \tag{4.52}$$

where the Monte Carlo weight $W(\mathcal{C})$ has been defined in Eq. (4.37). The behavior of this probability distribution is plotted, as an example, in the left panel of figure 4.4 for increasing values of the measuring time $t_\star$ starting from $t_\star = 0$, which corresponds to the equilibrium initial preparation. We note that all histograms are strongly peaked around an average value $\bar{k}$, larger perturbative orders $k > \bar{k}$ appearing with an exponentially small probability. Notice that whenever this would not be the case, namely if arbitrarily large

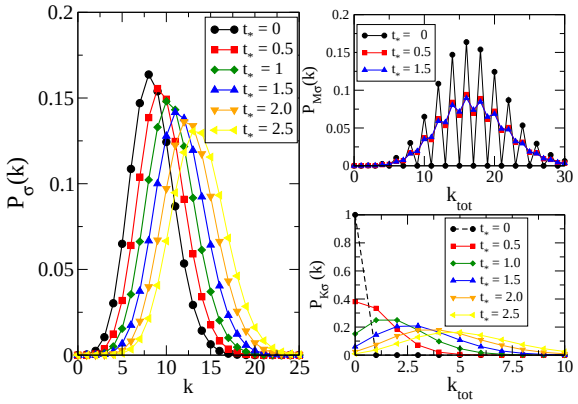

Figure 4.4: Probability distribution of different perturbative orders k sampled during the simulation. Data refers to a local quench in the Anderson Impurity Model, starting from $U_- = 0$ to $U_+ = 10\Gamma$ at particle-hole symmetry, for $T = 0.1\Gamma$ and $W = 10\Gamma$. Left panel shows the statistics ok kinks along the whole contour, while the top and bottom right panels display the histograms for the Matsubara and Keldysh sector, respectively.

perturbative orders ($k \gg \bar{k}$) would give a finite contribution to the result, a diagMC algorithm to work would need an explicit cut-off k_{max} on the perturbative order and the result would then require an extrapolation[2] to $k_{max} \to \infty$. However for quantum impurity models, at least for the weak and strong coupling algorithms[159, 187, 86], this is not the case. Figure 4.4 confirms that all orders are included and contribute, with their own weight, to the final result. This fact ensures that the outcome of our diagMC calculation is an unbiased result which do not correspond to any truncation at finite-order of the perturbative expansion but rather represents a numerical resummation of a formal expansion. From figure 4.4 we note that upon increasing $t_\star$ the whole histogram shifts toward larger values of k since kinks start to be added on the two Keldysh branches. It is therefore interesting to *resolve* this increased perturbative order in the two sectors of the simulation, namely the Matsubara and the Keldysh one. To this extent, we plot in the right panel of the same figure the probability distribution of having k_{tot} kinks

[2]This is what happens, for example, in diagMC simulation of lattice models with the bold-line trick[145], where the fermionic sign problem is so severe that a simulation with arbitrary (unbounded) self-consistent perturbative orders turns to be unstable and an explicit cut-off is needed.

with spin σ on the Matsubara axis, $P_{M\sigma}(k)$ (top right panel), or k_{tot} kinks with spin σ on the Keldysh branches, $P_{K\sigma}(k)$ (bottom right panel), where k_{tot} means that we are considering both creation and annihilation vertex. At $t_\star = 0$, the initial state, the Keldysh branches are empty while the Matsubara sector is filled with an even number of kinks (to ensure particle conservation). Upon increasing $t_\star > 0$, the system starts evolving in real-time and we note a transfer of weight in the Keldysh sector toward finite values of k. At the same time the Matsubara probability distribution does not change its center of gravity and rapidly converges to a final distribution, now allowing also for an odd number of kinks (the total particle conservation is ensured by kinks in the Keldysh sector). The scaling of the average number of kinks $\bar{k}$ with measuring time $t_\star$, temperature and other physical parameters is also relevant and instructive. In the equilibrium case (corresponding here to $t_\star = 0$), $\bar{k}$ has been shown in Ref. [86] to be proportional to inverse temperature β with a prefactor given by the average hybridization energy per spin,

$$\bar{k}_\sigma = -\beta \langle \mathcal{H}^\sigma_{hyb} \rangle. \tag{4.53}$$

Since $\langle \mathcal{H}_{hyb} \rangle$ decreases upon increasing the correlation strength U the diagMC method in imaginary time works extremely well in the regime $U \gg \Gamma$ being able to reach very low temperatures compared to the energy scales in the problem. Unfortunately, the very convenient scaling of Eq. (4.53) does not hold anymore for the real-time dynamics, as was also noted in previous works[191]. In figure 4.5 (left panel) we plot $\bar{k}$ as a function of time $t_\star$ for different initial preparations $U_- = 0, 5, 10$. We note an almost perfect linear scaling with time, as expected, while the effect of starting from a correlated initial state $U_- \neq 0$ generally helps since it decrease the value of $\bar{k}$ at $t = 0$. Nonetheless, a finite Coulomb interaction in the final state, $U_+ \neq 0$, has no effect on the average number of kinks sampled, as shown by the dashed line in left panel which exactly lies on top of the $U_+ = 0$ results.

Summarizing, we conclude that the scaling of the average number of diagrams for the real-time algorithm generally reads

$$\bar{k}_\sigma = \alpha\, t + \bar{k}^{eq}_\sigma\,, \tag{4.54}$$

α being a constant independent on U. It is therefore natural to ask what is the energy scale controlling this prefactor. As we show in the right panel of Figure 4.5, α strongly increases with the conduction bandwidth W (and presumably also on the hybridization strength). As a consequence of Eq. (4.54), accessing large time scales in the regime $W \gg \Gamma$ becomes increasingly difficult with this approach. This is due to the fact that both the computational

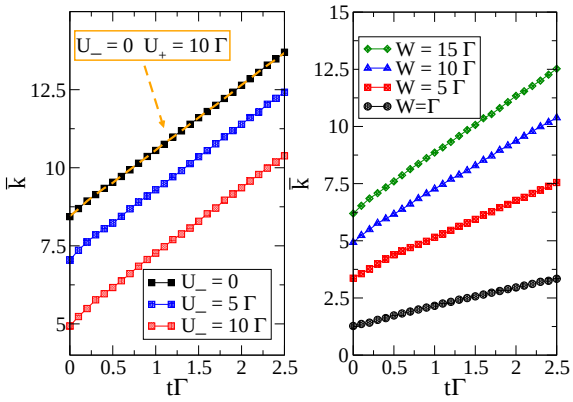

Figure 4.5: Scaling of the average number of kinks with maximum time $t_\star$. Left panel shows data at fixed $U_+ = 0$, tuning the strength of the Coulomb repulsion $U_- = 0, 5, 10$. See the perfect linear scaling with the same slope $\alpha = d\bar{k}/dt$. Right panel displays data at fixed $U_- = 10$, $U_+ = 0$ tuning the strength of the conduction bandwidth W. We see how the slope α increases with bandwidth making increasingly difficult to access large time scales in the regime $W \gg \Gamma$.

cost of the algorithm and, in particular, the average sign of the MC weights strongly depend on the average number of kinks $\bar{k}$, exponentially the former and power-law the latter.

Average Sign

Another important quantity to monitor during the simulation is the average sign of the MonteCarlo configurations, which is tightly related to the accuracy we can get on physical quantities at fixed CPU time. Indeed a vanishing average sign turns into very large error bars on MonteCarlo averages that makes the simulation unstable. In the specific case of the hybridization expansion diagMC, it is known that, for what concerns the equilibrium (imaginary-time) algorithm, the single impurity Anderson Model has always positive signs and that even multi-orbital impurity models with rotationally-invariant interaction can be efficiently simulated up to moderate low temperatures. This situation drastically change when dealing with real-time dynamics since even the simple non-interacting resonant level model faces a severe sign problem at large enough times scales. This seems to be due to

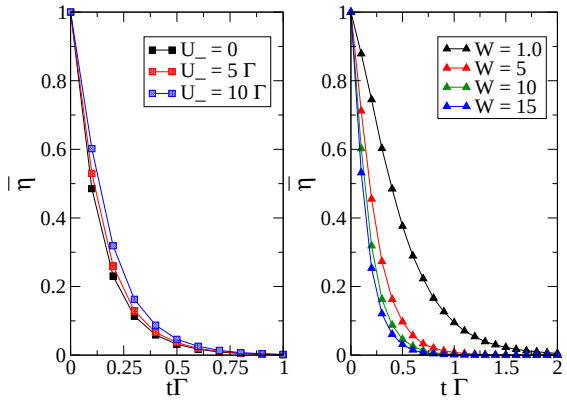

Figure 4.6: Average Sign as a function of time t for different initial preparations. We clearly see an exponential decay on a vey short-time scale. Left panel shows data obtained fixing the final value of the interaction $U_+ = 0$ and tuning the initial value $U_=0, 5, 10$. We see a slight increase of the average sign. Right panel shows the dependence of $\bar{\eta}$ from the bandwidth of conduction electrons and suggest that much longer time scales can be reached in the regime $W \sim \Gamma$.

the intrinsic nature of unitary quantum evolution and clearly appears from the definition we gave of the dynamical partition function $\mathcal{Z}(t)$ in section 4.2. Indeed exact cancellations are built in the whole formalism to ensure unitarity.

In the real-time diagMC one should in general talk about average phase, since as we mentioned the Monte Carlo weights are complex numbers. Nevertheless this quantity, which is defined as

$$\bar{\eta}(t) = \frac{\sum_{\mathcal{C}} |W(\mathcal{C})| \, \eta(\mathcal{C})}{\sum_{\mathcal{C}} |W(\mathcal{C})|} . \tag{4.55}$$

turns to be directly related to the probability of visiting configurations in the Matsubara sector, namely to the probability of having no kinks on the real-time branches. As a consequence of this result, which comes directly from unitarity, we conclude the the average phase is indeed a purely real number even for $t > 0$ and therefore, without further misunderstanding, we refer to it as the average Monte Carlo sign. As we show in figure 4.6, $\bar{\eta}(t)$ depends exponentially on the measuring time $t_\star$, namely on the length of the Keldysh contour. In the left panel, we plot the average sign for different

values of the Coulomb repulsion U_- in the initial density matrix. We see that $\bar{\eta}(t)$ uniformly increases with U_-, namely starting from a correlated initial state may result into a larger average sign even if the effect is rather small. In the left panel we study how the sign depends on the bandwidth W of conduction electrons. We see that moving from $W = \Gamma$ to $W = 15\Gamma$ there is a sizeable increasing of the average sign, which means that larger time scales can be reached with present algorithm in the regime $W \simeq \Gamma$. While this is not of direct relevance for quantum impurities, it can be very interesting for Non Equilibrium DMFT, where the conduction bandwidth is of the same order as the coupling between the impurity and the bath itself.

In the next chapter we describe two relevant applications of the present method. First we will investigate the non equilibrium dynamics of single impurity Anderson Model after a local quantum quench. Then we will move the attention to the problem of non equilibrium transport and study the effect of local vibrations on the differential conductance within a simple model of molecular conductor.

4.5 Conclusions

In this chapter we have introduced a novel numerical approach to describe non equilibrium real-time dynamics in correlated quantum impurity models. The method is based on the hybridization expansion of the evolution operator on the full Kadanoff-Baym-Keldysh contour and on a stochastic sampling of the resulting perturbation theory within Diagrammatic Monte Carlo.

The resulting algorithm represents a completely general and numerically exact approach to real-time dynamics in quantum impurity models, which interpolates between the standard equilibrium diagMC[187] defined on the Matsubara imaginary-time axis and its recent non equilibrium extensions[162, 127, 191] that works on the Keldysh contour and requires a special choice of the initial condition for the dynamics. Merging together these two approaches, we are able to deal with the most generic setup, namely a strongly correlated quantum impurity model initially in thermal equilibrium, which is driven out of equilibrium by some external time dependent perturbation. As a consequence, several kind of initial preparations as well as driving protocols can be considered with our approach that allow studying a wide class of non equilibrium problems.

More interestingly, we notice that no constraints are required on the nature of the fermionic *bath*, which enters in our approach as an input, encoded in the contour-ordered hybridization function $i\Delta_C(t, t')$. This allows us to deal with the intriguing problem of studying the real-time dynamics of the

quantum impurity coupled to a non equilibrium bath and opens the way to applying our method to solve Non Equilibrium Dynamical Mean Field Theory. In this perspective the effective action formulation of the algorithm we have presented at the end of section 4.2 represents the most natural one. The natural extension of this research is to study relaxation dynamics in correlated macroscopic quantum systems using Non Equilibrium Dynamical Mean Field Theory.

Chapter 5

Local Quenches and Non-Linear Transport

In this chapter we discuss two relevant applications of the Real-Time Diagrammatic Monte Carlo approach we have introduced in the previous chapter. Firstly we focus on local quenches in the Anderson Impurity Model addressing in particular the role of the low-energy properties of the fermionic bath. Then we consider the problem of non equilibrium transport in a simple toy model of molecular conductor.

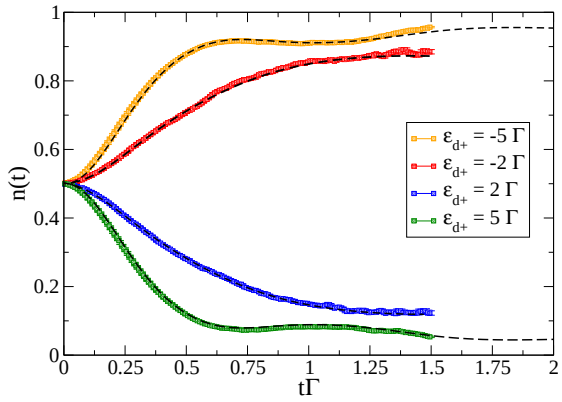

Figure 5.1: Quench dynamics in a Resonant Level Model after a sudden change of the energy level from $\varepsilon_{d-} = 0$ to $\varepsilon_{d+} \neq 0$. Dashed lines is the exact solution for $n(t)$ as obtained by a standard methods. Points are diagMC results obtained at $T = 0.1\Gamma$. We also add the dynamics for the trivial case $\varepsilon_{d+} = \varepsilon_{d-} = 0$ to show that unitarity is actually preserved by diagMC.

5.1 Charge and Spin Dynamics in the Anderson Model after a local quantum quench

We start by considering the non interacting case, the so called resonant level model with $U_- = U_+ = 0$, which allows for an exact solution and can be therefore used to benchmark the algorithm. We consider for this simple resonant level model a quench of the energy level ε_d that we tune from the on-resonance value $\varepsilon_- = 0$ to the off-resonance one $\varepsilon_+ \neq 0$. We note that this kind of quench can be realized in optical absorption experiments with quantum dots, as recently proposed in Ref. [181]. In Figure 5.1 we plot the real-time dynamics of the impurity density $n(t)$ for two different quenches, respectively above and below the on-resonance value $\varepsilon_d = 0$, and compare the result of diagMC (datapoints) with the exact dynamics which can be obtained using standard methods [115]. The excellent agreement with exact results confirms the reliability of our numerical approach.

We then move to the interacting case, namely consider a local quantum quench in the Anderson Model with local Hamiltonian (4.49). In Figure 5.2 we show the dynamics of the double occupation $D(t) = \langle n_\uparrow(t)\, n_\downarrow(t)\rangle$ after a sudden quench of the local interaction strength U. Two different cases

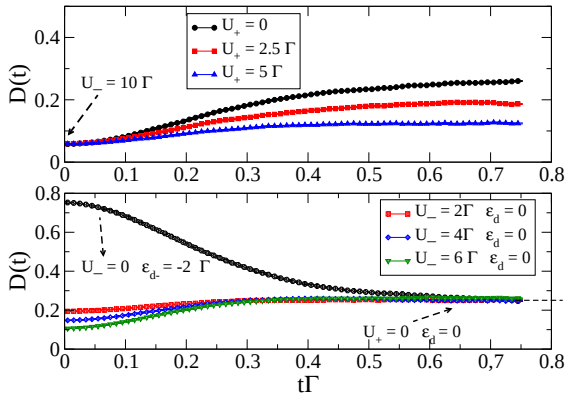

Figure 5.2: Non Equilibrium Dynamics of double occupancy $D(t)$ in the Anderson Impurity Model after a local quantum quench of the interaction strength at $T = 0.1\Gamma$ and particle-hole symmetry. In the upper panel we start from an initial state with $U_- = 10\Gamma$ and a very low double occupation and quench to different values of $U_+/\Gamma = 0, 2.5, 5$ from top to bottom. In the lower panel the opposite protocol is considered, namely we start from different values of $U_-/\Gamma = 2, 4, 6$ from top to bottom and quench to the same final U_+=0. In both cases we see that after a rather short transient the system relaxes to a new equilibrium state.

are considered. In the upper panel of Figure 5.2, we start from the same initial preparation, $U_- = 10\Gamma$, and quench to different final values of the interaction $U_+/\Gamma = 0, 2.5, 5$ (from top to bottom). In the lower panel of the same figure, we start from different initial preparations $U_-/\Gamma = 2, 4, 6$ (from top to bottom) and quench to the same final state $U_+ = 0$.

The dynamics at short times, soon after the quench, is controlled by the initial density matrix as expected on general grounds. After a short time scale, $t_{short} \sim 0.1/\Gamma$, the system starts feeling the quench and in fact the curves in the upper/lower panel start to deviate from/approach to each other. The time scale controlling the approach to the steady state is set mainly by $1/\Gamma$ - without coupling to the bath no dynamics for the charge would arise at all. However the final value of the interaction also affects the dynamics, as one can see from data in the top panel of figure 5.2. We also compare these findings with the non-interacting case, where the quench is performed on the energy level which is suddenly placed out of resonance

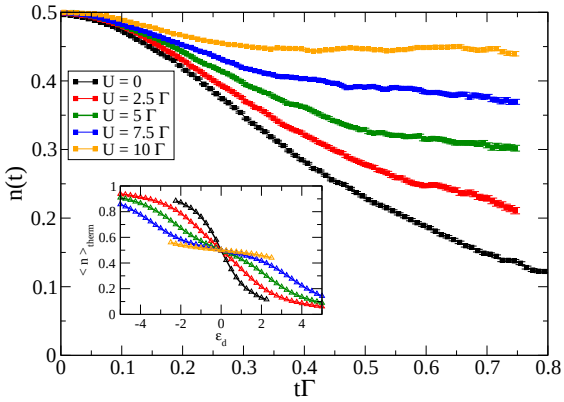

Figure 5.3: Non equilibrium dynamics of the impurity density after a quench of the energy level from $\varepsilon_{d-} = 0$ to $\varepsilon_{d+} = 2.5\Gamma$. We compare the dynamics for different values of the Coulomb repulsion $U = 0, 2.5, 5, 7.5, 10$ from bottom to top, revealing a much faster thermalization in the correlated case due to Coulomb blockade. Inset: thermal value of the impurity density as a function of the level position for $U = 0, 2.5, 5, 7.5, 10$ from top to bottom. For $U \gg \Gamma$ the curve is almost flat around $\varepsilon_d = 0$ hence departure from equilibrium is suppressed after a short transient.

(see lower panel black curve). In this situation the dynamics appears much slower than the previous cases, at least a factor of two. In Figure 5.3 the problem of quenching the impurity energy level is considered for different values of the Coulomb repulsion U, starting from a level which is initially half-filled. As compared to the non interacting $U = 0$ case, the effect of interaction is to make the whole relaxation dynamics much faster and the steady state value closer to the starting one, resulting in some sense into a less pronounced deviation from equilibrium. This can be rationalized by considering how the density depends, in equilibrium, on the energy level (see inset): upon increasing the interaction the curve $n(\varepsilon_d)$ becomes flat around $\varepsilon_d = 0$, a signature of Coulomb blockade phenomenon. As a consequence, any perturbation which moves the impurity occupation out of integer filling is quickly suppressed on a short-time scale. The overall picture confirms what also found in a similar investigation with the time-dependent NRG in [5], namely that charge dynamics is sensitive to high-energy scales, thus resulting into a generally fast relaxation. As opposite to the charge sector,

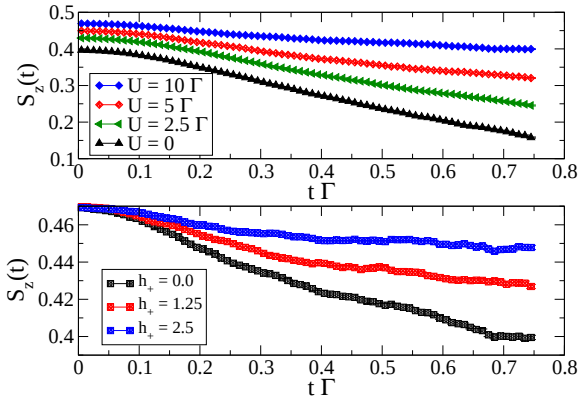

Figure 5.4: Spin Dynamics in the Anderson Model after a sudden quench of a local magnetic field. We start from a partially polarized impurity, with $h_- = 5.0$, $T = 0.1\Gamma$ and different values of local interaction U (top panel). At time $t > 0$ the magnetic field is switched off and the magnetization is allowed to relax toward an unpolarized steady state. We see that upon increasing the interaction U the dynamics slows down. Due to fine-time resolution we cannot follow the decay of the spin toward zero magnetization. However a large magnetic field in the final state gives rise to a rather fast relaxation.

the dynamics of spin degree of freedom is sensitive to the low-energy physics of the model. To probe this dynamics in real-time we imagine to add a magnetic field h_- to the local Hamiltonian, which partially polarizes the impurity, and suddenly switch it off for $t > 0$. The local Hamiltonian Eq. (4.49) now reads

$$\mathcal{H}^{\pm}_{loc}(h_{\pm}) = \mathcal{H}^{\pm}_{loc}(h_{\pm} = 0) - \frac{h_{\pm}}{2}\sum_{\sigma}\sigma n_{\sigma} \tag{5.1}$$

In Figure 5.4 we plot the spin dynamics $\langle S_z(t)\rangle$ starting from $h_- = 5\Gamma$ and switching it off, $h_+ = 0$, for different values of the interaction U. Since the final state in the absence of Zeeman splitting is fully simmetric, we expect to recover, for large enough times, a relaxation to an unpolarized state with $\langle S_z\rangle = 0$. We see that this relaxation is very slow and controlled by a time scale which *increases* with U (see top panel), as opposite to what found in previous cases, when the dynamics of charge degrees of freedom was probed by quenching the interaction or the level position. Indeed, the spin dynamics in the strong coupling regime is controlled by the lowest energy

scale in the problem, namely the Kondo temperature, as explicitly shown in [5]. Accessing such a long time scale seems so far unfeasable within the present approach, since diagMC simulations become increasingly unaccurate at large times due to sign problem, as we will discuss in the next section. As shown in the bottom panel of Figure 5.4, the effect of a large magnetic field in the final state is to destroy Kondo effect, thus resulting again into a fast relaxation toward a new steady state. An interesting direction for future investigation is to study the spin dynamics in the Kondo regime under the effect of more general non equilibrium processes, other than a quantum quenches. In this respect the present approach can deal with explicitly time dependent phenomena, such as for example an oscillating magnetic field, without any truncation of the dynamics.

5.1.1 Non Equilibrium Dynamics for a quantum impurity in a gapped or pseudogapped fermionic reservoir

In all cases considered above, we observe at large times a convergence to a new equilibrium state which is the thermal one described by the final hamiltonian $\mathcal{H}_+$, namely

$$\langle O\left(t\to\infty\right)\rangle = \frac{\mathrm{Tr}\left[e^{-\beta\mathcal{H}_+}O\right]}{\mathrm{Tr}\left[e^{-\beta\mathcal{H}_+}\right]} \tag{5.2}$$

This is explicitly shown by the dashed line in figure 5.2, which represent the result of an equilibrium calculation done with imaginary time diagMC with the final Hamiltonian $\mathcal{H}_+$. We also note that no effective heating arises, namely the temperature entering in Eq. (5.2) is the same as in the initial condition (4.2). This is due to the fact that within diagMC the fermionic reservoir is treated as an infinite system. The onset of thermalization in a quantum impurity model is not surprising[26], and it is related to the fact that the conduction electrons play the role of a thermal bath[44], able to absorbe the energy pumped locally after quench, which is dissolved in the interior of the bulk. It is worth noting that this feature is not generic of any bath – meant as a macroscopic (infinite) system – but rather depends on its spectral properties. In the present case, as we are going to see, thermalization is related to the *gapless* nature of the metallic state, whose energy spectrum goes down to arbitrarily small energies. To further investigate this issue, we consider now the out-of-equilibrium dynamics of an Anderson impurity coupled to gapped and pseudo-gapped fermionic bath. Even though QI models traditionally deal with genuine metallic hosts, the problem of gapped (or pseudo-gapped) fermionic reservoirs has a vast literature[194, 73, 33, 130],

that received a large boost in recent years. Eminent examples of such a physical situation are provided by adatoms in graphene sheet or by nanostructures built up with superconducting materials.

The equilibrium phase diagram of an Anderson impurity embedded in a non-metallic host it is by now rather well established[73, 32, 23]. As opposite, the non equilibrium real-time dynamics in this class of quantum impurity models is much less explored. A detailed study of this issue is left for future investigations. Here we limit to elucidate the role played by the presence/absence of low energy bath spectral weight on the single impurity dynamics after a local quantum quench. It is worth to notice that this issue can be also relevant to study, within Non Equilibrium DMFT, the relaxation dynamics of interacting electrons after quantum quenches. Indeed DMFT amounts to solve a quantum impurity self-consistently, using the contour ordered impurity Green's function as a seed to generate the new fermionic out-of-equilibrum bath.

Gapped Fermionic Reservoir

We start our discussion considering the case of a true gapped fermionic bath. In other words we consider as a model for the conduction electrons DoS the following

$$\rho_g(\varepsilon) = \begin{cases} 0 & 0 < |\varepsilon| < E_g \\ \rho_0 & E_g < |\varepsilon| < E_g + W \end{cases} , \tag{5.3}$$

where $2E_g$ is the band gap at the Fermi Level. This density of states results into an energy dependent hybridization function $\Gamma(\varepsilon)$ that we define as in Eq. (4.50), namely $\Gamma(\varepsilon) = \pi V^2 \rho(\varepsilon)$. A plot of this function for different values of E_g is given in figure 5.5. We note that in the following we will adopt as unit of energy the hybridization width $\Gamma = \pi V^2/2W$, the same as in the metallic case.

The equilibrium properties of an Anderson Impurity coupled to a gapped reservoir have been studied with NRG in [32] and more recently with a perturbative approach in [62]. The model at particle-hole (PH) symmetry flows at low temperature to the local moment fixed point where the impurity is asymptotically decoupled from the bath. Out of PH the model displays a transition between local moment fixed point and strong coupling fixed point depending on wheter the gap E_g is larger or smaller than the Kondo temperature. Here we consider for simplicity the PH symmetric point which correspond to setting $\varepsilon_{d-} = \varepsilon_{d+} = 0$ in the local hamiltonian Eq. (4.49) and discuss the real-time dynamics for the double occupancy $D(t) = \langle n_\uparrow(t)\, n_\downarrow(t) \rangle$

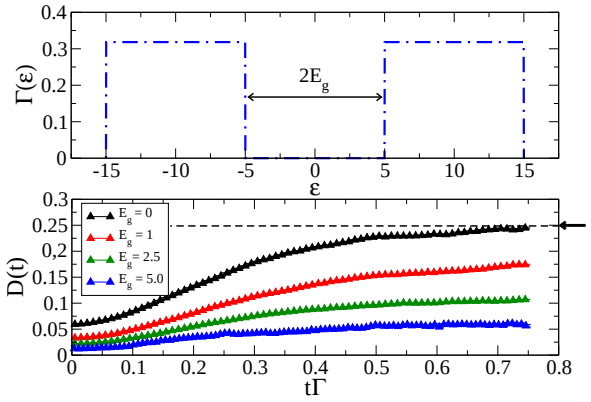

Figure 5.5: Non equilibrium dynamics for an Anderson Impurity coupled to a *gapped* fermionic reservoir. We plot the real-time dynamics for double occupancy at the impurity site after a quench of the interaction from $U_- = 10\Gamma$ to $U_+ = 0$, at particle-hole symmetry $\varepsilon_{d+} = \varepsilon_{d-} = 0$ and for $T = 0.1\Gamma$. Different values of the gap in the bath $E_g = 0, 1, 2.5, 5.0$ are considered, resulting into very different dynamics. Contrarily to the gapless case ($E_g = 0$, black points) which quickly approaches the thermal plateau fixed by PH symmetry and indicated by an arrow, $D_{therm} = 1/4$, we see that due to the finite gap in the spectrum the real-time dynamics slows down thus preventing us to conclude on the long time behaviour of $D(t)$. However, for very large values of E_g (see $E_g = 5\Gamma$) the dynamics seems actually to reach a steady state where the double occupation is different from D_{therm}.

on the impurity site after a sudden change of the local Coulomb interaction.

In figure 5.5 we show the double occupancy dynamics after a quench from $U_- = 10\Gamma$ to $U_+ = 0$ for different values of E_g at $T = 0.1\Gamma$. Due to PH symmetry the thermal value of D computed on the final hamiltonian $\mathcal{H}_+$ has to be equal to $D_{therm} = 1/4$ for $U_+ = 0$. Indeed, we see that in the metallic case ($E_g = 0$) $D(t)$ approaches rather quickly the expected thermal plateau. At the same time opening a finite gap $E_g \neq 0$ in the bath reflects into a much slower dynamics which prevents us from a firm conclusion on the asymptotic behaviour of $D(t)$. We note, however, that for large values of E_g the dynamics seems actually to reach a stationary state which looks quite different from the expected one. Such a behaviour

could be interpreted in terms of the equilibrium properties of the gapped Anderson impurity model which, as we mentioned, at PH symmetry flows to the local moment regime with the impurity effectively decoupled from the bath. Given such an initial condition and taking into account the large value

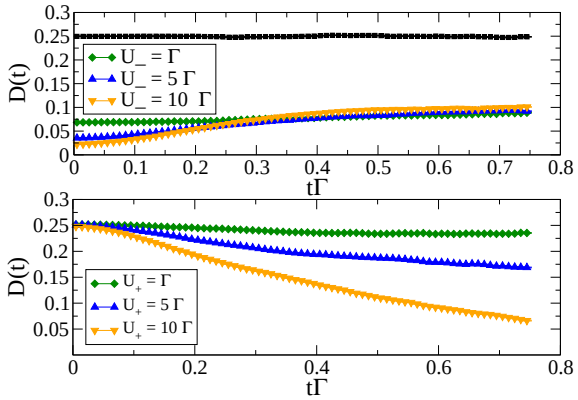

Figure 5.6: Non equilibrium dynamics for an Anderson Impurity coupled to a *gapped* fermionic reservoir. We set the gap in the spectrum equal to $E_g = 1.0$ and plot the real-time dynamics for the double occupancy after a quench of the interaction, at $T = 0.1\Gamma$ and PH symmetry. Two kind of processes are considered, namely a quench from $U_- = 0$ to $U_+ \neq 0$ and the reverse process from $U_- \neq 0$ to $U_+ = 0$, which differ among each other for the average work done during the quench, see Eq. (5.5) in the main text. Top panel shows data for $U_- = 10\Gamma$, $U_+ = 0$ and viceversa, while bottom panel data for $U_- = 2.5\Gamma$, $U_+ = 0$ and viceversa. We see that, provided the average work done is sufficiently larger than the gap $2E_g$, a fast thermalization can occurr also in a gapped model (see top panel, black points). As opposite, when the amount of energy pumped into the system is too small the dynamics slows down and we cannot conclude with present data wheter thermalization takes place or not.

of the gap, which strongly affects the bath properties, one can rationalize the slowing-down of the impurity dynamics. Indeed, in the limit of very large gaps $E_g \to \infty$, a free impurity would have no available mechanism to exchange energy and relax to the steady state described by $\mathcal{H}_+$. While this argument could be in principle satisfying to explain results plotted in figure 5.5, at least in the large gap regime, it does not take into account completely

the nature of a quantum quench process. To further investigate this point we now reverse the perspective, namely we fix the gap E_g in the spectrum and change the strength of the quench, namely we change the final value of the interaction U_+ while keeping fixed $U_- = 0$ as well as the level position so to ensure PH symmetry. This allows to study how the non equilibrium dynamics depends on the amount of *work done* during the quantum quench. As was recently suggested in[171] the statistics of the work is a key quantity to characterize a non equilibrium process such as a quantum quench. Its average value $\bar{W}$ gives a measure of the energy pumped into the system and turns to be given[171], in the case of an istantaneous quench, by

$$\bar{W} = \langle \mathcal{H}_- - \mathcal{H}_+ \rangle_- \,, \tag{5.4}$$

where the average $\langle \cdot \rangle_-$ is taken over the initial equilibrium density matrix $\rho_{eq} \propto e^{-\beta \mathcal{H}_-}$. In the case of a local quantum quench such as the one we are considering, the average work $\bar{W}$ is given by

$$\bar{W} = (U_- - U_+) \langle D \rangle_- \,. \tag{5.5}$$

We see therefore that the work $\bar{W}$ depends not only on the strength of the quench, namely the change in the interaction, but also on the initial condition. As we are going to see, this quantity greatly affects the resulting non equilibrium dynamics.

In figure 5.6 (top panel) we plot the dynamics of double occupancy $D(t)$ at PH symmetry after a quench of the local interaction. We set $T = 0.1\Gamma$ and choose a fixed value of the gap $E_g = \Gamma$. We compare two kind of processes: one starting from $U_- = 0$ to $U_+ \neq 0$ and the reverse one, which starts from $U_- \neq 0$ and quenches to $U_+ = 0$. Quite interestingly we see that, provided the average work $\bar{W}$ is *above* the threshold of the (semi)gap E_g, as for the process $U_- = 0 \to U_+ = 10\Gamma$ (black curve in top panel) for which $|\bar{W}| = 2.5\Gamma$, a rather fast thermalization can occurr also in the gapped model. Notice indeed that the expected thermal value for D, which is set by the dashed line in figure 5.6 (top panel) and which corresponds to the value of double occupation computed at equilibrium for $U_+ = 10\Gamma$, is approached on a rather short time scale. We compare these findings with the inverse quench process, starting from $U_- = 10\Gamma$ and quenching to $U_+ = 0$, which in force of Eq. (5.5) is characterized by a rather small average work $\bar{W} < E_g$. As we see in figure 5.6 the dynamics looks much slower in this case and we cannot conclude, on the basis of our data, wheter the thermal plateau at $D_{therm} = 1/4$ is actually approached or not at longer times. A similar comparative study is performed for quenches from $U_- = 0$ to $U_+ = 2.5\Gamma$ and viceversa and the results are plotted in bottom panel of figure 5.6.

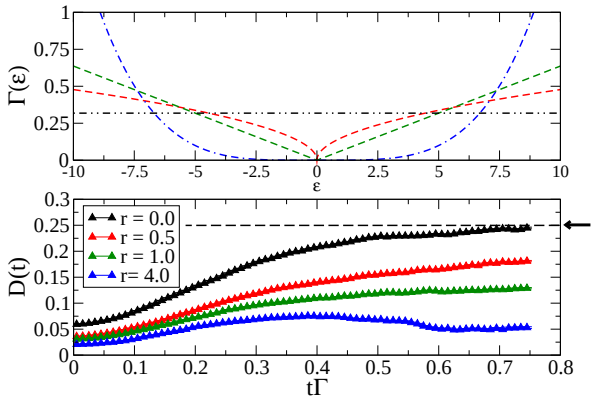

Figure 5.7: Non equilibrium dynamics for an Anderson Impurity coupled to a *pseudo-gapped* fermionic reservoir. We consider the model at PH symmetry and $T = 0.1\Gamma$. We fix the quench parameters, namely the initial and final value of the interaction, equal respectively to $U_- = 10$ and $U_+ = 0$, and tune the pseudo-gap exponent from $r = 0$ (gapless metallic state) to $r = 4$. The depletion of low energy states in the DoS reflects into a much slower dynamics which eventually, for large enough r, seems to prevent the system from reaching the value of $D_{therm} = 1/4$ which is fixed by PH symmetry and by the choice of $U_+ = 0$. However, due to finite time resolution we cannot conclude with present data wheter thermalization occurs or not on a longer time scale.

Pseudo-gapped Fermionic Reservoir

We now consider the dynamics of an Anderson impurity coupled to a pseudogap reservoir. We consider as DoS a pure power-law function, namely

$$\rho_{pg}(\varepsilon) = \begin{cases} \alpha|\varepsilon|^r & 0 < |\varepsilon| < W \\ 0 & |\varepsilon| > W \end{cases} , \tag{5.6}$$

where $\alpha = (r+1)/(2W^{r+1})$ ensures the proper normalization. This gives rise to a power-law hybridization function $\Gamma(\varepsilon)$, that we define in complete analogy with the previous cases see Eq. (4.50). Again, we choose as unit of energy the hybridization width $\Gamma = \pi V^2/2W$.

The equilibrium phase diagram of the pseudo-gap Anderson Impurity model is extremely rich, featuring at particle-hole (PH) symmetry and for $0 < r < 1/2$, a quantum phase transition at a critical value of the hybridiza-

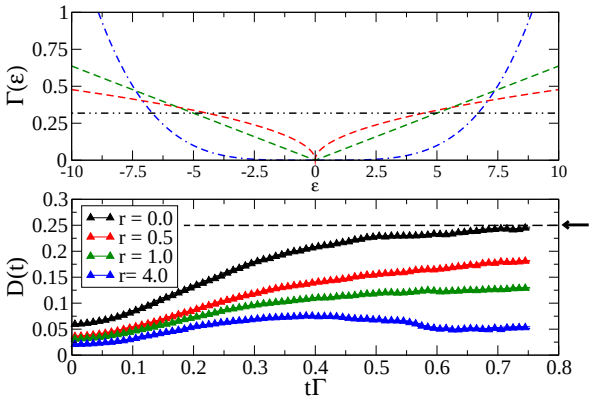

Figure 5.8: Non equilibrium dynamics for an Anderson Impurity coupled to a *pseudo-gapped* fermionic reservoir. We consider the PH simmetric point, at $T = 0.1\Gamma$ and for $r = 1$. We study how the dynamics changes while tuning the average work $\bar{W}$ done during the quench (see text). We fix the initial interaction $U_- = 0$ and perform a quench to $U_+ = 10\Gamma$ (top panel). We compare the results with the reverse process, from $U_- \neq 0$ to $U_+ = 0$. Despite the power-law DoS, the dynamics in the case of a large quantum quench (large average work) turns to be quite fast. On the contrary, in the low work regime (bottom panel) the dynamics is much slower and we cannot see wheter thermalization take place or not at longer time scales.

tion Γ_c between a strong coupling regime (for $\Gamma > \Gamma_c$) where Kondo screening occurs and a local moment one (for $\Gamma < \Gamma_c$) where the impurity becomes asymptotically free at low temperature. As opposite, at PH symmetry and for $r > 1/2$ the only stable fixed point is the local moment one and no Kondo effect can be stabilized for an Anderson Impurity in a gapless reservoir[73]. In the following we will focus for simplicity on this latter case ($r > 1/2$ at PH symmetry) so to avoid any complication related to the dynamics across criticality. We note that the topic of non equilibrium dynamics across quantum phase transitions is indeed an extremely intriguing problem [4], which may deserves furhter investigations in the future.

As we did for the gapped case, we consider as a starting point a quantum quench of the local Coulomb interaction between $U_- = 10\Gamma$ and $U_+ = 0$, at $T = 0.1\Gamma$ and for $\varepsilon_{d+} = \varepsilon_{d-} = 0$. In figure 5.7 we plot the dynamics of double occupancy as a function of time, while tuning the exponent r from

the metallic case $r = 0$ to the almost gapped one $r = 4$. As we can see the results we found look very similar to what already discussed in the case of a gapped reservoir. While for $r = 0$, namely for a finite hybridization at the Fermi level, the dynamics is pretty fast in approaching the thermal plateau (we are at PH simmetry and $U_+ = 0$, therefore again $D_{therm} = 1/4$), for $r \neq 0$ the dynamics slows down and for $r = 4$ seems actually to get stucked into a non thermal steady state. However from these data it is difficult to conclude wheter this is really the case or rather that thermalization emerges on a very long time scale.

We conclude this section by discussing how the dynamics in the pseudo-gapped case changes as a function of the work done during the quantum quench. To this extent we plot in figure 5.8 the double occupancy as a function of time, $D(t)$, for $T = 0.1\Gamma$ and at PH symmetry. As we have previously done, we fix the initial value of the interaction to $U_- = 0$ while tuning the final value U_+ (see top of panel) so to change the average work $\bar{W}$. At the same time, we study the dynamics for the reverse process where we fix the final value of the repulsion to $U_+ = 0$, while changing the initial condition U_-. As we have already found in the gapped case, the dynamics turns out to be very sensitive to the average work done, namely to the amount of energy pushed into the system. In particular we can see from figure 5.8 that quenches with sufficiently large work $\bar{W}$ can result into a rather fast dynamics and thermalization at long times. This seems to be the case, for example, of quenches from $U_- = 0$ to $U_+ = 10\Gamma$ (black points, top panel) where the thermal value of double occupation with $U_+ = 10\Gamma$ is set by the arrow at the bottom of the panel. In other cases, where the work done is not that large, the dynamics turns to be slow and we cannot conclude about the long time behaviour.

Discussion

To summarize, in this section we have discussed the non equilibrium quench dynamics of the Anderson Impurity model in a gapped or pseudo-gapped fermionic reservoir after a quantum quench of the local Coulomb interaction. For the sake of simplicity we have considered only the particle-hole simmetric case and we have chosen the parameters in such a way to be always in the local moment regime in equilibrium for both gapped and pseudo-gapped cases, so to avoid further complications due to local quantum criticality which may result into very low-energy/long-time scales controlling the dynamics.

An important issue we have tried to discuss concerns the onset of thermalization at long times. While this is expected to occurr for quantum

quenches in a conventional metallic reservoir, one may wonder wheter or not the lack of available states close to the Fermi energy could result into a lack of thermalization at long times. We have shown that the real-time dynamics is strongly affected, even on short-to-intermediate time scales, by the modified spectral function of the bath. In particular, the opening of a gap or pseudo-gap at the Fermi level results into a slower transient dynamics. While it is tempting to explain this fact by invoking the equilibrium properies of the model and the mentioned flow to the local moment fixed point, one have to take into account also the intrinsic out-of-equilibrium nature of the quantum quench process. In this perspective we have identified the work $\bar{W}$ done during the quench as a relevant physical quantity to describe the non equilibrium dynamics after the quench. In particular, for the gapped and pseudogapped models, we have shown that a rather fast thermalization can occur provided the work done $\bar{W}$ is sufficiently large (for example with respect to the (semi)gap E_g). As opposite for small quantum quenches characterized by a small amount of work done $\bar{W} \ll E_g$, the dynamics turns to be much slower and we cannot conclude, with present data, wheter thermalization occurs or not on a longer time scale, thus leaving the question open to further investigations.

5.2 Dc Transport Through a Molecular Conductor

We now move our attention to a different problem, namely the relevance of vibrational effects in non equilibrium quantum transport through a simple model of molecular conductor. As already noticed in chapter 4 the problem of finite bias steady state transport can be also addressed within DiagMC provided that a proper non equilibrium initial condition is chosen.

5.2.1 Current through a Resonant Level Model

To begin our analysis we benchmark the method on the biased spinless RLM. Its nonequilibrium real-time dynamics, despite being analytically solvable by standard methods, has proven to be very difficult to access within other numerical approaches [127, 186], expecially in at low-bias and low-temperature, where the correlations induced by the fermionic leads decay slower than exponential in time. To test the reliability of our method, we compute the occupation number $\langle n(t) \rangle$ at zero temperature as a function of time t and for different values of the level position ε_d, both in equilibrium, $eV = 0$, as well as out of equilibrium, $eV \neq 0$, and compare the exact results with diagMC data. In this simple case, we expect that a single energy scale,

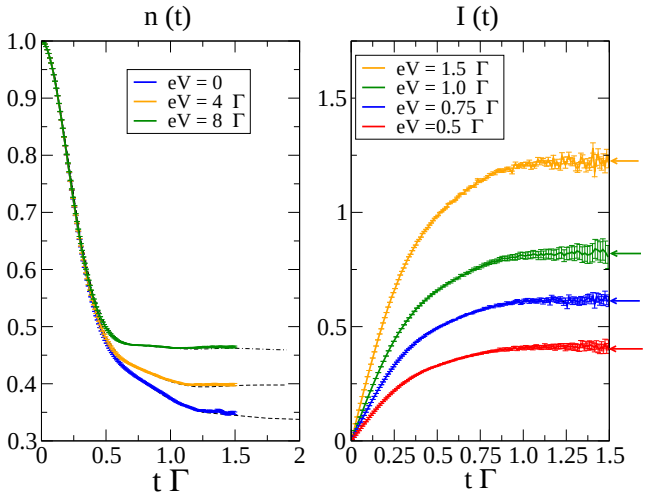

Figure 5.9: Zero-temperature real-time dynamics for different bias values eV of the dot population, $\langle n(t)\rangle$, from an initially occupied dot (left panel) and of the current, $\langle I(t)\rangle$ (right panel) of the resonant level model. DiagMC results (dots) are compared with the exact solution (full line). We take $\epsilon_d = \Gamma$ and consider a flat density of states in the leads with an half-bandwidth 10Γ. The increasing error bars for larger times is due to the limited simulation time.

namely the level broadening $\Gamma = \pi \sum_k |V_k|^2 \delta(\varepsilon_k)$, will control the approach to the steady-state. As can be seen in Fig. 5.9, the diagMC calculation perfectly matches the exact solution. We are able to resolve both the short-time transient after the initial configuration and the approach to steady state. A finite applied bias $eV \neq 0$ cuts off the Keldysh evolution operator (the steady state is reached earlier than at $eV = 0$), as pointed out by Ref. [123], thus making the expansion more convergent. Moreover, within the present approach we can easily measure the current flow through the impurity $I(t) = \frac{1}{2}\langle I_L(t) - I_R(t)\rangle$ on a fine real-time grid in a very efficient way. Results shown in Fig. 5.9 confirm that a true *non-equilibrium* steady state with a finite value of the current is reached at long times, due to the infinite size of the bath. Dissipation occurs entirely within the fermionic reservoir and we do not need to include any ficticious bosonic bath to reach a steady state [127]. A delicate issue to discuss when sampling real-time quantum dynamics is the so called sign problem, namely the exponential scaling of relative statistical errors in the Monte Carlo estimate of any observable in the infinite-size limit. In this respect, the main advantage of the Diagrammatic Monte Carlo method is that one pointed out in Ref. [145]: both the

thermodynamic limit as well as the zero temperature/zero bias limit can be safely taken with no numerical effort, while the computational demanding part is related to the long-time limit, because the average number of sampled diagrams scales roughly linearly in time. While for the simple RLM model we can reach the steady state running the code for a couple of days on a laptop, when an exponentially small energy scale in the tunneling controls the physics, as e.g. in the Kondo regime, *ad hoc* resummation [145] or more efficient sampling criteria must be used to improve accuracy.

5.2.2 Step-up Step-down Crossover

As a first nontrivial application we consider a simple model of a molecular conductor, namely a spinless fermionic level coupled to Holstein phonons. The local Hamiltonian is

$$\mathcal{H}_{loc}(n) = \frac{\omega_0}{2}(x^2 + p^2) + gx(n - \frac{1}{2}) + \varepsilon_d(n - \frac{1}{2}) \tag{5.7}$$

where g the electron-phonon coupling, ω_0 is the phonon frequency (x is the phonon displacement and p its conjugate momentum), ε_d is the energy of the level and n its occupancy. Our Keldysh diagMC can be naturally extendend to include local phonons [189], the only difference appearing in the trace over local degrees of freedom, now involving fermionic operators time-evolved according to the hamiltonian (5.7) for the electron-phonon subsystem. This trace can be evaluated analytically by observing that the local Hamiltonians with different level occupancy $n = 0, 1$ are related one to the other by a unitary transformation, $\mathcal{H}_{loc}(0) + \epsilon_d = U^\dagger \mathcal{H}_{loc}(1) U$, with $U = \exp(igp/\omega_0)$. It follows that the bosonic contribution to the local trace reduces to the following bosonic correlation-function

$$\mathcal{L}_k^{ph} = Tr\left(\rho_{ph}\, U^\dagger(t_k^e)\, U(t_k^s)\, U^\dagger(t_{k-1}^e) \ldots U(t_1^s)\right), \tag{5.8}$$

which can be easily evaluated analytically for most common initial phonon density matrices ρ_{ph}, which we assume the equlibrium distribution at zero temperature. In (5.8) $U(t)$ and $U^\dagger(t)$ are the unitary operators evolved with $\mathcal{H}_{loc}(1)$, and we have assumed the level initially occupied. The coupling to molecular vibrations is known to significantly affect inelastic electron tunneling. [61] When the bias hits a vibrational frequency, the differential conductance dI/dV changes sharply. Experimentally, it is observed that dI/dV increases in the tunneling regime, but decreases in the opposite case of a high transmission barrier. Although simple physical arguments can be invoked [95, 142] to explain this phenomenon, theoretical calculations have so

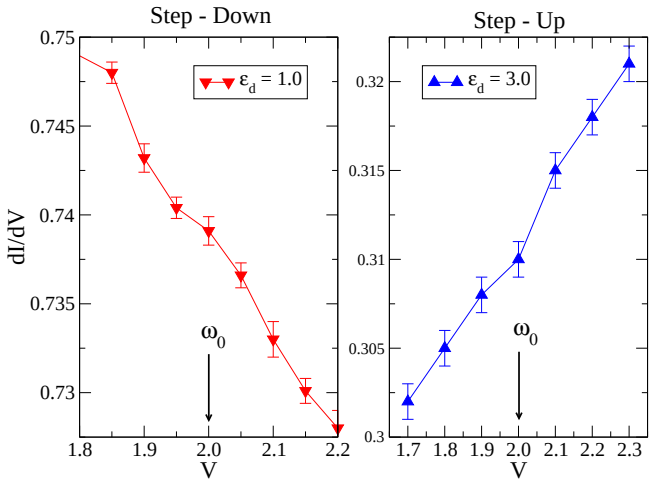

Figure 5.10: Zero-temperature differential conductance dI/dV (in unit of e^2/h) for bias values eV around $\omega_0 = 2.0\Gamma$. Electron-phonon coupling is $g = 0.5\omega_0$. We consider two different values of the fermionic level position ε_d in order to reproduce the crossover from reducted (step-down) to enhanced (step-up) conductance.

far been restricted to lowest orders in the electron-phonon coupling [140, 51]. In the simple resonant level model that we are considering, previous perturbative calculations predicted that dI/dV at bias $eV = \omega_0$ should decrease or increase if the zero-bias conductance $G > 0.5$ or $G < 0.5$, respectively, in units of the unitary value (in our spinless case e^2/h). Evidences for this was very recently reported by Tal and coworkers with H_2O molecules bridging a Pt break junction. Since the Keldysh diagMC is non perturbative in the electron-phonon coupling, it offers the possibility to verify this perturbative predictions. We model the two regimes of $G \gtrless 0.5$ by two different values of the level position $\varepsilon_d = 1$ and 3, the former closer to resonance than the latter, and compute directly the differential conductance dI/dV. As can be seen from Fig. 5.10, either step-down or step-up features do appear around the threshold for vibronic excitations, $eV \simeq \omega_0$, when the zero bias conductance is greater or lower than 0.5, respectively, in agreement with perturbative results [140, 51]. We also note that the step is not as abrupt as in perturbation theory, likely signaling a significant phonon damping.

5.3 Conclusions

In this chapter we have studied two applications of the Real-Time Diagrammatic Monte Carlo method to real-time dynamics in quantum impurity models. Two non equilibrium situations have been addressed corresponding respectively to a local quantum quench and to non equilibrium steady state transport.

As a first application of our algorithm we have studied the real-time in an Anderson Impurity Model after a local quantum quench. In the case of a metallic reservoir we have discussed time scales controlling charge and spin relaxation. While the former is a rather fast process mainly controlled by hybridization Γ, the latter turns to be a much slower process associated with the lowest energy scale in the problem, namely the Kondo temperature T_K. As we have shown in section 5.1 , the charge time scale can be reached within the present approach, while the decay of a polarized spin cannot, due to sign problem which makes calculations at very long times increasingly difficult. Finally we have addressed the non equilibrium dynamics of an Anderson Impurity coupled to a gapped or a pseudo-gapped reservoir. Even though we restrict our attention to the PH symmetry and to power-law exponents $r > 1/2$, for which the equilibrium phase diagram in both gapped and pseudo-gapped cases only features a local moment fixed point, the real-time dynamics for charge degrees of freedom turns out to be rather intriguing. In particular we distinguish two regimes depending on wheter the amount of work done during the quench, $\bar{W}$, is large or small with respect to typical energy scale in the DoS. In the former case we observe a rather fast dynamics which may give rise to thermalization, while in the latter case a much slower dynamics which prevent us from drawing definite conclusions on the long-time behaviour. The investigation of real-time dynamics in this class of quantum impurity models represents, in this perspective, a very intriguing and challenging open problem.

As a second application we have considered the problem of non linear transport in a simple toy model of molecular conductor where a single spinless fermionic level is coupled to an Holstein vibronic mode. To this extent we formulate the problem in a different non equilibrium set-up, where the tunnel coupling between the dot/molecule and the biased leads is suddenly switched on at time $t > 0$, see figure 4.1 (bottom panel). The dynamics is evaluated numerically using the real-time diagMC method on the two branches Keldysh contour.

We firstly consider the non interacting problem, with no coupling between electrons and phonons, which can be solved exactly using standard methods

and serves as a benchmark for the numerical algorithm. We confirm that the real-time diagMC can describe a true non equilibrium steady state with a finite currently flowing through the impurity. Dissipation takes place within the continuum of gapless fermionic reservoirs.

We then address the role of coupling the electrons tunneling into the dot to vibronic excitations, within a simple Holstein Model. As soon as the bias voltage becomes comparable to the typical energy scale of the vibrations, $eV \sim \omega_0$, a feature in the differential conductance dI/dV appears. Interestingly, while lowest order calculations predict a sharp threshold behaviour, we find signatures of phonon damping which act to broaden out the step, in fair agreement with recent experimental results [178]. These are effects due to vertex corrections which are difficult to include within Keldysh perturbation theory but that are naturally accounted for within our method, which is non perturbative in the electron-vibron coupling. We also find a crossover between step-up and step-down in the dI/dV curve, depending on the value of the zero-bias conductance which can be tuned by gate voltage.

Many other interesting issues concerning the role of vibrations in quantum transport can be addressed with the method we have presented in this chapter. Particularly intriguing is the role played by phonon distribution function during the transport process as well as the signatures of electron vibron coupling in the transient dynamics.

Part III

Quantum Quenches in Isolated Systems

Chapter 6

Variational Description of Correlated Electrons Out of Equilibrium

A simple and very flexible variational approach to the out-of-equilibrium quantum dynamics in strongly correlated electron systems is introduced through a time-dependent Gutzwiller wavefunction. As an application, we study the simple case of a sudden change of the interaction in the fermionic Hubbard model and find at the mean field level an extremely rich behaviour. In particular, a dynamical transition between small and large quantum quench regimes is found to occur at half-filling, in accordance with the analysis of Eckstein et al., Phys. Rev. Lett. **103**, *056403 (2009), obtained by dynamical mean field theory, that turns into a crossover at any finite doping.*

6.1 Introduction

Since the discovery of high-temperature superconductivity in copper based materials [128] up to the recent experimental realization of fermionic Mott Insulators in cold atomic gases loaded in optical lattices [96], strong electron-electron correlations keep playing a major role in condensed matter physics. This is certainly due to the large variety of striking novel phenomena that result from competing interactions among electronic degrees of freedom. During last decades the experimental and theoretical efforts have been focused on low temperature equilibrium properties, which typically probe ground state or low-lying excited states correlations, mapping out complex phase diagrams as a function of external control parameters. The exciting possibility of probing the dynamics of high-energy excited states, offered by recent experimental breakthrough in the field of cold atomic gases [84] and time-resolved spectroscopies [66], have opened a new window on the non equilibrium physics of strongly correlated systems, which is still largely unexplored.

From a theoretical perspective strong correlations are known to be very difficult to treat, since are intrinsically non perturbative effects. This has triggered the development of sophisticated many body techniques to deal with this physics, the Dynamical Mean Field Theory [65] (DMFT) being one of the most relevant example. Interestingly enough, however, many basic concepts in the theory of strongly correlated systems, have been originated from calculations based on very simple and physically transparent variational approaches. Among them we mention, for example, the Brinkman-Rice scenario for the Mott transition [22], built on early works by Gutzwiller [80], or the famous RVB scenario for high temperature superconductivity, proposed by Anderson in its seminal paper [9] and based on the idea of a projected groundstate wavefunction [136, 175]. Variational approaches to the strong correlation problem have therefore a long standing tradition. Due to their physical appeal and their intrinsic non perturbative nature they are still largely used, either with further analytical (mean-field like) approximations or in connection with very efficient numerical algorithms to optimize the wavefunction [173, 174] that have greatly extended the range of application of these methods [28, 117].

It is therefore tempting to see whether a proper extension of those ideas to the out of equilibrium strong correlation problem is somehow possible. This would clearly provides us with a very powerful approach, although less rigorous than others, which would represents one of the few non perturbative yet analytically manageable techniques to study correlated systems out of

equilibrium.

An obvious observation at this point is that, differently from ground state physics which is *protected* by a clear variational principle, non equilibrium states cannot in general be formulated in terms of minimizing some energy functional. While this is likely the case for non equilibrium *stationary states* such as those with currents flowing through them, although some attempts have been done in this direction [89, 85, 45], the situation may be different for what concerns time evolution, hence transient states. Indeed unitary quantum dynamics can be shown to derive from a *variational* principle on a real-time action.

This leaves open the possibility to describe, by means of a suitable time dependent variational approach, many non equilibrium problems such as for example the relaxation dynamics of an isolated many body systems or, even more generally, the dynamics induced by tuning in time any Hamiltonian parameters.

This is actually the aim of the present chapter. In particular we will first introduce a general variational scheme for quantum dynamics in correlated systems. This will allow us to cast the original problem of solving the time-dependent many-body Schroedinger into a simpler, yet non trivial, one. As often happens with correlated wavefunctions the resulting variational problem cannot be solved exactly, in general, unless some further approximation is introduced. This can be either numerical, in the spirit of Variational Monte Carlo techniques, or analytical, along the well known Gutzwiller approximation. We follow the latter, properly generalized to deal with time dependent situations. As an application we study the simplest non equilibrium problem, namely the relaxation dynamics after a quantum quench in the single band Hubbard model.

6.2 A General Formulation

For simplicity, we assume initially a many-body wavefunction $|\Psi_0\rangle$, which, for times $t > 0$, is let evolve with a Hamiltonian $\mathcal{H}$ that includes sizable on-site interactions. In the spirit of the Gutzwiller approach, we make the following variational ansatz for the time-dependent wavefunction $|\Psi_{exact}(t)\rangle = \mathrm{e}^{-i\mathcal{H}t}\,|\Psi_0\rangle$

$$|\Psi_{exact}(t)\rangle \simeq |\Psi(t)\rangle = \prod_i \mathrm{e}^{-i\mathcal{S}_i(t)}\,\mathcal{P}_i(t)\,|\Phi(t)\rangle, \tag{6.1}$$

where $|\Phi(t)\rangle$ is a time-dependent Slater determinant. $\mathcal{P}_i(t)$ and $\mathcal{S}_{i\alpha}$ are hermitian operators that act on the Hilbert space of site i and we assume

they depend, respectively, on some variables $\lambda_{i\alpha}(t)$ and $\phi_{i\alpha}(t)$ such that

$$\frac{\partial}{\partial\lambda_{i\alpha}}\mathcal{P}_i = \mathcal{O}_{i\alpha} \qquad \frac{\partial}{\partial\phi_{i\alpha}}\,\mathrm{e}^{-i\mathcal{S}_i} = -i\,\mathcal{O}_{i\alpha}\,\mathrm{e}^{-i\mathcal{S}_i}, \tag{6.2}$$

where $\mathcal{O}_{i\alpha}$ is any local hermitian operator. Since (6.1) is just a variational ansatz, it does not solve the full Schrœdinger equation. Our proposal is to determine the variational parameters by requiring: (*i*) that the Heisenberg equations of motion of the local operators $\mathcal{O}_{i\alpha}$ are satisfied when averaging over (6.1), namely that

$$\dot{O}_{i\alpha} \equiv \frac{d}{dt}\,\langle\Psi(t)|\mathcal{O}_{i\alpha}|\Psi(t)\rangle = -i\langle\Psi(t)|\,[\mathcal{O}_{i\alpha},\mathcal{H}]\,|\Psi(t)\rangle \tag{6.3}$$

and (*ii*) that the average energy $E = \langle\Psi(t)|\,\mathcal{H}\,|\Psi(t)\rangle$ is, as it should be, conserved during the real-time evolution,

$$\frac{d\,E}{dt} = \langle\,\partial_t\Psi(t)|\mathcal{H}|\Psi(t)\rangle + \langle\Psi(t)|\mathcal{H}|\,\partial_t\Psi(t)\rangle = 0\,. \tag{6.4}$$

Let us start from the first condition (6.3) noticing that, by definition (6.2),

$$\frac{\partial}{\partial\phi_{i\alpha}}\,\mathrm{e}^{i\mathcal{S}_i}\,\mathcal{H}\,\mathrm{e}^{-i\mathcal{S}_i} = i\,\mathrm{e}^{i\mathcal{S}_i}\,[\mathcal{O}_{i\alpha},\mathcal{H}]\,\mathrm{e}^{-i\mathcal{S}_i}.$$

Hence it follows that

$$-i\langle\Psi(t)|\,[\mathcal{O}_{i\alpha},\mathcal{H}]\,|\Psi(t)\rangle = -\frac{\partial E}{\partial\phi_{i\alpha}}$$

from which we get the equation of motion for $O_{i\alpha}$

$$\dot{O}_{i\alpha} = -\frac{\partial E}{\partial\phi_{i\alpha}}\,. \tag{6.5}$$

Concerning the second condition we notice that, by definition, the time derivative of the variational wave-function reads

$$|\partial_t\Psi(t)\rangle = (\partial_t\,P)\,|\Phi(t)\rangle + P|\partial_t\Phi(t)\rangle\,,$$

where we have defined for simplicity $P(t) = \prod_i \mathrm{e}^{-i\mathcal{S}_i(t)}\,\mathcal{P}_i(t)$. A simple calculation, that we report in Appendix B for completeness, gives the result

$$(\partial_t\,P)\,|\Phi(t)\rangle = \frac{d}{dt}\,\mathcal{P}(t) = \left(\sum_{i\alpha}\dot{\lambda}_{i\alpha}\,\mathcal{P}_i^{-1}\mathcal{O}_{i\alpha} - i\dot{\phi}_{i\alpha}\,\mathcal{O}_{i\alpha}\right)\,\mathcal{P}(t)\,, \tag{6.6}$$

When this expression is plugged into (6.4) it gives, using eq. (6.5) and after some simple algebra,

$$\begin{aligned}\frac{d\,E}{dt} \;=\; & \sum_{i\alpha}\dot{O}_{i\alpha}\left(-\dot{\phi}_{i\alpha} + \frac{\partial E}{\partial O_{i\alpha}}\right) + \\ & +\langle\Phi(t)|\mathcal{H}_\star(t)|\partial_t\Phi(t)\rangle + \langle\partial_t\Phi(t)|\mathcal{H}_\star(t)|\Phi(t)\rangle \;= 0\end{aligned} \tag{6.7}$$

where $\mathcal{H}_*(t) = P^\dagger(t)\mathcal{H}P(t)$ is an effective Hamiltonian that depends on all time-dependent variational parameters defining $\mathcal{P}_i$ and $\mathcal{S}_i$. In general, these parameters can be expressed in terms of $\phi_{i\alpha}$ and $O_{i\alpha}$.

The condition (6.4) can be therefore readily satisfied if we impose that $|\Phi(t)\rangle$ is the solution of the time-dependent Schrœdinger equation

$$-i\frac{\partial}{\partial t}|\Phi(t)\rangle = \mathcal{H}_*(t)\,|\Phi(t)\rangle, \tag{6.8}$$

and furthermore that

$$\dot{\phi}_{i\alpha} = \frac{\partial E}{\partial O_{i\alpha}}\,. \tag{6.9}$$

We see from equations (6.5) and (6.9) that $\phi_{i\alpha}$ and $O_{i\alpha}$ act like classical conjugate variables and the energy functional E as their effective Hamiltonian.

Interestingly, the above dynamical equations for the variational parameters can be equivalently obtained from a stationarity principle on the real-time action. Indeed if we define the action functional as

$$\mathcal{S}[\Psi^\dagger, \Psi] = \int dt\, \langle\Psi(t)|\, i\partial_t - \mathcal{H}|\Psi(t)\rangle \tag{6.10}$$

we immediately see that the stationarity condition $\delta\mathcal{S} = 0$ is fully equivalent to the solution of the original time-dependent Schrœdinger problem. If we now assume the ansatz (6.1) for the time-dependent many body wave function $\Psi(t)$ and compute the corresponding action $\mathcal{S}$ (6.10) we obtain a functional of the variational parameters $\{\phi_{i\alpha}, O_{i\alpha}, \Phi\}$ which reads

$$\mathcal{S}_{trial} = \int dt\, \left(\frac{i}{2}\partial_t\langle\Psi(t)|\Psi(t)\rangle + \sum_{i\alpha}\dot{\phi}_{i\alpha}O_{i\alpha} - E[\phi_{i\alpha}, O_{i\alpha}]\right) \tag{6.11}$$

and whose stationarity conditions

$$\frac{\delta\mathcal{S}}{\delta\phi_{i\alpha}} = 0 \qquad \frac{\delta\mathcal{S}}{\delta O_{i\alpha}} = 0 \qquad \frac{\delta\mathcal{S}}{\delta\Phi} = 0$$

give back the dynamical equations (6.5,6.9) and (6.8).

Notice that, in the present case where the original Hamiltonian does not depend explicitly on time, the conservation of energy immediately follows from the stationarity principle. However in the case of time-dependent problems which may be relevant for cold atoms applications the above formulation in terms of real-time action is still valid even though the energy is no more a conserved quantity.

In conclusion, within the above variational scheme, the quantum many body evolution has been translated into a classical problem for the variational parameters, with Hamiltonian $\mathcal{H}_{class}$

$$\mathcal{H}_{class} = \langle\Psi(t)|\mathcal{H}|\Psi(t)\rangle\,,$$

coupled to a time-dependent Schroedinger equation 6.8 for the Slater determinant. Finally, it is worth mentioning that the above scheme is variationally exact, as far as the effective Hamiltonian $\mathcal{H}_{class}$ can be computed in closed form. For strongly correlated problems this is often not the case and one has to resort to analytical approximations or to numerical methods. In the next section we will apply this method to the simplest example of correlated lattice electrons out of equilibrium, namely the Hubbard Model after a quantum quench.

6.3 Quantum Quenches in the Hubbard Model

The simplest way one could imagine to induce a non trivial dynamics is through a so called *quantum quench*. Here the system is firstly prepared in the ground-state of some given Hamiltonian $\mathcal{H}_i$, and then suddenly let evolved under the action of a new Hamiltonian $\mathcal{H}_f$. Recently, quantum quenches have been the subject of a vast literature focusing on integrable systems [47, 156] one dimensional models [30, 108, 116] or systems close to a quantum criticality [41]. The interest on these class of non equilibrium problems relies both on the dynamics itself [11] as well as on the long-time properties where the issue of thermalization or its lack of is still highly debated [149, 16]. For what concerns strongly correlated electrons in more than one dimension, the subject is still largely unexplored and progresses have been done only very recently. The single band fermionic Hubbard model is likely the simplest lattice model of correlated electrons embodying the competition between metallic and insulating behavior driven by a local Hubbard repulsion U. Its Hamiltonian reads

$$\mathcal{H}(t) = -\sum_{\sigma}\sum_{\langle i,j\rangle} t_{ij}\, c^{\dagger}_{i\sigma}\, c_{j\sigma} + U(t)\sum_{i} n_{i\uparrow}\, n_{i\downarrow}\,. \tag{6.12}$$

In two pioneering works [125, 48] the response of a Fermi sea to a sudden switch-on of the Hubbard U has been studied in infinite dimensions using respectively the flow-equation method and the Dynamical Mean Field Theory (DMFT). Results suggest the existence of two different regimes in the real-time dynamics depending on the final interaction strength U_f. At weak coupling [125] the systems is trapped at long-times into a quasi-stationary regime where correlations are more effective than in equilibrium. This *prethermalization* phenomenon has been confirmed by DMFT results [48] which further indicate a true dynamical transition above a critical U_{fc} towards another regime with pronounced oscillations in the dynamics of physical quantities. These intriguing results have been so far restricted to a quench starting

from a non interacting system ($U_i = 0$) and, more importantly, limited to rather short accessible time scales and weak quenches, thus leaving open many important issues.

In this section we address this problem using the time dependent variational scheme previously introduced. In particular we study the dynamics after a sudden change of the local interaction, starting from the zero-temperature ground state with $U(t \leq 0) = U_i$ then quenching the interaction to $U(t > 0) = U_f$. Notice that since the initial state is described within the equilibrium Gutzwiller approximation, which provides a poor description of the Mott Insulator, we have to restrict our analyis to strongly correlated yet metallic initial conditions, namely to $U_i < U_c$ where U_c is the critical interaction strength where Mott transition occurs (see Appendix B). Moreover in the following we will completely disregard magnetism, considering only paramagnetic and homogeneous wave functions.

6.3.1 Time Dependent Gutzwiller Approximation

In the following we assume $\mathcal{H}$ to be the single band Hubbard model (6.12) and assume for the correlated time-dependent wave function the form (6.1) with

$$\mathcal{P}_i(t) = \sum_{n=0}^{2} \lambda_{i,n}(t)\, \mathcal{P}_{i,n}\,, \tag{6.13}$$

and

$$\mathcal{S}_i(t) = \sum_{n=0}^{2} \phi_{i,n}(t)\, \mathcal{P}_{i,n}\,, \tag{6.14}$$

where $\mathcal{P}_{i,n}$ is the projector at site i onto configurations with $n = 0, \ldots, 2$ electrons. Notice that equations (6.13-6.14) imply that $\phi_{i,n}(t)$ plays the role of the conjugate variable of the occupation probability $P_{i,n} = \langle \Psi(t)|\mathcal{P}_{i,n}|\Psi(t)\rangle$.

As we already mentioned the concrete evaluation of the energy functional E on the trial state (6.1) is still a very challenging task, for which analytical results generally lack. However, as in equilibrium, calculations can be done exactly in the limit of large lattice connectivity or within the so called Gutzwiller approximation, provided the following conditions are imposed [55, 24].

$$\langle \Phi(t)|\mathcal{P}_i^2(t)|\Phi(t)\rangle = 1\,,\ \langle \Phi(t)|\mathcal{P}_i^2(t)\, c_{i\sigma}^\dagger c_{i\sigma}|\Phi(t)\rangle = \frac{n_i}{2}\,, \tag{6.15}$$

where $n_i = \sum_\sigma \langle \Phi(t)|c_{i\sigma}^\dagger c_{i\sigma}|\Phi(t)\rangle$. Using these constraints one can show [24] that averages over the correlated wave function $|\Psi(t)\rangle$ of local and non local

operators read, respectively, as

$$\langle\Psi(t)|\,\mathcal{O}_i\,|\Psi(t)\rangle = \langle\Phi(t)|\,\mathcal{P}_i(t)\,\mathcal{O}_i\,\mathcal{P}_i(t)\,|\Phi(t)\rangle \tag{6.16}$$

and

$$\langle\Psi(t)|\,c^\dagger_{i\alpha}c_{j\beta}\,|\Psi(t)\rangle = \sum_{\gamma\delta}\sqrt{Z^\star_{i\alpha\gamma}}\,\sqrt{Z_{j\beta\delta}}\,\langle\Phi(t)|\,c^\dagger_{i\gamma}c_{j\delta}\,|\Phi(t)\rangle\,, \tag{6.17}$$

where $\sqrt{Z_{i\alpha\beta}}$ plays the role of a time-dependent quasiparticle renormalization factor defined through the equation

$$\sum_\gamma\sqrt{Z_{i\alpha\gamma}}\,\langle\Phi(t)|\,c^\dagger_{i\gamma}c_{i\beta}|\Phi(t)\rangle = \langle\Phi(t)|\,\mathcal{P}_i\,e^{i\mathcal{S}_i}c^\dagger_{i\alpha}e^{i\mathcal{S}_i}\mathcal{P}_i\,c_{i\beta}|\Phi(t)\rangle\,. \tag{6.18}$$

In the case of present interest this gives

$$\sqrt{Z_i} = \frac{\sqrt{P_{i,1}}}{\sqrt{n_i\,(1-n_i/2)}}\left(\sqrt{P_{i,2}}\,e^{i(\phi_{i,2}-\phi_{i,1})} + \sqrt{P_{i,0}}\,e^{i(\phi_{i,1}-\phi_{i,0})}\right)\,. \tag{6.19}$$

From the constraints (6.15) it immediately follows that, by defining $P_{i,2}\equiv D_i$

$$P_{i,0} = 1-n_i+D_i\,,\qquad P_{i,1} = n_i-2D_i\,. \tag{6.20}$$

Using the above results and further assuming $\phi_{i,0}=\phi_{i,2}=\phi_i$ while $\phi_{i,1}=0$, we can write the energy functional E as

$$E = \langle\Psi(t)|\mathcal{H}|\Psi(t)\rangle = U_f\sum_i D_i + \sum_{\langle ij\rangle} w_{ij}\,\sqrt{Z^\star_i\,Z_j} + h.c. \tag{6.21}$$

where $w_{ij}(t) = t_{ij}\,\sum_\sigma\langle\Phi(t)|\,c^\dagger_{i\sigma}c_{j\sigma}\,|\Phi(t)\rangle$ while $Z_i\,(t)$ defined in equation (6.18-6.19) reads

$$\sqrt{Z_i} = \sqrt{\frac{n_i-2D_i}{n_i\,(1-n_i/2)}}\left(\sqrt{D_i+\delta_i}\,e^{i\phi_i} + \sqrt{D_i}\,e^{-i\phi_i}\right)\,. \tag{6.22}$$

Using the result (6.21) for the variational energy we can readily obtain the equations of motion for the double occupancy D_i and its conjugate variable ϕ_i using (6.5,6.9). In addition, the dynamics of these variational parameters is further coupled to a time dependent Schroedinger equation for the Slater determinant.

In the next subsection we will discuss the quench dynamics in the limit of infinite lattice coordination and further assuming a time-independent Slater determinant such that $w_{ij}(t)=w$. This will allow us to simplify the problem and make it amenable to a full analitical treatment. The results provide a very simple time-dependent mean field theory for the quench dynamics in the fermionic Hubbard model [164].

6.3.2 Connection with Quantum Ising Model in a Transverse Field

Before proceeding further, it is worth to notice that the expression (6.22) we have obtained for the quasiparticle weight simplifies in the half-filled case, $n_i = 1$

$$\sqrt{Z_i} = 4\sqrt{D_i\,(1/2 - D_i)}\,cos\phi_i\,. \tag{6.23}$$

Then, if we parametrize the double occupation D_i as

$$D_i = (1 - \cos\theta_i)/4\,, \tag{6.24}$$

we can recast the energy into a form which resembles the mean field energy of an Ising model in a transverse field

$$\mathcal{H}_{QI} = \frac{U_f}{4}\sum_i (1 - \sigma_i^z) - \sum_{ij} w_{ij}(t)\,\sigma_i^x\,\sigma_j^x, \tag{6.25}$$

where $\langle\sigma_i^z\rangle = \cos\theta_i$ and $\langle\sigma_i^x\rangle = \sin\theta_i\,\cos\phi_i$.

Remarkably, this connection can be established in much more generality [163], and agrees with the Z_2-slave-spin theory recently introduced [92, 160]. Therefore, it is not surprising that the equations of motion that we obtain through Eqs. (6.3) and (6.4) are just those of the Ising model $\langle\partial_t\,\sigma_i^a\rangle = -i\langle[\sigma_i^a, \mathcal{H}_I]\rangle$ within mean field. In other words, under the above assumption of homogeneous and paramagnetic wavefunctions, a quantum quench in the half-filled Hubbard model is equivalent, within the Gutzwiller variational scheme, to a quench in a Ising model in the presence of a transverse field. In particular, if $|\Phi(t)\rangle$ is taken to be the half-filled Fermi sea, then $w_{ij}(t) = w$ and (6.25) is the conventional ferromagnetic Ising model with constant and uniform exchange w and transverse field $U_f/4$. Quantum dynamics after step-like variations of the transverse field has been recently investigated in one-dimension, where the model is integrable [156], and on a fully connected lattice within a large spin approximation [39].

6.4 Time-Dependent Mean Field Theory

In the limit of infinite coordination lattices all spatial fluctuations are frozen out and we can safely assume the variational parameters $\{D_i, \phi_i\}$ to be independent of lattice site. The resulting classical Hamiltonian (6.21) for one single degree of freedom D and its conjugate variable ϕ reads

$$E[D, \phi] = U_f D(t) + \bar{\varepsilon}_n\,Z(D, \phi)\,, \tag{6.26}$$

where $\bar{\varepsilon}_n$ is the average kinetic energy for a Fermi sea with density $n = 1-\delta$ while Z is the effective quasiparticle weight, which reads from equation (6.22)

$$Z(D,\phi) = \frac{2(n-2D)}{n(2-n)} \times \left[\left(\sqrt{D+\delta}-\sqrt{D}\right)^2 + 4\cos^2\phi\sqrt{D}\sqrt{D+\delta}\right] . \tag{6.27}$$

The classical equations of motion for this integrable system immediately follow from (6.26)

$$\dot{\phi} = \frac{U_f}{2} + \frac{\bar{\varepsilon}_n}{2}\frac{\partial Z}{\partial D} \tag{6.28}$$

$$\dot{D} = -\frac{\bar{\varepsilon}_n}{2}\frac{\partial Z}{\partial \phi} \tag{6.29}$$

In the following we will use the MIT critical interaction, $U_c = -8\bar{\varepsilon}_{n=1}$, as the basic unit of energy and define accordingly the adimensional quantities $u_f = U_f/U_c$ and $u_i = U_i/U_c$.

The initial conditions for the classical dynamics (6.28-6.29) read

$$D(0) = D_{eq}(u_i,\delta)\,, \qquad \phi(0) = 0\,, \tag{6.30}$$

where $D_{eq}(u_i,\delta)$ is the zero temperature double occupancy for interaction u_i and filling δ that can be easily computed from an equilibrium Gutzwiller calculation (see appendix B).

It is worth to notice that, apart from the trivial case in which $u_f = u_i$, the classical dynamics (6.28-6.29) admits a non-trivial stationary solution $D = 0$ and $\cos^2\phi = u_f$, which is compatible with the initial conditions only at half-filling and $u_f = u_{fc} = (1+u_i)/2$. It turns out that u_{fc} identifies a dynamical critical point that separates two different regimes similarly to a simple pendulum. When $u_f < u_{fc}$, $2\phi(t)$ oscillates around the origin, while, for $u_f > u_{fc}$, it performs a cyclic motion around the whole circle. In order to characterize the different regimes, we focus on three physical quantities, the double occupancy $D(t)$, the quasiparticle residue $Z(t)$ and their period of oscillation, $\mathcal{T}$.

Just before discussing in some detail the results of the classical dynamics (6.28-6.29) it is useful to cast it into a closed first-order differential equation for one of the two conjugate variables D, ϕ. Indeed the dynamics is such that

$$E_0(U_f,U_i,\delta) = U_f D(t) + \bar{\varepsilon}_n\, Z(t)\,, \qquad t > 0 \tag{6.31}$$

where $E_0(U_f,U_i,\delta)$ is the total energy soon after the quench, which reads

$$E_0(U_f,U_i,\delta) = U_f\, D_{eq}(U_i,\delta) + \bar{\varepsilon}_n\, Z_{eq}(U_i,\delta)\ . \tag{6.32}$$

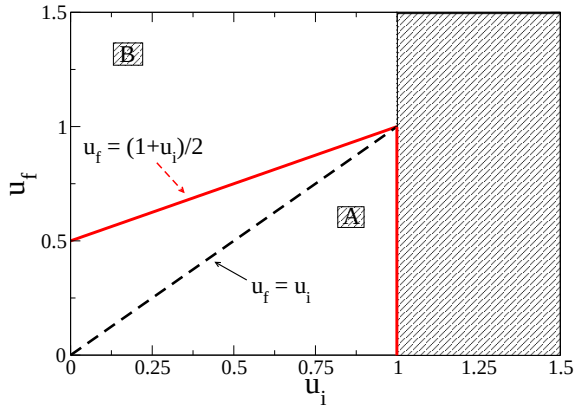

Figure 6.1: Sketch of the *phase diagram* in the u_i, u_f plane for the quench dynamics of the single band Hubbard model within the Gutzwiller approximation at half-filling. Two different dynamical regimes corresponding to weak and strong coupling dynamics (A and B in the plot) are found depending whether the final interaction u_f lies above or below the critical quench line $u_f = \frac{1+u_i}{2}$. For quantum quenches along this line the dynamics features an exponential relaxation toward a steady state.

A quick look to the definition of the quasiparticle weight Z in (6.27) is enough to convince us that the simplest way to proceed is to eliminate ϕ from Eq.(6.31) in order to close the problem for the double occupancy $D(t)$. From Eq.(6.27) and using the fact that $\bar{\varepsilon}_n = n\,(2-n)\,\bar{\varepsilon}$ we obtain

$$cos^2\phi = \frac{E_0 - U_f D - 2\bar{\varepsilon}\,(n-2D)\left(\sqrt{D+\delta} - \sqrt{D}\right)^2}{8\bar{\varepsilon}\,(n-2D)\sqrt{D\,(D+\delta)}}\,. \tag{6.33}$$

which can be inserted into the equation (6.29) for $D(t)$, which reads after evaluating the derivative of Z with respect to ϕ

$$\dot{D} = -8\bar{\varepsilon}\,(n-2D)\sqrt{D\,(D+\delta)}\,sin\phi\,cos\phi\,. \tag{6.34}$$

After some simple but lengthly algebra we end up with a differential equation for the time-dependent double occupation whose general structure is

$$\dot{D} = \pm\sqrt{\Gamma(D)}\,, \tag{6.35}$$

where $\Gamma(D) = 2u_f\,(D_{2+} - D)\,(D - D_{1+})\,(D - D_-)$ can be thought as an effective potential controlling the dynamical behavior of $D(t)$. Here $D_{2+} \geq$

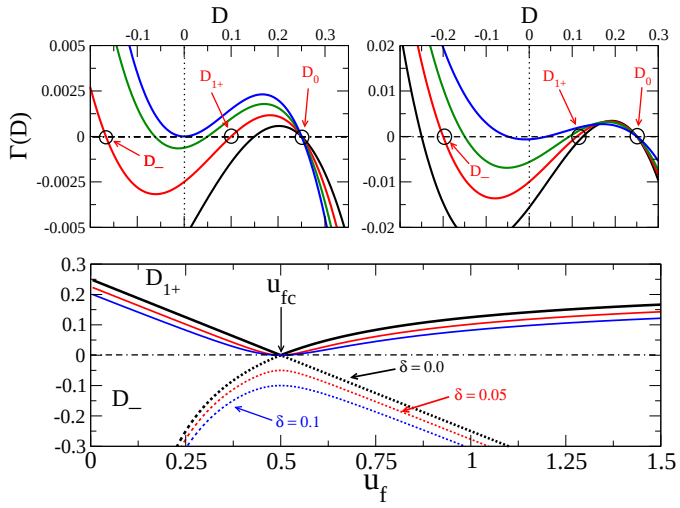

Figure 6.2: Top Panel: Effective potential $\Gamma(D)$ for $u_f = 0.2, 0.3, 0.4, 0.5$ (right) and $u_f = 0.6, 0.8, 0.9, 1.0$ (left). Bottom panel: Inversion points D_{1+}, D_- as a function of u_f at fixed $u_i = 0$ for zero and finite doping.

$D_{1+} \geq 0$ and $D_- \leq 0$ are the three roots of $\Gamma(D)$ whose explicit expression will be given hereafter. We note that since the problem is one dimensional many properties of the solution (6.35) can be inferred directly from the knowledge of $\Gamma(D)$ without explicitly solving the dynamics.

It turns out that the equilibrium zero temperature Gutzwiller solution $D_{eq}(u_i, \delta) \equiv D_i$ is always a root of the effective potential $\Gamma(D)$, see figure 6.2, hence a stable solution for the dynamics. This is not surprising but simply reflects the fact that to induce a non-trivial dynamics one has to start from an highly excited state for the Hamiltonian $\mathcal{H}_f$. As opposite the remaining roots strongly depend on u_f and δ, thus resulting into a very rich dynamical behavior.

6.4.1 Quench Dynamics at Half-Filling

We start considering the half-filled case ($\delta = 0$) and for the time being fix $u_f > u_i$ see figure 6.1. In this regime the behavior of the effective potential $\Gamma(D)$ is plotted in figure 6.2. As one can see in addition to $D_{2+} = D_i = \frac{1-u_i}{4}$, there are two roots $D_- < 0 < D_{1+}$ which strongly depend on u_f (see bottom panel). As we are going to argue those roots merge together at a *critical* interaction quench $u_{fc} = (1 + u_i)/2$ thus turning into a stationary point

for the effective potential $\Gamma(D)$. As a consequence two different dynamical regimes can be identified which are divided by a true dynamical transition.

Weak Coupling

Let us start from the weak coupling side $u_i < u_f < u_{fc}$ when the accessible regions for the dynamics (6.28-6.29) ($\Gamma(D) \geq 0$) are bounded by

$$D_{2+} = D_i \qquad D_{1+} = (u_{fc} - u_f)/2 = D_i\,(1 - u_f/2D_i)\ . \tag{6.36}$$

Here the double occupation dynamics *oscillates* between these two values with amplitude $\mathcal{A}_D = (u_f - u_i)/2$ and period $\mathcal{T}$ given by

$$\mathcal{T} = 2\int_{D_{1+}}^{D_i} \frac{dD}{\sqrt{\Gamma(D)}} = \frac{4\sqrt{2}\,\mathcal{K}(k)}{\sqrt{Z_i}}\,, \tag{6.37}$$

where $\mathcal{K}(k)$ is the complete elliptic integral of the first kind with argument $k^2 = 4u_f\,(u_f - u_i)/Z_i$. Here we have defined $Z_i = 1 - u_i^2$ as the Gutzwiller zero temperature quasiparticle weight (see appendix B). In the limit of a small quantum quench, $\delta u = u_f - u_i \to 0$, the amplitude of those oscillations vanishes linearly while the period stays finite, $\mathcal{T} \simeq \mathcal{T}_0\,(1 + u_i\,\delta u/Z_i)$, with $\mathcal{T}_0 = 4\pi/\sqrt{Z_i}$. Upon further increasing u_f both the period $\mathcal{T}$ and the amplitude $\mathcal{A}_D$ of oscillations increase their size as shown in figure 6.3. As the critical quench line is approached the period increases further, eventually diverging logarithmically right at $u_f = u_f^c$. This can be shown explicitly from Eq.(6.37). Indeed we notice that for $u_f \to u_f^c$ the argument of the complete elliptic integral approaches $k = 1$, since $\frac{u_f^c - u_i}{2} = D_i$. Therefore, using the known asymptotic result $K(k) \simeq log\left(4/\sqrt{1-k^2}\right)$ we get

$$1 - k^2 = \left(u_f^c - u_f\right)\left(1 + \frac{u_f}{2\,u_f^c\,D_i}\right) \tag{6.38}$$

from which we obtain

$$\mathcal{T} \sim \frac{4}{\sqrt{1-u_i^2}}\,log\left(\frac{1}{u_f^c - u_f}\right)\,. \tag{6.39}$$

Such a diverging time scale signals a sharp transition to a completely different dynamical regime for $u_f > u_{fc}$. This clearly appears by looking at the effective potential $\Gamma(D)$ whose positive smaller root D_{1+}, which is perturbatively connected to D_i, linearly approaches zero for $u_f \to u_{fc}$, see equation (6.36). Here it merges with the negative roots

$$D_- = D_0\left(1 - \frac{u_{fc}}{u_f}\right)\,, \tag{6.40}$$

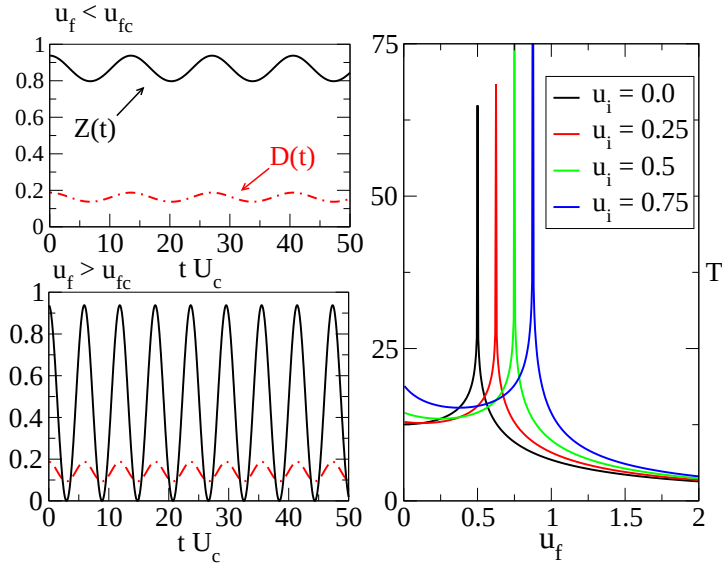

Figure 6.3: Left Panel: Mean-field dynamics for quantum quenches to u_f below (top) and above (bottom) the critical line. Right Panel: Period of oscillation $\mathcal{T}_D$ as a function of u_f for $u_i = 0.0, 0.25, 0.5, 0.75$. Notice the log-singularity at u_{fc}.

which is also connected to D_i but for $u_f \to \infty$. Hence, upon further increasing the quench strenght u_f above the critical line, the two roots D_{1+}, D_- swap their role and the dynamics enters the strong-coupling regime.

Finally it is worth to briefly discuss the dynamics of the quasiparticle weight $Z(t)$ and that one of the phase $\phi(t)$. The former shows an oscillating behavior with the same period $\mathcal{T}$ given in (6.37), as a consequence of energy conservation. For what concerns the phase $\phi(t)$, its dynamics can be obtained by eliminating the double occupation $D(t)$ from the original dynamical system (6.28-6.29), as we show explicitly in the Appendix B. Interestingly as we can see from figure 6.4 in the weak quench regime we are considering ($u_f < u_{fc}$) the phase oscillates around the *equilibrium* fixed point $\phi = 0$, with a period which increases upon approaching u_{fc}. As we are going to discuss in the next paragraph, it is just the phase which shows the most striking change in the dynamics as the critical line is crossed.

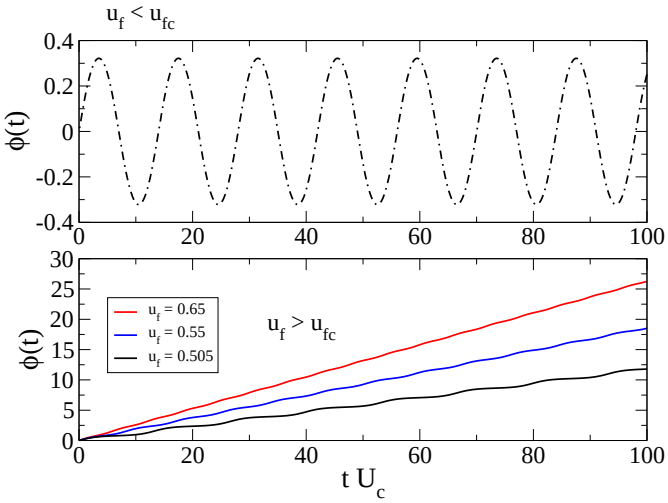

Figure 6.4: Dynamics of the phase in for quenches below and above the critical value u_{fc}. Notice that for small quenches the phase oscillates around zero while for $u_f > u_{fc}$ the dynamics is no more bounded since the energy is sufficient to overcome the potential barrier.

Strong Coupling

As we anticipated, for quenches above the critical value u_f^c the effective potential $\Gamma(D)$ shows again two simple roots, hence the motion of double occupation $D(t)$ (and quasiparticle weight $Z(t)$) is still periodic.

In particular, the period $\mathcal{T}$ of these strong coupling oscillations can be still expressed in terms of the complete elliptic integral

$$\mathcal{T} = 2\sqrt{\frac{2}{u_f}}\frac{K(k')}{\sqrt{D_i - D_+}} = \frac{4\,K(k')}{\sqrt{u_f\,(u_f - u_i)}}\,, \tag{6.41}$$

with argument k' given by

$$k' = \sqrt{\frac{D_i - D_-}{D_i - D_+}} = \frac{1}{k} = \sqrt{\frac{2D_i\,u_f^c}{u_f\,(u_f - u_i)}}\,. \tag{6.42}$$

As the critical quench line is approached from above $u_f \to u_f^c+$ the period of oscillations shows the same logarithmic singularity found on the weak-coupling side. Indeed in this limit k' approaches unity from below while k stays always greater than one. Therefore we can use the previous asymptotic

result to write $K\left(1/k\right) \simeq log\left(4k/\sqrt{k^2-1}\right)$ from which we readily obtain

$$\mathcal{T} \sim \frac{4}{\sqrt{1-u_i^2}} log\left(\frac{1}{u_f - u_f^c}\right), \tag{6.43}$$

namely the same singularity, with the same prefactor, appears on the two side of the dynamical transition.

However as the quench is increased further the resulting dynamics features remarkable differences from the weak-coupling case. Indeed both the amplitude and the period of these strong coupling oscillations *decrease* upon increasing the strength of the quench.

Let us start by discussing the dynamics of double occupancy. Deep in the strong coupling regime, $u_f \gg u_i$, period and amplitude vanish as

$$\mathcal{T} \simeq \frac{2\pi}{u_f}, \qquad \mathcal{A}_D = \frac{u_f^c\, D_i}{u_f}, \tag{6.44}$$

smoothly matching the atomic limit result. Hence the resulting dynamics shows very fast oscillations with a reduced amplitude. In the strong quench limit the double occupation dynamics is completely frozen, doublons have no available elastic channel to decay [155].

Similarly, quasiparticle weight $Z(t)$ also shows fast oscillations with period $\mathcal{T}$ given by (6.44) at strong coupling. However the amplitude of those oscillations keeps large even for infinite u_f, a consequence of the very non trivial dynamics of the phase $\phi(t)$. Indeed as we plot in figure 6.4 and show explicitly in the Appendix B, as soon as the critical line is crossed the phase starts precessing around the whole circle. Such an unbounded dynamics reflects directly into the quasiparticle weight $Z(t)$ which at half-filling simply reads

$$Z(t) = 16\, D(t)\left(1/2 - D(t)\right)\, cos^2\phi(t) \equiv Z_{eq}(t) cos^2\phi(t) \tag{6.45}$$

Notice that $Z(t)$ does not depends only on the double occupation $D(t)$, as one would expect in equilibrium, but features a phase-renormalization which is a peculiar non-equilibrium effect. As a consequence, even thought the double occupancy, and hence $Z_{eq}(t)$, oscillates with a vanishing amplitude the correction due to the unbounded dynamics of $\phi(t)$ results into a finite amplitude of oscillations for the effective quasiparticle weight. This transition from a localized phase with small oscillations around $\phi = 0$ to a delocalized phase where the dynamics is unbounded is, from a mathematical point of view, completely analogous to what happen in a simple pendulum. Right

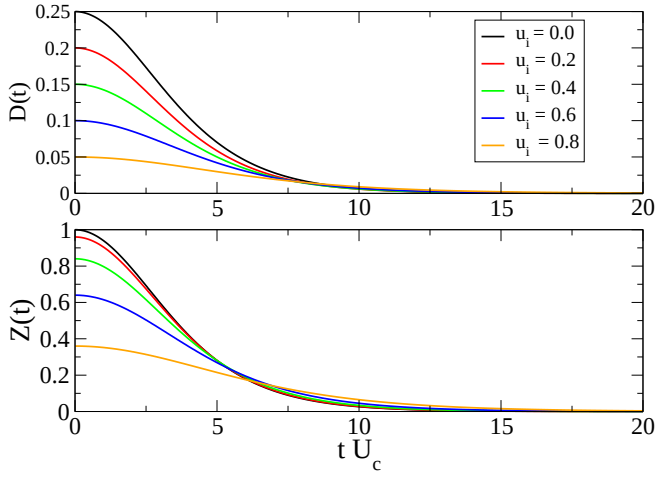

Figure 6.5: Dynamics after a quench at the critical interaction u_{fc}, for different initial conditions u_i. Both double occupation $D(t)$ and quasiparticle weight $Z(t)$ decay exponentially to zero with a relaxation time $\tau_\star \sim 1/\sqrt{Z_i}$ which increases with u_i approaching the initial Mott Insulator.

at the critical quench line the dynamics is on the separatrix and the phase takes infinite time to reach its metastable configuration. As we are going to see in the next paragraph this metastable configuration corresponds to a featureless Mott Insulator.

Critical Line

Quite interestingly, the weak and the strong coupling regimes that we have so far discussed are separated by a critical quench line u_{fc} at which mean-field dynamics exhibits *exponential relaxation*. This can be seen explicitly since in this limit the effective potential is simply given by $\Gamma(D) = \alpha D\sqrt{D_i - D}$ with $\alpha = \sqrt{2u_f^c}$ and the dynamics can be easily integrated

$$\alpha t = \int_D^{D_i} \frac{dD}{D\sqrt{D_i - D}} = \frac{2}{\sqrt{D_i}}\, atanh\left(\sqrt{\frac{D_i - D}{D_i}}\right) \tag{6.46}$$

from which we get the double occupation dynamics at the critical quench

$$D(t) = D_i\left(1 - tanh^2\left(t/\tau_\star\right)\right) . \tag{6.47}$$

We notice that, independently on the initial value of the correlation u_i for $u_f = u_f^c$ the double occupancy relaxes toward zero with a characteristic time scale $\tau_\star = 4/\sqrt{Z_i}$ that increases upon approaching the Mott insulator $u_i \to 1$. Analogously, also the quasiparticle weight $Z(t)$ approaches zero for long-time, with the same exponential behavior,

$$Z(t) = Z_i \left(1 - tanh^2 \left(t/\tau_\star\right)\right) .$$

We see therefore that for quenches at the critical line u_{fc} the system reaches a steady state featuring a complete suppression of charge fluctuations, that is the Mott insulating state within the Gutzwiller mean field picture. Interestingly, the line u_{fc} is such to make the energy soon after the quench exactly vanishing

$$E_0 \left(u_{fc}, u_i\right) = u_{fc} D_i + Z_i = 0 . \tag{6.48}$$

6.4.2 Integrated Dynamics and Long-time Behavior

As we have seen so far, the mean field Gutzwiller dynamics is periodic in the main part of the phase diagram excluding the quench to the critical value u_{fc} where an exponential behaviour emerges. Inspite of that, it is however worth to investigate a properly defined *long-time* behaviour of the dynamics which, as we are going to show, features many interesting properties. To this extent we firstly introduce, for any given function $O(t)$ an *integrated* (average) dynamics defined through

$$\langle O \rangle_t = \frac{1}{t} \int_0^t dt' \, O\left(t'\right) . \tag{6.49}$$

Then it is natural to define the long-time average as

$$\bar{O} = \lim_{t \to \infty} \langle O \rangle_t . \tag{6.50}$$

Notice that, since the relevant observables are periodic functions of time with period $\mathcal{T}_O$ admitting a Fourier decomposition

$$O\left(t\right) = \sum_n O_n \, e^{i \omega_n \, t} , \qquad \omega_n = \frac{2\pi n}{\mathcal{T}_O} , \tag{6.51}$$

the above definition (6.50) can be equivalently written as

$$\bar{O} = \frac{1}{\mathcal{T}_O} \int_{\mathcal{T}_O} dt \, O(t) . \tag{6.52}$$

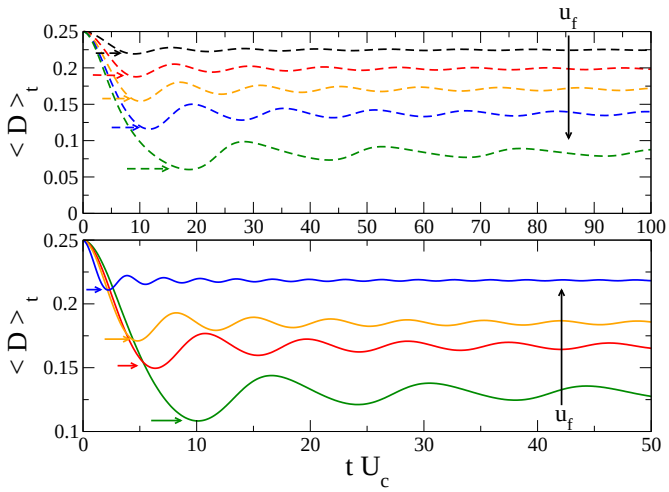

Figure 6.6: Average Dynamics for double occupation as defined in the main text (see Eq. 6.50). We show data for a quench from $u_i = 0.0$ to $u_f = 0.1, 0.2, 0.3, 0.4, 0.49$ (top panel from top to bottom) and from $u_i = 0.0$ to $u_f = 0.6, 0.8, 1.0, 1.2$ (bottom panel from bottom to top). Notice the different trend of the time scale $t_\star$ as a function of u_f in the weak and strong quench regime. For very large quenches $u_f \gg u_i$ the dynamics of double occupancy is trapped in the initial configuration.

Before discussing the long-time average behaviour of double occupancy and quasiparticle weight it is worth to briefly comment their average dynamics which contains interesting information on how the plateau is approached. As we can see from top panels of figures 6.6-6.7 the average dynamics shows a fast transient followed by small oscillations which are progressively damped out. We stress that this comes *entirely* from the averaging procedure (6.49) and not from an intrinsic damping mechanism that, as we have already shown is missing in our mean field dynamics. However the overall picture, including the behaviour of the steady state averages that we are going to discuss, displays some interesting features that is worth addressing. First we notice that the fast time scale $t_\star$, which can be roughly estimated as the time at which first minimum occurs, is basically controlled by the period $\mathcal{T}$ of oscillations as we explicitly show in the inset of figure 6.7. It increases as a function of final interacion quench u_f in the weak quench regime eventually diverging at the critical line. In the strong quench regime the behaviour of

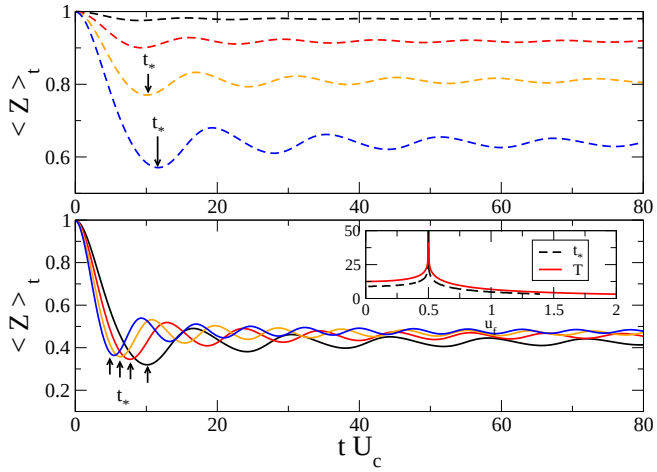

Figure 6.7: Average Dynamics for quasiparticle weight as defined in the main text (see Eq. 6.50). We show data for a quench from $u_i = 0.0$ to $u_f = 0.1, 0.2, 0.3, 0.4$ (top panel from top to bottom) and from $u_i = 0.0$ to $u_f = 0.6, 0.7, 0.8, 0.9$ (bottom panel from right to left arrow). The inset shows the behaviour of the time scale $t_\star$ as a function of u_f in comparison with the period $\mathcal{T}$ of oscillations. Notice the singularity at u_{fc}.

this time scale changes, as we can see from the bottom panels of both figures. In particular $t_\star$ decreases with the strength of the quench for $u_f > u_{fc}$. This has a direct consequence for the average dynamics of both double occupation and quasiparticle weight (see bottom panels of figures 6.7-6.6), which shows a different trend. Indeed not only the transient is faster but also the oscillations get quenched on a much shorter time scale and a steady state is quickly approached.

We now move the attention to the behaviour of steady state avererages as a function of the initial and final values of the interaction. To this extent we compute the average double occupation $\bar{D}$ using equation (6.52) which reads

$$\bar{D} = \frac{2}{\mathcal{T}_D} \int_{D_1}^{D_2} \frac{D\, dD}{\sqrt{\Gamma(D)}}, \tag{6.53}$$

Remarkably such an integral can be expressed in terms of the complete elliptic integrals of the first and second kind, $K(k)$ and $E(k)$ respectively.

The result for $\bar{D}$ reads therefore

$$\bar{D} = D_- + (D_2 - D_-)\,\frac{E\,(k)}{K\,(k)}\,, \tag{6.54}$$

with $k = \sqrt{\frac{D_2 - D_1}{D_2 - D_-}}$, where we have defined $D_{1,2}$ as the two positive roots of the effective potential $\Gamma\,(D)$ while D_- as the negative one. In addition, due to energy conservation, the knowledge of the average double occupancy $\bar{D}$ completely fixes the average quasiparticle weight which reads

$$\bar{Z} = Z_i + 8u_f\left(\bar{D} - D_i\right)\,. \tag{6.55}$$

We now evaluate the long-time average $\bar{D}$ and $\bar{Z}$ as given in Eq. (6.54-6.55) in the three different dynamical regimes we have previously identified.

Weak Coupling

In the weak coupling regime and for $u_f > u_i$ the average double occupation at long times reads

$$\begin{aligned} \bar{D} &= D_i\left(1 - \frac{u_f^c}{u_f}\right) + D_i\frac{u_f^c}{u_f}\,\frac{E\,(k)}{K\,(k)} \\ &= D_i\left[1 + \frac{u_f^c}{u_f}\left(\frac{E(k) - K(k)}{K(k)}\right)\right] \end{aligned} \tag{6.56}$$

with $k^2 = \frac{u_f\left(u_f - u_i\right)}{2D_i\,u_f^c}$. Similarly using the Eq. (6.55) we get for the average quasiparticle weight the result

$$\bar{Z} = Z_i\,\frac{E(k)}{K(k)}\,. \tag{6.57}$$

It is interesting to consider the asymptotic regime of a small quantum quench $\delta u = u_f - u_i \to 0$. Then we can expand the elliptic integrals for small k to get

$$\bar{D} \simeq D_i - \frac{\delta u}{4} = \frac{1 - u_f}{4}\,. \tag{6.58}$$

We see therefore that for small quenches the double occupation follows the zero temperature equilibrium curve, independently on the initial value of the interaction u_i. This is clearly shown in figure 6.8. Since to lowest order in δu no heating effects arise, this result implies that after a small quench of the interaction the average double occupation $\bar{D}$ is thermalized. In addition, this result has an interesting consequence for what concerns the behavior of the quasiparticle weight $\bar{Z}$. A simple calculation to lowest order in δu gives

$$\bar{Z} \simeq Z_i - 2\,u_f\,\delta u \tag{6.59}$$

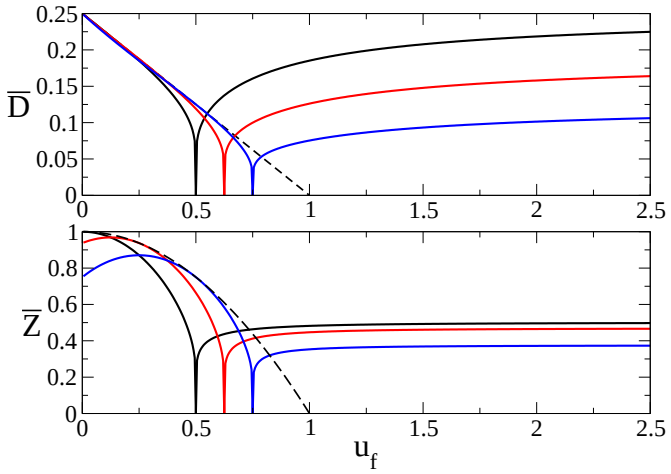

Figure 6.8: Average double occupation $\bar{D}$ (top) and quasiparticle weight $\bar{Z}$ (bottom) as a function of u_f at fixed $u_i = 0.0, 0.25, 0.5$ compared to the zero temperature equilibrium result (dashed lines).

from which we conclude that, as opposite to the double occupation $\bar{D}$, the long-time average quasiparticle weight differs from the zero temperature equilibrium result even at lowest order in the quench δu. In particular if we evaluate $\bar{Z}$ for the special case of a quench from a non interacting Fermi Sea ($u_i = 0$) we get the result, $1 - \bar{Z} = 2\,(1 - Z_{eq})$, firstly obtained in [125] within the flow equation approach. This peculiar mismatch between equilibrium and non equilibrium quasiparticle weight is a general result of quenching a Fermi Sea [126, 124]. It signals the onset of a *prethermal* regime where quasiparticle are well defined objects, momentum-averaged quantities such as kinetic and potential energy are thermalized while relaxation of distribution function is delayed to later time scales. Interestingly we see that our simple mean field theory correctly captures the onset of this long-lived state but fails in describing its subsequent relaxation toward equilibrium.

Interestingly when approaching the critical quench line from below the average double occupation $\bar{D}$ vanishes logarithmically. Indeed for $k \to 1$ we have

$$K(k) \simeq \log\left(4/\sqrt{1-k^2}\right) + o\left(1-k^2\right) , \tag{6.60}$$

and

$$E\left(k\right) \simeq 1 + o\left(1-k^2\right) , \tag{6.61}$$

therefore

$$\bar{D} \simeq D_i \left(\frac{u_f - u_f^c}{u_f} \right) + \frac{2D_i}{\log\left(\frac{1}{u_f^c - u_f}\right)} \tag{6.62}$$

The leading term is therefore logarithmic as mentioned, with linear corrections in $\delta u = u_f^c - u_f$

$$\bar{D} \simeq \frac{2D_i}{\log\left(\frac{1}{u_f^c - u_f}\right)} \left(1 + \frac{\delta u \log \delta u}{2u_f^c} \right) \tag{6.63}$$

A similar behavior is found for the quasiparticle weight $\bar{Z}$ which reads

$$\bar{Z} \simeq \frac{2Z_i}{\log\left(\frac{1}{u_{fc} - u_f}\right)} \tag{6.64}$$

Strong Coupling

In the strong coupling regime the average double occupation reads

$$\bar{D} = \frac{u_f^c - u_f}{2} + \frac{u_f - u_i}{2} \frac{E(k)}{K(k)}, \tag{6.65}$$

with the argument given by $k^2 = \frac{2\,D_i\,u_f^c}{u_f\left(u_f - u_i\right)}$.

Deep in the strong coupling regime, $u_f \gg u_i$, k goes to zero and we can use the asymptotic for $E(k)$ and $K(k)$

$$\frac{E(k)}{K(k)} \simeq 1 - \frac{k^2}{2} \tag{6.66}$$

to obtain

$$\bar{D} \simeq D_i \left(1 - \frac{u_f^c}{2u_f} \right). \tag{6.67}$$

We see therefore that, for infinitely large quenches, $u_f \to \infty$, the dynamics is trapped into the initial state. Interestingly enough, for quenches starting from $u_i = 0$ the scaling 6.67 exactly matches the strong coupling perturbative result obtained in [48] for the prethermal plateau. Indeed using the fact that for $u_i = 0$ we have $D_i\,u_{fc} = 1/8 = |\bar{\varepsilon}|$, we find

$$\bar{D} \simeq D_i - \frac{|\bar{\varepsilon}|}{2U_f},$$

where $\bar{\varepsilon}$ is the kinetic energy of the Fermi Sea, in accordance with strong coupling perturbation theory.

As opposite, when approaching the critical quench line from above we obtain a vanishing long-time average, with the same logarithmic behavior we have found on the weak coupling side. Indeed for $u_f \to u_f^c$ from above we have that $k \to 1^-$ and therefore we can again make use of the asymptotic for the complete elliptic integrals. We thus obtain

$$\bar{D} \simeq \frac{2D_i}{\log\left(\frac{1}{u_f - u_f^c}\right)} \left(1 + \frac{\delta u \log \delta u}{4D_i}\right) . \tag{6.68}$$

Note that the approach to zero is the same in both sides of the phase diagram, while the corrections are slightly different.

For what concerns the quasiparticle weight $\bar{Z}$ to get the leading behavior $o\left(1/u_f\right)$ we need the double occupancy to next-to-leading order. Expanding the ratio between elliptic functions we get

$$\frac{E\left(k\right)}{K\left(k\right)} \simeq 1 - \frac{k^2}{2} - \frac{k^4}{8} + o(k^6) \tag{6.69}$$

and using the expression for $k \simeq Z_i/4u_f^2$ we obtain the following asymptotic behavior for $\bar{Z}$

$$\bar{Z} \simeq Z_i - 2u_f^2\, k^2 \left(1 + k^2/4\right) \simeq \frac{Z_i}{2}\left(1 - \frac{Z_i}{16u_f^2}\right) \tag{6.70}$$

which shows that also $\bar{Z}$ increases from the critical line to large u_f and deep in the strong coupling regime it saturates to a finite plateau which, however does not coincide with its initial value Z_i but rather it is smaller by a factor of two due to energy conservation.

6.4.3 Quench Dynamics away from half-filling

As soon as we dope the system away from half-filling the picture we have obtained in the previous section dramatically change. In particular, as we are going to show, any finite doping $\delta \neq 0$ is enough to wash out the dynamical transition, cutting off the logarithmic divergence in the oscillation period $\mathcal{T}$.

To see how this may arise it is worth to consider again the effective potential $\Gamma\left(D\right)$ which enters the dynamics (6.35) for the double occupation. The qualitative analysis we have performed in section 6.4.1 can be done even for finite doping. In particular, since the equilibrium zero temperature Gutzwiller solution $D_{eq}(u_i, \delta) \equiv D_i$ is always a root of $\Gamma(D)$ we can still write the effective potential as

$$\Gamma(D) = 2u_f\ \left(D_i - D\right)\left(D - D_{1+}\right)\left(D - D_-\right) .$$

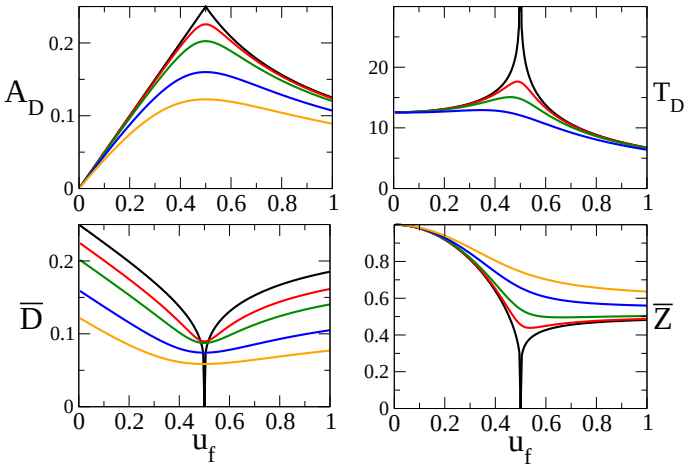

Figure 6.9: Top Panel: amplitude $\mathcal{A}_D$ (left) and period $\mathcal{T}_D$ at $u_i = 0$ and $\delta = 0.0, 0.05, 0.10, 0.20, 0.30$. Bottom Panel: averages double occupancy $\bar{D}$ (left) and quasiparticle weight $\bar{Z}$ (right) at $u_i = 0$ and $\delta = 0.0, 0.05, 0.10, 0.20, 0.30$.

All the differences between the doped and the half-filled case are therefore hidden in the behavior of the two non-trivial roots D_{1+}, D_- as a function of u_f. Their explicit expression is however quite lengthy and it is reported for completeness in Appendix B. As we can see from figure 6.2 those two roots, which at half-filling degenerate at u_{fc}, are always different for finite doping. In particular at the critical quench line we have

$$D_{1+}(u_{fc}) - D_-(u_{fc}) \simeq \delta\,.$$

As a consequence the dynamics of double occupancy (and hence of quasiparticle weight) always features a *finite* period given by

$$\mathcal{T} = \frac{2\sqrt{2}\,K\,(k)}{\sqrt{u_f\,(D_i - D_-)}}\,, \tag{6.71}$$

with the argument k of the elliptic function defined in term of the inversion points as

$$k = \sqrt{(D_i - D_+)\,/\,(D_i - D_-)}\,. \tag{6.72}$$

Notice that, due to the above mentioned finite difference between D_{1+} and D_-, this argument is always strictly lesser than one, $k < 1$ and no singularity in $\mathcal{T}$ arises. In figure 6.9 (top panels) we plot the period $\mathcal{T}$ and the amplitude

$\mathcal{A}$ of the double occupancy oscillations in the doped case, as a function of u_f at fixed u_i. We notice that both quantities are smooth across u_{fc}, and in particular the logarithmic singularity in the period turns into a sharp peak which broadens out as the doping increases.

Notice finally that a small doping not only affects the dynamics, but also drastically changes the long-time averages properties with respect to the results we have depicted in section 6.4.1. This can be worked out explicitly by using the same equations we have obtained for the half-filling case, (cfr. section 6.4.2), provided the correct expression for the roots D_{1+}, D_- is used. As we can see from figure 6.9 both double occupation and quasiparticle weight stay always finite as u_f increases and only show a dip around the critical quench line which is gradually smoothed out as the doping increases.

In summary we have shown that the dynamical transition described in section 6.4.1 is a peculiar feature of the half-filled case, a finite doping is enough to turn it into a sharp crossover.

6.4.4 Discussion

It is worth discussing the results of the time dependent mean field theory in light of those recently obtained with the Flow Equation method [125, 126] and with Non Equilibrium Dynamical Mean Field Theory [48, 49] for quantum quenches starting from a non interacting Fermi Sea.

We first of all notice that the suppression of quantum fluctuations, which is at the ground of our results, give rise to an oversimplified periodical dynamics that lacks relaxation toward a steady state and even more thermalization. This is at odd with results of both Flow Equation and DMFT which, thanks to a more careful treatment of quantum fluctuations, are able to damp out these oscillations. We guess that a similar result could be obtained from our variational treatment, for example, by allowing fluctuations in the Fermi sea and treating the Quantum Ising Model beyond the simplest mean field level [92]. Further investigations are required to clarify this point.

Beside this obvious drawback we can say that, quite remarkably, our mean field theory catches many interesting features of the problem which are also present in the results of Flow Equation and DMFT.

In particular our variational ansatz is able to exactly capture both regimes of prethermalization found at weak [125] and strong coupling [48], the former due to the non equilibrium mismatch in the quasiparticle weight while the latter to long-lived double occupations (see equations 6.59-6.67). The agreement at strong coupling is particularly remarkable if thought from the point of view of thermal equilibrium, where one knows the Gutzwiller wavefunction

cannot capture the Hubbard bands. We stress however that for the reasons mentioned above our simplified mean field theory wrongly make those two regimes stable up to infinite times without any relaxation to thermal equilibrium. Furthermore, the Gutzwiller ansatz makes clear and transparent the existence, in between of those two metastable regimes, of some critical value of the quench at which an exponentially fast relaxation can emerge, as firstly proposed in [48]. In this perspective our results are very promising and can be seen as a first step in the direction of a more detailed understanding of the physics of intermediated-to-strong interaction quenches in the fermionic Hubbard Model.

6.5 Conclusions

In this chapter we have introduced a variational approach to strongly correlated electrons out of equilibrium. The idea is to give an ansatz on the time dependent many-body wave function and to obtain dynamical equations for the parameters by imposing a saddle point on the real-time action. While this strategy is widely used for non interacting fermionic systems, in the spirit of time dependent Hartree-Fock, its extension to strongly correlated electrons represents an interesting novelty, with many possibilities for further developments. We have applied this variational scheme to the single band Hubbard model using a proper generalization of the Gutzwiller wavefunction. It is worth mentioning, however, that the method is general and can be applied also to other correlated wavefunctions, as long as a suitable numerical or analytical approach is available to calculate the *variational energy* controlling the classical dynamics of the variational parameters.

As a first application we have studied the dynamics of the Hubbard model after a quantum quench of the interaction. This is an interesting open problem for which results have been obtained only very recently using sophisticated non equilibrium many body techniques (see section 3.3.2 for a discussion). Remarkably, although extremely simple, our approach seems to capture many non trivial effects of the problem and shows a good overall agreement with the picture provided by DMFT. From this perspective it can be seen as a simple and intuitive mean field theory for quench dynamics in interacting Fermi systems.

Finally we note that the possibility to describe variationally the unitary dynamics of strongly correlated systems opens interesting perspectives for further investigations. This represents an important research line that it is worth pursuing in the next future.

Part IV

Appendix

Appendix A

Contour-ordered Hybridization Functions

In this appendix we discuss with some more details the contour-ordered Hybridization Function $i\Delta_C(t,t')$ we have introduced in the text, which is the basic object entering the hybridization expansion on the Kadanoff-Baym-Keldysh contour $\mathcal{C}$. This function encodes the effect of the bath on the impurity degrees of freedom, as it clearly appears in the effective action formulation of the theory. As we have shown in section in the case of a quantum impurity coupled to an equilibrium fermionic bath the hybridization function $i\Delta_C(t_1,t_2)$ can be written as

$$i\Delta_C(t_1,t_2) \equiv \sum_{\mathbf{k}} V_{\mathbf{k}}^2 \langle T_C\, f_{\mathbf{k}}(t_1)\, f_{\mathbf{k}}^\dagger(t_2)\rangle_{bath}\,, \tag{A.1}$$

while in general, i.e. for out of equilibrium fermionic baths, a parametrization of this function in terms of time independent Anderson impurity Hamiltonian is not possible. From the previous expression we see that $i\Delta_C(t_1,t_2)$ is given by the contour-ordered bath Green's function evaluated at the impurity site. The meaning of this function is the following. We consider a bath of free fermionic excitations in equilibrium at temperature T, whose hamiltonian generally reads

$$\mathcal{H}_{bath} = \sum_{\mathbf{k}\,a} \varepsilon_{\mathbf{k}}\, f_{\mathbf{k}\,a}^\dagger\, f_{\mathbf{k}\,a} \tag{A.2}$$

We take as initial density matrix ρ_0 the statistical one,

$$\rho_{in} = \frac{e^{-\beta\,\mathcal{H}_{bath}}}{Z}\,, \tag{A.3}$$

and define the contour-ordered bath Green's function as

$$g_{\mathbf{k}\,a}(t,t') = -i\langle T_{\mathcal{C}}\left(f_{\mathbf{k}\,a}(t)\, f_{\mathbf{k}\,a}^\dagger(t')\right)\rangle\,, \qquad t,t'\in\mathcal{C} \tag{A.4}$$

where both time arguments t and t' live on the three branch contour $\mathcal{C}$, while the average is taken over the initial density matrix. The contour time ordering $T_{\mathcal{C}}$ acts as described in the main text, namely ordering operators according to their time argument on the contour $\mathcal{C}$. Concerning the contour-time evolution of creation and annihilation operators it is defined as usual

$$f_{\mathbf{k}\,a}\left(t\right) \;=\; e^{i\mathcal{H}_{bath}t}\, f_{\mathbf{k}\,a}\, e^{-i\mathcal{H}_{bath}t}\,. \tag{A.5}$$

We now discuss the possible time orderings arising from the choice of t and t' along the contour $\mathcal{C}$, which naturally lead to a 3×3 matrix structure for the contour-ordered hybridizaton function.

$$i\Delta_C\left(t,t'\right) \rightarrow\; i\Delta_{ab}\left(t,t'\right) \qquad a,b=1,2,3 \tag{A.6}$$

A.1 Matsubara Sector

When both arguments live on the imaginary time axis, namely $t=-i\tau$ and $t'=-i\tau'$, we recover the standard Matsubara Green's function, a part from the i-factor

$$g^{33}_{\mathbf{k}\,a}\left(\tau,\tau'\right) = -i\langle T_\tau\,\left(f_{\mathbf{k}\,a}\left(\tau\right) f^{\dagger}_{\mathbf{k}\,a}\left(\tau'\right)\right)\rangle\,. \tag{A.7}$$

We note this function is antiperiodic and time-traslational invariant, therefore we can set $\tau'=0$ and compute it in the interval $\tau\in[0,\beta]$. We obtain for the hybridization function the standard result used also in equilibrium diagMC

$$\Delta_{33}\left(\tau\right) = -i\int\frac{d\varepsilon}{\pi}\,\Gamma\left(\varepsilon\right) n\left(\varepsilon\right)\, e^{-\varepsilon\tau}\,, \tag{A.8}$$

where $n\left(\varepsilon\right)$ is the Fermi distribution function and we had explicitly introduced the energy-dependent the hybridization $\Gamma\left(\varepsilon\right)$

$$\Gamma(\varepsilon) = \pi\sum_k |V_k|^2\,\delta(\varepsilon-\varepsilon_k)\,. \tag{A.9}$$

A.2 Keldysh Sector

When t and t' are both on real-time branches we are in the Keldysh subspace. The Green's function acquires a 2×2 matrix form, depending on the branch position $(a,b=1,2)$ of the two time arguments, and consequently also the hybridization function in Eq. (A.1) can be written as a matrix

$$\Delta_{ab}\left(t,t'\right) = \begin{pmatrix} \Delta^{11}\left(t,t'\right) & \Delta^{12}\left(t,t'\right) \\ \Delta^{21}\left(t,t'\right) & \Delta^{22}\left(t,t'\right) \end{pmatrix}. \tag{A.10}$$

In particular, when t is greater/lesser than t' on the contour we get the Δ^{21}/Δ^{12} component, which reads respectively

$$\Delta^{21}\left(t,t'\right)=\int\frac{d\varepsilon}{\pi}\,\Gamma\left(\varepsilon\right)\,\left(1-n_{F}\left(\varepsilon\right)\right)\,e^{-i\,\varepsilon\,\left(t-t'\right)} \tag{A.11}$$

and

$$\Delta^{12}\left(t,t'\right)=-\int\frac{d\varepsilon}{\pi}\,\Gamma\left(\varepsilon\right)\,n_{F}\left(\varepsilon\right)\,e^{-i\,\varepsilon\,\left(t-t'\right)}\,. \tag{A.12}$$

On the contrary when the two times are on the same branch we obtain the time-ordered Δ^{11} or anti-time ordered Δ^{12} hybridization function, which reduce to the off-diagonal ones depending on the time interval, namely

$$\Delta^{11}\left(t,t'\right)=\begin{cases}t>t' & \Delta^{21}\left(t,t'\right)\\ t<t' & \Delta^{12}\left(t,t'\right)\end{cases} \tag{A.13}$$

and

$$\Delta^{22}\left(t,t'\right)=\begin{cases}t>t' & \Delta^{12}\left(t,t'\right)\\ t<t' & \Delta^{21}\left(t,t'\right)\end{cases} \tag{A.14}$$

We note that, by construction, since we are considering a time independent quantum impurity model, all the four Keldysh components only depend on time differences $t-t'$. This property is peculiar of a bath which is in thermal equilibrium and do not hold in general for other kinds of non equilibrium driving protocols or in the case we are solving Non-Equilibrium DMFT.

A.3 Mixed Sector

Finally we have to consider the case in which the two time arguments live in different sectors. These mixed hybridization functions usually take into account the short-time memory effects, namely the transient correlations due to the chosen initial density matrix. We can distinguish two cases, depending on wheter $t>_{C}t'$ or viceversa. In the former case, namely when $t=-i\tau$ is on the Matsubara branch while t' lies on the Keldysh branches we have

$$\Delta_{31}\left(\tau,t'\right)=-\int\frac{d\varepsilon}{\pi}\,\Gamma\left(\varepsilon\right)\,\left(1-n_{F}\left(\varepsilon\right)\right)\,e^{-\varepsilon\,\tau}\,e^{-i\,\varepsilon\,t'} \tag{A.15}$$

as well as

$$\Delta_{32}\left(\tau,t'\right)=-\int\frac{d\varepsilon}{\pi}\,\Gamma\left(\varepsilon\right)\,\left(1-n_{F}\left(\varepsilon\right)\right)\,e^{-\varepsilon\,\tau}\,e^{-i\,\varepsilon\,t'}\,. \tag{A.16}$$

We note that in this case, as usual for off-diagonal terms, the contour-time ordering is fixed independently from the values of the time arguments since

the Keldysh branches are always lesser on the contour $\mathcal{C}$ than the imaginary branch. Moreover, we note there is no difference in the value of the hybridization function if the real-time is placed on the upper or lower branch, namely

$$\Delta^{31}\left(\tau, t'\right) = \Delta_{32}\left(\tau, t'\right) . \tag{A.17}$$

. As opposite, when t lies on the Keldysh contour while $t' = -i\tau'$ is on the Matsubara branch we obtain the other two mixed components

$$\Delta^{13}\left(t, \tau'\right) = -\int \frac{d\varepsilon}{\pi} \Gamma\left(\varepsilon\right) n_F\left(\varepsilon\right) e^{\varepsilon\,\tau'} e^{-i\,\varepsilon\,t} = \Delta^{23}\left(t, \tau'\right) . \tag{A.18}$$

Appendix B

Few details on the Gutzwiller Calculation

B.1 Gutzwiller Approximation in Equilibrium

In this section we briefly recall the Gutzwiller variational approach to the single band Hubbard model in equilibrium. For simplicity we will disregard symmetry breaking effects and only focus on the simplest paramagnetic case. The Gutzwiller ansatz for the many-body ground state wave function $|\Psi\rangle$ reads

$$|\Psi\rangle = \mathcal{P}|\Phi\rangle\,, \tag{B.1}$$

where $|\Phi\rangle$ is an uncorrelated Fermi Sea while $\mathcal{P}$ reads

$$\mathcal{P} = \prod_i \mathcal{P}_i \qquad \mathcal{P}_i = \sum_n \lambda_n \mathcal{P}_{i,n}\,, \tag{B.2}$$

where $\mathcal{P}_{i,n} = |\,i,n\,\rangle\langle\,i,n\,|$ are local operators acting at site i which project onto configurations with n electrons, with $n = 0, 1, 2$.

At zero temperature when the variational solution is obtained by minimizing the total energy written as

$$E_{var} = \langle\Phi|\mathcal{P}^\dagger\mathcal{H}\mathcal{P}|\Phi\rangle\,. \tag{B.3}$$

This calculation can be done exactly in the infinite dimensional limit (or in any-finite dimension within the Gutzwiller approximation), by imposing the following two constraints on the variational wave function

$$\langle\Phi|\mathcal{P}_i^2|\Phi\rangle = 1\,,\ \langle\Phi|\mathcal{P}_i^2\, c_{i\sigma}^\dagger c_{i\sigma}|\Phi\rangle = \frac{n_i}{2}\,. \tag{B.4}$$

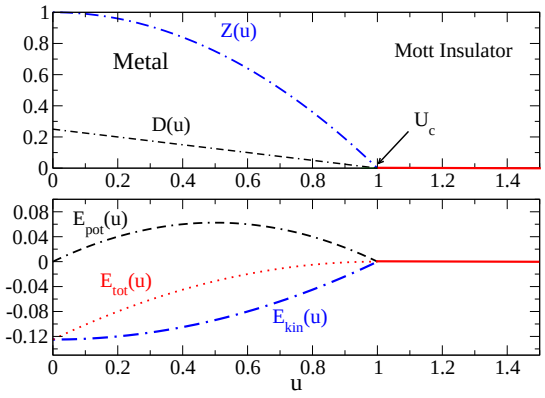

Figure B.1: Gutzwiller equilibrium phase diagram at zero temperature for the single band Hubbard model. The paramagnetic weakly correlated metal is destroyed at a critical value of the interaction $u = 1$ when the Metal-Insulator transition occurs. Right at the transition both the fraction of doubly occupied sites and the quasiparticle weight vanishes. The Mott insulator is featureless, with zero energy and no charge flucutations.

Using these constraints one can show [24] that averages over the correlated wave function $|\Psi(t)\rangle$ of local and non local operators read, respectively, as

$$\langle\Psi|\,\mathcal{O}_i\,|\Psi\rangle = \langle\Phi|\,\mathcal{P}_i\,\mathcal{O}_i\,\mathcal{P}_i\,|\Phi\rangle \tag{B.5}$$

and

$$\langle\Psi|\,c^\dagger_{i\alpha}c_{j\beta}\,|\Psi\rangle = \sum_{\gamma\delta}\sqrt{Z^\star_{i\alpha\gamma}}\,\sqrt{Z_{j\beta\delta}}\,\langle\Phi|\,c^\dagger_{i\gamma}c_{j\delta}\,|\Phi\rangle\,, \tag{B.6}$$

where $\sqrt{Z_{i\alpha\beta}}$ is the quasiparticle renormalization factor defined through the equation

$$\sum_\gamma \sqrt{Z_{i\alpha\gamma}}\,\langle\Phi|\,c^\dagger_{i\gamma}c_{i\beta}|\Phi\rangle = \langle\Phi|\,\mathcal{P}_i\,c^\dagger_{i\alpha}\,\mathcal{P}_i\,c_{i\beta}|\Phi\rangle\,. \tag{B.7}$$

In what follows we will only consider homogeneous wave functions hence we will drop out the site-index i from the forthcoming expressions. Notice however that the Gutzwiller approximation has been recently extended to deal with inhonogeneous effects [18, 19]

To proceed further it is convenient to define, as independent variational parameters, the correlated local probabilites P_n which are defined in terms

of the original λ_n as

$$P_n = \langle \Psi | n \rangle \langle n | \Psi \rangle = \lambda_n^2 \, p_n \,, \tag{B.8}$$

where in the right-hand side we have used equation (B.5) and we have also introduced the uncorrelated probabilities

$$p_n = \langle \Phi | n \rangle \langle n | \Phi \rangle \,.$$

In terms of these new variational parameters the constraints (B.4) can be easily written as

$$P_0 = 1 - n + P_2 \,, \qquad P_1 \equiv \sum_\sigma P_\sigma = n - 2P_2 \,. \tag{B.9}$$

A simple calculation gives for the uncorrelated probabilities p_n the result

$$\tilde{p}_a = \begin{cases} (1 - n/2)\,(1 - n/2) & a = 0 \\ (1 - n/2)\, n/2 & a = 1 \\ n^2/4 & a = 2 \end{cases}$$

The quasiparticle renormalization factor $\sqrt{Z_{\sigma\,\sigma'}}$ is written in terms of the variational parameters P_n as

$$\sqrt{Z_{\sigma\,\sigma'}} = \delta_{\sigma\,\sigma'} \, \frac{\left(\sqrt{P_0\, P_\sigma} + \sqrt{P_2\, P_{-\sigma}}\right)}{\sqrt{n_\sigma\,(1 - n_\sigma)}} \tag{B.10}$$

from which we get in the case of our interest (and posing $P_2 \equiv D$)

$$Z(D, n) = \frac{2\,(n - 2D)}{n\,(2 - n)} \left(\sqrt{1 - n + D} + \sqrt{D}\right)^2 \tag{B.11}$$

Notice that for D equal to its uncorrelated value ($D = n^2/4$) we correctly get $Z = 1$, independently on the filling n. All in all the variational energy in the most general paramagnetic case reads

$$E\,(D) = UD + \bar{\varepsilon}_n \, Z(D, n) \,, \tag{B.12}$$

where $\bar{\varepsilon}_n$ is the average kinetic energy for Fermi sea with filling n. This quantity can be expressed as an integral over the single particle DoS $\rho(\varepsilon)$

$$\begin{aligned} \bar{\varepsilon}_n &= 2 \int d\varepsilon \, \varepsilon \, \rho(\varepsilon) f(\varepsilon - \mu(n)) \\ n &= 2 \int d\varepsilon \, \rho(\varepsilon) f(\varepsilon - \mu(n)) \end{aligned}$$

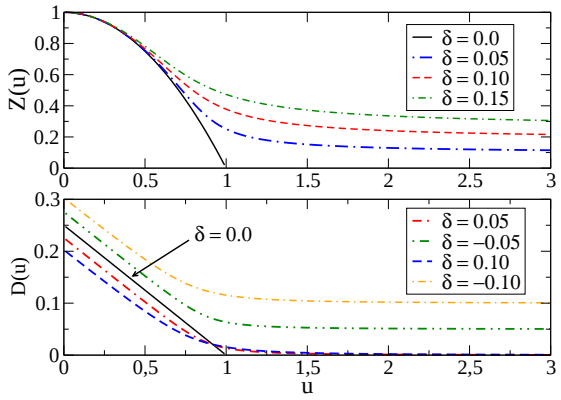

Figure B.2: Gutzwiller equilibrium mean field solution for the single band Hubbard model at zero temperature and finite doping δ. We see that for $\delta \neq 0$ the Mott transition disappears and the system always displays metallic features, such as a finite quasiparticle weight Z even at large u (see top panel) or a finite fraction of doubly occupied sites D (bottom panel).

A simple calculation reveals that $\bar{\varepsilon}_n = \bar{\varepsilon}\, n\,(2-n)$ where $\bar{\varepsilon} < 0$ is the average kinetic energy for an half-filled band. We are now in the position to derive the saddle point equation for the equilibrium double occupancy D. After some algebra we obtain

$$\frac{U}{U_c} = F(D,\delta)\,, \tag{B.13}$$

where the function $F(D,\delta)$ is given by

$$\begin{aligned} F(D,\delta) \;\; = \;\; & \frac{1}{2}\,(1-2\delta) - 2D - \sqrt{D\,(D+\delta)} + \\ & + \frac{(n-2D)\,(2D+\delta)}{4\sqrt{D\,(D+\delta)}} \end{aligned} \tag{B.14}$$

while we have defined $U_c = -8\bar{\varepsilon}$. Let us start discussing the half-filled case $\delta = 0$. As we can see from equation (B.14) in this limit the function $F(D,\delta)$ grealty simplifies and the saddle point equation can be solved analitically. The result reads, by defining $u = U/U_c$,

$$D(u) = \frac{1}{4}\,(1-u)\,. \tag{B.15}$$

From this result, using equation (B.11) we can easily compute the quasipar-

ticle weight $Z(u)$ which reads

$$Z(u) = 1 - u^2 \,. \tag{B.16}$$

Both these functions are plotted in figure B.2 as a function of the correlation strength u (see dashed lines). We see that the Gutzwiller wave function correctly accounts for the decrease of double occupations and quasiparticle weight as the correlation strength u is increased. Moreover, it also features a quantum phase transition, at a critical value of the interaction $u = 1$, between a paramagnetic metal and a paramagnetic Mott insulator which is mimicked, in the Gutzwiller approximation, by a system with zero fraction of doubly occupied sites and a complete suppression of charge fluctuations[1].

As soon as the system is moved away from half-filling due to a finite doping the transition disappears and the system behaves as a correlated metal with a finite amount of double occupations and with a finite quasiparticle weight. This can be seen directly from the expression (B.14). Indeed we see that for any finite doping δ the function $F(D, \delta)$ features a square-root singularity for $D \to 0$ which is cutted off for $\delta = 0$. Due to this peculiar behaviour we can immediately conclude that the critical strength $U_c(\delta)$ to obtain a vanishing double occupancy (and therefore a Mott insulator in the Gutzwiller approximation) is pushed to infinity for any finite δ. A numerical solution of the saddle point equation is plotted in figure B.2 and correctly reproduces the metallic behaviour for any finite u.

B.2 Evaluating the time-derivative on the trial wave function

Let us evaluate the time derivative on the Gutzwiller trial wave function (6.1). By definition this amounts to compute two terms

$$|\partial_t \Psi(t)\rangle = (\partial_t \mathcal{P})\, |\Phi(t)\rangle + \mathcal{P}|\partial_t \Phi(t)\rangle \,.$$

To compute the time-derivative of the operator $\mathcal{P}(t)$ defined as

$$\mathcal{P}(t) = \prod_i e^{-i\mathcal{S}_i(t)} \mathcal{P}_i(t) \tag{B.17}$$

[1] We mention that, strictly speaking, the Gutzwiller metal-insulator transition at half-filling is an artifact of the infinite dimensional limit. Indeed in any finite dimension the Gutzwiller wavefunction (B.1) shows genuine metallic behaviour with a finite quasiparticle weight and no transition. In order to describe variationally the Mott transition in finite dimension a more rich wave function is actually needed [28]

we take its logarithm

$$\mathrm{Log}\,\mathcal{P}(t) = \sum_i e^{-i\mathcal{S}_i(t)}\,\mathcal{P}_i(t)$$

and take the derivative with respect to time

$$\sum_i \frac{d}{dt}\,\mathrm{Log}(e^{-i\mathcal{S}_i(t)}\,\mathcal{P}_i(t)) = \frac{d}{dt}\,\mathrm{Log}\,\mathcal{P}(t) = \mathcal{P}^{-1}(t)\frac{d}{dt}\,\mathcal{P}(t) \tag{B.18}$$

from which we conclude that

$$\frac{d}{dt}\,\mathcal{P}(t) = \left(\sum_i \frac{d}{dt}\,\mathrm{Log}(e^{-i\mathcal{S}_i(t)}\,\mathcal{P}_i(t))\right)\,\mathcal{P}(t)\,, \tag{B.19}$$

where we have used the fact that the operator $\mathcal{P}(t)$ commutes with itself at different times. Using equations (6.2), the result (B.19) can be written also as

$$\frac{d}{dt}\,\mathcal{P}(t) = \left(\sum_{i\alpha} \dot{\lambda}_{i\alpha}\,\mathcal{P}_i^{-1}\mathcal{O}_{i\alpha} - i\dot{\phi}_{i\alpha}\,\mathcal{O}_{i\alpha}\right)\,\mathcal{P}(t) \;\equiv \chi(t)\,\mathcal{P}(t) \tag{B.20}$$

We now will derive the expression (6.7) for the total time derivative of the average energy, given in the main text.

$$\begin{aligned}\frac{d\,E}{dt} \;=\; & \langle\Phi(t)|\chi^\dagger(t)\mathcal{H}|\Phi(t)\rangle + \langle\Phi(t)|\mathcal{H}\chi(t)|\Phi(t)\rangle \\ & + \langle\Phi(t)|\mathcal{H}_\star(t)|\partial_t\Phi(t)\rangle + \langle\partial_t\Phi(t)|\mathcal{H}_\star(t)|\Phi(t)\rangle\end{aligned} \tag{B.21}$$

By using the result for $\chi(t)$ as well as the equation of motion for $\dot{O}_{i\alpha}$, equation (6.5), we can write the first line as

$$\begin{aligned}\langle\Phi(t)|\chi^\dagger(t)\mathcal{H}|\Phi(t)\rangle + \langle\Phi(t)|\mathcal{H}\chi(t)|\Phi(t)\rangle \;=\; \\ \sum_{i\alpha} -\dot{\phi}_{i\alpha}\dot{O}_{i\alpha} + \langle\{\mathcal{P}_i^{-1}\mathcal{O}_{i\alpha},\mathcal{H}\}\rangle\dot{\lambda}_{i\alpha}\,,\end{aligned} \tag{B.22}$$

where in the second line the average is taken with respect to the correlated wave function $|\Psi(t)\rangle$. It is now easy to show, by the same line of reasoning, that

$$\frac{\partial\,\mathcal{P}}{\partial\lambda_{i\alpha}} = \mathcal{P}_i^{-1}\,\mathcal{O}_{i\alpha}\,\mathcal{P}$$

hence the derivative of the energy with respect to $\lambda_{i\alpha}$ reads

$$\frac{\partial E}{\partial\lambda_{i\alpha}} = \langle\{\mathcal{P}_i^{-1}\mathcal{O}_{i\alpha},\mathcal{H}\}\rangle\,. \tag{B.23}$$

Using this last result in equations (B.21) and (B.22) the desired result (6.7) immediately follows by simple chain-rule differentiation.

B.3 Explicit Expression for the Effective Potential

In the main text we have introduced an effective potential $\Gamma(D)$ controlling the dynamics for the double occupation $D(t)$

$$\dot{D} = \pm\sqrt{\Gamma(D)}\,.$$

Its explicit expression reads, from equations (6.33-6.34), $\Gamma\left(D\right) = \Gamma_{+}\left(D\right)\Gamma_{-}\left(D\right)$ where

$$\Gamma_{\pm}\left(D\right) = \pm\left[E_0 - UD - 2\bar{\varepsilon}\left(n-2D\right)\left(\sqrt{D+\delta}\pm\sqrt{D}\right)^2\right]. \tag{B.24}$$

From this expression we notice that, for any u_f, the equilibrium zero temperature Gutzwiller solution $D_0\left(u_i,\delta\right)$ is always an inversion point for the effective potential. Indeed it is easy to show, see equation (B.13), that $\Gamma_{+}\left(D_0\right) = 0$, since by construction $D_0(u_i,\delta)$ satisfies the equation

$$E_0 = u_f\, D_0 + 2\bar{\varepsilon}\left(n-2D_0\right)\left(\sqrt{D_0+\delta}+\sqrt{D_0}\right)^2. \tag{B.25}$$

As a consequence we can write the effective potential as

$$\Gamma\left(D\right) \equiv \left(D-D_0\right)\Phi\left(D\right), \tag{B.26}$$

with $\Phi(D)$ that can be formally written as

$$\Phi\left(D\right) = \gamma_3\, D^2 + \left(\gamma_2 + D_0\gamma_3\right)D + \left(\gamma_1 + D_0\gamma_2 + D_0^2\gamma_3\right) \tag{B.27}$$

once the effective potential $\Gamma(D)$ given in equation (B.24) is written as a polynomial in D. From this result we obtain for the other two inversion points $D_{\pm}$ the following result

$$D_{\mp} = \frac{\left(\gamma_2 + D_0\gamma_3\right) \mp \sqrt{\Delta}}{4u_f}, \tag{B.28}$$

with $\Delta = \left(\gamma_2 + D_0\gamma_3\right)^2 - 4\gamma_3\left(\gamma_1 + D_0\gamma_2 + D_0^2\gamma_3\right)$. The explicit expression for the coefficients γ_a can be easily found after some simple but lengthy algebra. These read

$$\begin{cases} \gamma_3 &= -2u_f \\ \gamma_2 &= -u_f^2 + 2E_0 + u_f\left(1-2\delta\right) - \delta^2/4 \\ \gamma_1 &= 2u_f E_0 + \frac{n\delta^2}{4} + \frac{u_f n\delta}{2} - E_0\left(1-2\delta\right) \end{cases}$$

with E_0 given by Eq. (B.25). Notice that all the dependence from the initial interaction u_i is hidden into the Gutzwiller equilibrium solution $D_0(u_i,\delta)$.

B.4 Phase Dynamics

In this section we will describe in some detail the mean-field dynamics of the phase variable, $\phi(t)$, which is conjugate to the double occupancy $D(t)$. We limit our analysis to the half-filled case which is the most interesting one featuring, as we have discussed, a dynamical transition similar to the one of the simple pendulum.

We start again from the classical dynamics (6.28-6.29) given in the main text and use the integral of motion for the energy soon after the quench E_0

$$E_0 = u_f\, D(t) - \frac{1}{8} Z(t)$$

to express the double occupation D as a function of the phase ϕ. This can be easily done since at half-filling the quasiparticle weight Z acquires the simple form (6.27)

$$Z = 16\, D\, (1/2 - D)\, \cos^2 \phi\,.$$

A simple algebra gives

$$D_\pm = \frac{(cos^2\phi - u_f) \pm \sqrt{\Delta}}{4\, cos^2\phi}\,, \tag{B.29}$$

where Δ reads

$$\Delta = (u_f - cos^2\phi)^2 + 8 cos^2\phi\, E_0(u_i, u_f)\,. \tag{B.30}$$

Using the zero-temperature Gutzwiller approximation described in section B.1 to evaluate the initial energy we get

$$E_0(u_i, u_f) = \frac{u_f}{4}\,(1 - u_i) - \frac{1}{8}\left(1 - u_i^2\right)\,, \qquad u_i \leq 1 \tag{B.31}$$

Note that Eq. (B.31) breaks down in the insulator ($u_i > 1$) where the Gutzwiller solution has exactly zero energy.

From equation (B.29) we get the quasiparticle weight $Z_\pm$ which reads

$$Z_\pm = cos^2\phi \left(1 + \frac{u_f \mp \sqrt{\Delta}}{cos^2\,\phi}\right)\left(1 - \frac{u_f \mp \sqrt{\Delta}}{cos^2\,\phi}\right) \tag{B.32}$$

We can now substitute the result for $D_\pm[\phi]$ into Eq.(6.28) thus obtaining a closed differential equation for the phase $\phi(t)$. Using the fact that

$$\frac{\partial\, Z_{eq}}{\partial D} = 8(1 - 4D) = \frac{8}{cos^2\phi}\left(u_f \mp \sqrt{\Delta}\right) \tag{B.33}$$

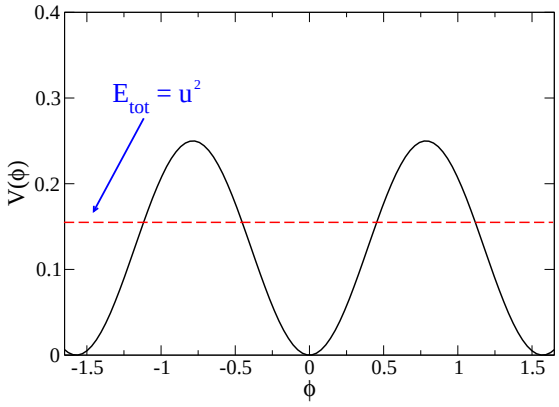

Figure B.3: Effective Potential $F(\phi)$ controlling the dynamics of $\phi(t)$.

and the equation of motion (6.28) we end up with the following dynamics for $\phi(t)$

$$\dot{\phi} = \mp \frac{U_c}{2} \sqrt{F(\phi)}\,, \tag{B.34}$$

describing a single degree of freedom ϕ in a potential $F(\phi)$, see figure B.3,

$$F(\phi) = cos^4\phi + 2\gamma\, cos^2\phi + u_f^2\,, \tag{B.35}$$

where $\gamma = \left(4E_0 - u_f^2\right)$. The regions of ϕ phase space which are classically accessibles are those for which $F(\phi) \geq 0$. It is therefore useful to study the sign and the stationary points of this function. By posing $x = cos^2\phi$ we obtain a second order equation

$$f(x) = x^2 + 2\gamma\, x + u_f^2 \tag{B.36}$$

whose discriminant is $Q = \gamma^2 - u_f^2$. For $Q < 0$ there are no zeros on the real axis and $F(\phi)$ is always positive. In this regime the dynamics for ϕ is not bounded (no inversion points) namely the phases is allowed to reach infinity. As opposite for $Q > 0$ the are inversion points $\phi_\pm$ and the motion for ϕ is periodic in the interval $[\phi_-, \phi_+]$ with period $\mathcal{T}(u_i, u_f)$, see figure B.3.

To get an expression for the inversion points it is useful to find the roots of the equation $f(x) = 0$ for $Q > 0$. These read

$$x_\pm = -\gamma \pm \sqrt{\gamma^2 - u_f^2}\,. \tag{B.37}$$

Using the result for γ, namely

$$\gamma = 4E_0 - u_f^2 = \frac{u_i^2}{2} - u_i\, u_f - \frac{1}{2} \tag{B.38}$$

we can check that only the positive root x_+ can be accepted. Indeed we have to impose that for $u_i = u_f$ no dynamics arises, namely that the phase $\phi = 0$. A simple calculation shows that for $u_i = u_f$

$$x_\pm = \frac{1 + u_i^2}{2} \pm \frac{1 - u_i^2}{2} \tag{B.39}$$

therefore only the positive root is meaningful.

Hence the phase dynamics for $u_f < u_{fc}$ is periodic between two simmetric inversion points $\phi_\pm(u_i, u_f)$ which can be written from equation (B.37) as

$$\phi_\pm = \pm\frac{1}{2} arcsin\xi(u_i, u_f)\,, \tag{B.40}$$

where ξ is defined as

$$\xi(u_i, u_f) = 2\sqrt{\frac{1}{4} - \left[u_i\,(u_f - u_i/2) + \sqrt{\gamma^2 + u_f^2}\right]^2}\,. \tag{B.41}$$

The condition $Q = 0$ identifies a special line of quenches where a pure relaxation dynamics for the phase is possible. Using Eq. (B.31) we obtain for this condition

$$\gamma^2 - u_f^2 = (u_i^2 - 1)\left(u_f^2 - u_i\, u_f + \frac{1}{4}\left(u_i^2 - 1\right)\right) \tag{B.42}$$

Aside from the special value $u_i = 1$, we can solve the quantity in parenthesis for u_f thus obtaining $u_{fc} = \frac{u_i \pm 1}{2}$. We notice that only the $+$ solution is meaningful in the region $u_i \leq 1$ we are considering, hence

$$u_{fc} = \frac{u_i + 1}{2}\,. \tag{B.43}$$

We now show that the critical quench line also corresponds to a change in the stability points of the function $F(\phi)$, resulting into a diverging period $\mathcal{T}$ and therefore into a dynamical transition from oscillation to relaxation. Let us compute the stationary points for the function $F(\phi)$. We get for the first derivative

$$\frac{\partial F}{\partial \phi} = -2sin\,2\phi\left(\gamma + cos^2\phi\right)\,, \tag{B.44}$$

which vanishes at $\phi = 0, \pi/2$ as well at $\pm\phi_\star$ such that

$$cos^2\phi_\star = -\gamma\,. \tag{B.45}$$

By computing the second derivative we get

$$\frac{\partial^2 F}{\partial \phi^2} = 2sin^2\, 2\phi - 4cos\, 2\phi \left(\gamma + cos^2\phi\right) \tag{B.46}$$

from which we can conclude that for $\gamma \in [-1, 0]$, which is always the case in the region we are considering $u_i < 1, u_f \leq u_f^c$, $\phi_\star$ is the only minimum while $0, \pi/2$ are maxima.

A dynamical transition occurs whenever the minimum $\phi_\star$ and the inversion point ϕ_+ given in equation (B.40) merge. Indeed if this happens the inversion point changes from a single to a double root of the equation $F(\phi) = 0$ thus resulting into a logarithmic singularity for the period $\mathcal{T}$ which is given by

$$\mathcal{T} = \frac{8}{U_c} \int_0^{\phi_+} \frac{d\phi}{\sqrt{F(\phi)}}\,. \tag{B.47}$$

The condition therefore reads $F(\phi_\star) = 0$ which gives us, when substituted in Eq.(B.35),

$$u_f^2 - \gamma^2 = Q = 0\,. \tag{B.48}$$

We see therefore that the condition $Q = 0$, namely $u_f = u_{fc}$, corresponds to a diverging time scale and to the onset of a relaxation dynamics. Finally we note that, upon inserting our definition for γ in terms of the conserved energy E_0 we obtain for the condition $Q = 0$ the result

$$u_f^2 - \gamma^2 = 8E_0\left(2E_0 - u_f\right)\,, \tag{B.49}$$

which stress the fact that, along the critical line $u_f = u_f^c$ the initial energy vanishes. Notice that the condition $E_0 = u_f/2$ does not introduce novel solutions but only gives us back the solution $u_f = (u_i - 1)/2$ which we have already rejected.

B.5 Elliptic Integrals

In this appendix we give some useful result on elliptic integrals. The elliptic integral of the firts kind, $F\left(\varphi, k\right)$ is defined as

$$F\left(\varphi, k\right) = \int_0^{\varphi} d\theta \frac{1}{\sqrt{1 - k^2\, sin^2\theta}}\,, \tag{B.50}$$

with $k^2 < 1$ being the *modulus* and $k' = \sqrt{1 - k^2}$ the *complementary modulus*. Similarly the elliptic integral of the second kind reads

$$E\left(\varphi, k\right) = \int_0^{\varphi} d\theta \sqrt{1 - k^2\, sin^2\theta}\,. \tag{B.51}$$

The complete elliptic integrals, of the first and second kind, are obtained when the argument φ is equal to $\pi/2$, namely

$$K(k) = F(\pi/2, k) \qquad E(k) = E(\pi/2, k) \ . \tag{B.52}$$

In the main text we have used the following results on definite integrals. For $a > u \geq b > c$ we have

$$\int_u^a \frac{dx}{\sqrt{(a-x)(x-b)(x-c)}} = \frac{2}{\sqrt{a-c}} F(\lambda, p) \ , \tag{B.53}$$

and similarly

$$\begin{aligned} \int_u^a \frac{xdx}{\sqrt{(a-x)(x-b)(x-c)}} &= \frac{2c}{\sqrt{a-c}} F(\lambda, p) + \\ &+ \sqrt{a-c}\, E(\lambda, p) \ , \end{aligned}$$

with $\lambda = \arcsin\left(\sqrt{\frac{a-u}{a-b}}\right)$ and $p = \sqrt{\frac{a-b}{a-c}}$.

Bibliography

[1] A. Abrikosov, I. Dzjaloshinsky, and L. Gorkov. *Methods of Quantum Field Theory in Statistical Mechanics*. Dover, 1963.

[2] I. L. Aleiner, P. W. Brouwer, and L. I. Glazman. Quantum effects in coulomb blockade. *Physics Reports*, 358(5-6):309 – 440, 2002.

[3] F. B. Anders. Steady-state currents through nanodevices: A scattering-states numerical renormalization-group approach to open quantum systems. *Phys. Rev. Lett.*, 101(6):066804, Aug 2008.

[4] F. B. Anders, R. Bulla, and M. Vojta. Equilibrium and nonequilibrium dynamics of the sub-ohmic spin-boson model. *Phys. Rev. Lett.*, 98:210402, 2007.

[5] F. B. Anders and A. Schiller. Real-time dynamics in quantum-impurity systems: A time-dependent numerical renormalization-group approach. *Phys. Rev. Lett.*, 95:196801, 2005.

[6] F. B. Anders and A. Schiller. Spin precession and real-time dynamics in the Kondo model:time-dependent numerical renormalization-group study. *Phys. Rev. B*, 74(24):245113, Dec 2006.

[7] M. H. Anderson, J. R. Ensher, M. R. Matthews, C. E. Wieman, and E. A. Cornell. Observation of Bose-Einstein Condensation in a Dilute Atomic Vapor. *Science*, 269(5221):198–201, 1995.

[8] P. W. Anderson. Localized magnetic states in metals. *Phys. Rev.*, 124:41, 1961.

[9] P. W. Anderson. The Resonating Valence Bond State in La2CuO4 and Superconductivity . *Science*, 235:1196–1198, 1987.

[10] R. Avriller and A. Levy Yeyati. Electron-phonon interaction and full counting statistics in molecular junctions. *Phys. Rev. B*, 80(4):041309, Jul 2009.

[11] P. Barmettler, M. Punk, V. Gritsev, E. Demler, and E. Altman. Relaxation of antiferromagnetic order in spin-1/2 chains following a quantum quench. *Phys. Rev. Lett.*, 102:130603, 2009.

[12] P. Barmettler, M. Punk, V. Gritsev, E. Demler, and E. Altman. Quantum quenches in the anisotropic spin-1/2 heisenberg chain: different approaches to many-body dynamics far from equilibrium. *New Journal of Physics*, 12(5):055017, 2010.

[13] J. Berges. Introduction to nonequilibrium quantum field theory. *arXiv:hep-ph/0409233*, 2004.

[14] J. Berges, S. Borsányi, and C. Wetterich. Prethermalization. *Phys. Rev. Lett.*, 93(14):142002, Sep 2004.

[15] J. Berges, A. Rothkopf, and J. Schmidt. Nonthermal fixed points: Effective weak coupling for strongly correlated systems far from equilibrium. *Phys. Rev. Lett.*, 101(4):041603, Jul 2008.

[16] G. Biroli, C. Kollath, and A. M. Lauchli. Does thermalization occur in an isolated system after a global quantum quench. *arXiv:0907.3731v1*, 2009.

[17] I. Bloch, J. Dalibard, and W. Zwerger. Many-body physics with ultracold gases. *Rev. Mod. Phys.*, 80:885, 2008.

[18] G. Borghi, M. Fabrizio, and E. Tosatti. Surface dead layer for quasiparticles near a Mott transition. *Phys. Rev. Lett.*, 102(6):066806, Feb 2009.

[19] G. Borghi, M. Fabrizio, and E. Tosatti. Strongly correlated metal interfaces in the gutzwiller approximation. *Phys. Rev. B*, 81(11):115134, Mar 2010.

[20] E. Boulat, H. Saleur, and P. Schmitteckert. Twofold advance in the theoretical understanding of far-from-equilibrium properties of interacting nanostructures. *Phys. Rev. Lett.*, 101(14):140601, Sep 2008.

[21] C. C. Bradley, C. A. Sackett, J. J. Tollett, and R. G. Hulet. Evidence of Bose-Einstein Condensation in an Atomic Gas with Attractive Interactions. *Phys. Rev. Lett.*, 75(9):1687–1690, Aug 1995.

[22] W. F. Brinkman and T. M. Rice. Application of Gutzwiller's Variational Method to the Metal-Insulator Transition. *Phys. Rev. B*, 2:4302, 1970.

[23] R. Bulla, T. A. Costi, and T. Pruschke. Numerical renormalization group method for quantum impurity systems. *Rev. Mod. Phys.*, 80:395, 2008.

[24] J. Bünemann, W. Weber, and F. Gebhard. Multiband Gutzwiller wave functions for general on-site interactions. *Phys. Rev. B*, 57:6896, 1998.

[25] P. Calabrese and J. Cardy. Time dependence of correlation functions following a quantum quench. *Phys. Rev. Lett.*, 96(13):136801, Apr 2006.

[26] A. O. Caldeira and A. J. Leggett. Influence of dissipation on quantum tunneling in macroscopic systems. *Phys. Rev. Lett.*, 46:211, 1981.

[27] E. A. Calzetta and B.-L. B. Hu. *Non Equilibrium Quantum Field Theory.* Cambridge University Press, 2008.

[28] M. Capello, F. Becca, M. Fabrizio, S. Sorella, and E. Tosatti. Variational Description of Mott Insulators. *Phys. Rev. Lett.*, 94(2):026406, Jan 2005.

[29] F. Carbone, D. S. Yanga, E. Giannini, and A. Zewail. Direct role of structural dynamics in electron-lattice coupling of superconducting cuprates. *Proc. Natl. Acad. Sci. USA*, 105, 2008.

[30] M. A. Cazalilla. Effect of suddenly turning on interactions in the luttinger model. *Phys. Rev. Lett.*, 97:156403, 2006.

[31] M. A. Cazalilla and M. Rigol. Focus on dynamics and thermalization in isolated quantum many-body systems. *New Journal of Physics*, 12(5):055006, 2010.

[32] K. Chen and C. Jayaprakash. Kondo effect in Fermi systems with a gap: A renormalization-group study. *Phys. Rev. B*, 57:5225, 1998.

[33] P. S. Cornaglia, G. Usaj, and C. A. Balseiro. Localized spins on graphene. *Phys. Rev. Lett.*, 102:046801, 2009.

[34] G. Coslovich *et al.* Inducing a superconducting-to-normal-state first-order phase transition in overdoped BiSCYCO by ultrashort laser pulses. *arXiv:1005.4320*, 2010.

[35] P. Courteille, R. S. Freeland, D. J. Heinzen, F. A. van Abeelen, and B. J. Verhaar. Observation of a Feshbach Resonance in Cold Atom Scattering. *Phys. Rev. Lett.*, 81(1):69–72, Jul 1998.

[36] S. M. Cronenwett, T. H. Oosterkamp, and L. P. Kouwenhoven. A Tunable Kondo Effect in Quantum Dots. *Science*, 281(5376):540–544, 1998.

[37] G. Cuniberti, G. Fagas, and K. Richter. *Introducing Molecular Electronic*. Springer Berlin and Hedelberg, 2005.

[38] A. Damascelli, Z. Hussain, and Z.-X. Shen. Angle-resolved photoemission studies of the cuprate superconductors. *Rev. Mod. Phys.*, 75(2):473–541, Apr 2003.

[39] A. Das, K. Sengupta, D. Sen, and B. K. Chakrabarti. Infinite-range Ising ferromagnet in a time-dependent transverse magnetic field: Quench and ac dynamics near the quantum critical point. *Phys. Rev. B*, 74(14):144423, Oct 2006.

[40] K. B. Davis, M. O. Mewes, M. R. Andrews, N. J. van Druten, D. S. Durfee, D. M. Kurn, and W. Ketterle. Bose-Einstein Condensation in a Gas of Sodium Atoms. *Phys. Rev. Lett.*, 75(22):3969–3973, Nov 1995.

[41] C. De Grandi, V. Gritsev, and A. Polkovnikov. Quench dynamics near a quantum critical point. *Phys. Rev. B*, 81:012303, 2010.

[42] B. DeMarco and D. S. Jin. Onset of Fermi Degeneracy in a Trapped Atomic Gas. *Science*, 285(5434):1703–1706, 1999.

[43] J. M. Deutsch. Quantum statistical mechanics in a closed system. *Phys. Rev. A*, 43(4):2046–2049, Feb 1991.

[44] B. Doyon and N. Andrei. Universal aspects of nonequilibrium currents in a quantum dot. *Phys. Rev. B*, 73:245326, 2006.

[45] P. Dutt, J. Koch, J. E. Han, and K. Le Hur. Effective Equilibrium Description of Nonequilibrium Quantum Transport I: Fundamentals and Methodology. *ArXiv:1004.5591*, Apr. 2010.

[46] J. Eckel, F. Heidrich-Meisner, S. G. Jakobs, M. Thorwart, M. Pletyukhov, and R. Egger. Comparative study of theoretical methods for non-equilibrium quantum transport. *New Journal of Physics*, 12(4):043042, 2010.

[47] M. Eckstein and M. Kollar. Nonthermal steady states after an interaction quench in the falicov-kimball model. *Phys. Rev. Lett.*, 100:120404, 2008.

[48] M. Eckstein, M. Kollar, and P. Werner. Thermalization after an interaction quench in the Hubbard model. *Phys. Rev. Lett.*, 103:056403, 2009.

[49] M. Eckstein, M. Kollar, and P. Werner. Interaction quench in the Hubbard model: Relaxation of the spectral function and the optical conductivity. *Phys. Rev. B*, 81(11):115131, Mar 2010.

[50] Eckstein, M., Hackl, A., Kehrein, S., Kollar, M., Moeckel, M., Werner, P., and Wolf, F.A. New theoretical approaches for correlated systems in nonequilibrium. *Eur. Phys. J. Special Topics*, 180:217–235, 2009.

[51] R. Egger and A. O. Gogolin. Vibration-induced correction to the current through a single molecule. *Phys. Rev. B*, 77(14):146404, 2008.

[52] R. Egger, L. Mühlbacher, and C. H. Mak. Path-integral monte carlo simulations without the sign problem: Multilevel blocking approach for effective actions. *Phys. Rev. E*, 61:5961, 2000.

[53] O. Entin-Wohlman, Y. Imry, and A. Aharony. Voltage-induced singularities in transport through molecular junctions. *Phys. Rev. B*, 80(3):035417, Jul 2009.

[54] O. Entin-Wohlman, Y. Imry, and A. Aharony. Transport through molecular junctions with a nonequilibrium phonon population. *Phys. Rev. B*, 81(11):113408, Mar 2010.

[55] M. Fabrizio. Gutzwiller description of non-magnetic Mott insulators: dimer lattice model. *Phys. Rev. B*, 76:165110, 2007.

[56] R. P. Feynmann. *Statistical Mechanics: A Set of Lectures*. Westview Press, 1998.

[57] K. Flensberg. Tunneling broadening of vibrational sidebands in molecular transistors. *Phys. Rev. B*, 68(20):205323, Nov 2003.

[58] J. K. Freericks, V. M. Turkowski, and V. Zlatić. Nonequilibrium dynamical mean-field theory. *Phys. Rev. Lett.*, 97:266408, 2006.

[59] P. Fritsch and S. Kehrein. Non-equilibrium scaling analysis of the Kondo model with voltage bias. *Annals of Physics*, 324(5):1105 – 1135, 2009.

[60] P. Fritsch and S. Kehrein. Nonequilibrium Kondo model with voltage bias in a magnetic field. *Phys. Rev. B*, 81(3):035113, Jan 2010.

[61] M. Galperin, M. A. Ratner, and A. Nitzan. Molecular transport junctions: vibrational effects. *Journal of Physics: Condensed Matter*, 19(10):103201, 2007.

[62] M. R. Galpin and D. E. Logan. Anderson impurity model in a semiconductor. *Phys. Rev. B*, 77:195108, 2008.

[63] T. Gasenzer, S. Kessler, and J. Pawlowski. Far-from-equilibrium quantum many-body dynamics. *arXiv:1003.4163*, 2010.

[64] M. Gell-Mann and F. Low. Bound states in quantum field theory. *Phys. Rev.*, 84(2):350–354, Oct 1951.

[65] A. Georges, G. Kotliar, W. Krauth, and M. J. Rozenberg. Dynamical mean-field theory of strongly correlated fermion systems and the limit of infinite dimensions. *Rev. Mod. Phys.*, 68:13, 1996.

[66] C. Giannetti, G. Coslovich, F. Cilento, G. Ferrini, H. Eisaki, N. Kaneko, M. Greven, and F. Parmigiani. Discontinuity of the ultrafast electronic response of underdoped superconducting BiSCCO strongly excited by ultrashort light pulses. *Phys. Rev. B*, 79:224502, 2009.

[67] C. Giannetti, G. Zgrablic, C. Consani, A. Crepaldi, D. Nardi, G. Ferrini, G. Dhalenne, A. Revcolevschi, and F. Parmigiani. Disentangling thermal and nonthermal excited states in a charge-transfer insulator by time- and frequency-resolved pump-probe spectroscopy. *Phys. Rev. B*, 80(23):235129, Dec 2009.

[68] A. Giraud and J. Serreau. Decoherence and thermalization of a pure quantum state in quantum field theory. *Phys. Rev. Lett.*, 104(23):230405, Jun 2010.

[69] L. I. Glazman and M. E. Raikh. Resonant Kondo transparency of a barrier with quasilocal impurity states. *JETP Lett.*, 47:452, 1988.

[70] L. I. Glazman and R. I. Shekhter. Phonon-assisted resonant tunneling. *Solid State Communications*, 66(1):65 – 69, 1988.

[71] D. Goldhaber-Gordon, J. Göres, M. A. Kastner, H. Shtrikman, D. Mahalu, and U. Meirav. From the Kondo Regime to the Mixed-Valence Regime in a Single-Electron Transistor. *Phys. Rev. Lett.*, 81:5225, 1998.

[72] D. Goldhaber-Gordon *et al.* Kondo effect in a single-electron transistor. *Nature*, 391:156, 1998.

[73] C. Gonzalez-Buxton and K. Ingersent. Renormalization-group study of Anderson and Kondo impurities in gapless Fermi systems. *Phys. Rev. B*, 57:14254, 1998.

[74] M. Greiner, O. Mandel, T. Esslinger, T. Hansch, and I. Bloch. Quantum phase transition from a superfluid to a Mott Insulator in a gas of ultracold atoms. *Nature*, 415:39, 2002.

[75] M. Greiner, O. Mandel, T. Hansch, and I. Bloch. Collapse and revival of the matter wave field of a Bose-Einstein condensate. *Nature*, 419:51, 2002.

[76] M. Grobis, I. G. Rau, R. M. Potok, H. Shtrikman, and D. Goldhaber-Gordon. Universal Scaling in Nonequilibrium Transport through a Single Channel Kondo Dot. *Phys. Rev. Lett.*, 100(24):246601, Jun 2008.

[77] E. Gull. *Continuous-Time Quantum Monte Carlo Algorithms for Fermions*. PhD Thesis, ETH Zurich, 2008.

[78] S. Gustavsson, R. Leturcq, M. Studer, I. Shorubalko, T. Ihn, K. Ensslin, D. Driscoll, and A. Gossard. Electron counting in quantum dots. *Surface Science Reports*, 64:191 – 232, 2009.

[79] M. C. Gutzwiller. Effect of correlation on the ferromagnetism of transition metals. *Phys. Rev. Lett.*, 10:159, 1963.

[80] M. C. Gutzwiller. Correlation of electrons in a narrow s band. *Phys. Rev.*, 137:A1726, 1965.

[81] A. Hackl and S. Kehrein. Real time evolution in quantum many-body systems with unitary perturbation theory. *Phys. Rev. B*, 78:092303, 2008.

[82] A. Hackl and S. Kehrein. A unitary perturbation theory approach to real-time evolution problems. *Journal of Physics: Condensed Matter*, 21(1):015601, 2009.

[83] A. Hackl, D. Roosen, S. Kehrein, and W. Hofstetter. Nonequilibrium spin dynamics in the ferromagnetic Kondo model. *Phys. Rev. Lett.*, 102(19):196601, May 2009.

[84] E. Haller, M. Gustavsson, M. J. Mark, J. G. Danzl, R. Hart, G. Pupillo, and H.-C. Nagerl. Realization of an Excited, Strongly Correlated Quantum Gas Phase. *Science*, 325(5945):1224–1227, 2009.

[85] J. E. Han. Imaginary-time formulation of steady-state nonequilibrium in quantum dot models. *Phys. Rev. B*, 81(24):245107, Jun 2010.

[86] K. Haule. Quantum monte carlo impurity solver for cluster dynamical mean-field theory and electronic structure calculations with adjustable cluster base. *Phys. Rev. B*, 75:155113, 2007.

[87] F. Haupt, T. c. v. Novotný, and W. Belzig. Phonon-assisted current noise in molecular junctions. *Phys. Rev. Lett.*, 103(13):136601, Sep 2009.

[88] F. Hedrich-Meisner, A. E. Feiguin, and E. Dagotto. Real-time simulations of nonequilibrium transport in the single-impurity anderson model. *Phys. Rev. B*, 79:235336, 2009.

[89] S. Hershfield. Reformulation of steady state nonequilibrium quantum statistical mechanics. *Phys. Rev. Lett.*, 70(14):2134–2137, Apr 1993.

[90] M. Heyl and S. Kehrein. The crooks relation in optical spectra - universality in work distributions for weak local quenches. *arXiv:1006.3522*, 2010.

[91] J. Hubbard. Electron correlations in narrow energy bands. *Proceedings of the Royal Society of London. Series A. Mathematical and Physical Sciences*, 276(1365):238–257, 1963.

[92] S. D. Huber and A. Rüegg. Dynamically generated double occupancy as a probe of cold atom systems. *Phys. Rev. Lett.*, 102:065301, 2009.

[93] S. Inoye *et al.* Observation of Feshbach resonances in a Bose-Einstein condensate. *Nature*, 392:151, 1998.

[94] A. Iucci and M. A. Cazalilla. Quantum quench dynamics of the luttinger model. *Phys. Rev. A*, 80(6):063619, Dec 2009.

[95] R. C. Jaklevic and J. Lambe. Molecular vibration spectra by electron tunneling. *Phys. Rev. Lett.*, 17(22):1139, Nov 1966.

[96] R. Jordens, N. Strohmaier, K. Gunter, H. Moritz, and T. Esslinger. A Mott insulator of fermionic atoms in optical lattices. *Nature*, 451, 2008.

[97] L. P. Kadanoff and G. Baym. *Quantum Statistical Mechanics.* Benjamin, New York, 1962.

[98] A. Kamenev. Keldysh technique and non-linear sigma-model: basic principles and applications. *Advances in Physics*, 58, 2009.

[99] A. Kaminski, Y. V. Nazarov, and L. I. Glazman. Suppression of the Kondo effect in a quantum dot by external irradiation. *Phys. Rev. Lett.*, 83(2):384–387, Jul 1999.

[100] A. Kaminski, Y. V. Nazarov, and L. I. Glazman. Universality of the Kondo effect in a quantum dot out of equilibrium. *Phys. Rev. B*, 62(12):8154–8170, Sep 2000.

[101] J. Kanamori. Electron correlation and ferromagnetism of transition metals. *Progress of Theoretical Physics*, 30(3):275–289, 1963.

[102] C. Karrasch, S. Andergassen, M. Pletyukhov, D. Schuricht, L. Borda, V. Meden, and H. Schoeller. Non-equilibrium current and relaxation dynamics of a charge-fluctuating quantum dot. *EPL (Europhysics Letters)*, 90(3):30003, 2010.

[103] S. Kehrein. Scaling and decoherence in the nonequilibrium Kondo model. *Phys. Rev. Lett.*, 95(5):056602, Jul 2005.

[104] K. Keiter and G. Morandi. Nca. *Phys. Rep*, 109, 1984.

[105] L. V. Keldysh. *Sov. Phys. JETP*, 20:1018, 1964.

[106] T. Kinoshita, T. Wenger, and D. S. Weiss. A quantum Newton's cradle. *Nature*, 440:900, 2006.

[107] S. Kirino, T. Fujii, J. Zhao, and K. Ueda. Time-dependent dmrg study on quantum dot under a finite bias voltage. *Journal of the Physical Society of Japan*, 77(8):084704, 2008.

[108] C. Kollath, A. M. Läuchli, and E. Altman. Quench dynamics and nonequilibrium phase diagram of the Bose-Hubbard model. *Phys. Rev. Lett.*, 98:180601, 2007.

[109] F. Krausz and M. Ivanov. Attosecond physics. *Rev. Mod. Phys.*, 81(1):163–234, Feb 2009.

[110] L. D. Landau and E. M. Lifshitz. *Physical Kinetics.* 1995.

[111] L. D. Landau and E. M. Lifshitz. *Statistical Physics, Part I.* 1995.

[112] P. A. Lee, N. Nagaosa, and X.-G. Wen. Doping a Mott insulator: Physics of high-temperature superconductivity. *Rev. Mod. Phys.*, 78(1):17–85, Jan 2006.

[113] D. Lobaskin and S. Kehrein. Crossover from nonequilibrium to equilibrium behavior in the time-dependent Kondo model. *Phys. Rev. B*, 71:193303, 2005.

[114] S. K. Ma. *Statistical Mechanics*. World Scientific, Singapore, 1985.

[115] G. Mahan. *Many-Particle Physics*. Plenum Press, 1990.

[116] S. R. Manmana, S. Wessel, R. M. Noack, and A. Muramatsu. Strongly correlated fermions after a quantum quench. *Phys. Rev. Lett.*, 98:210405, 2007.

[117] M. Marchi, S. Azadi, M. Casula, and S. Sorella. Resonating valence bond wave function with molecular orbitals: Application to first-row molecules. *The Journal of Chemical Physics*, 131(15):154116, 2009.

[118] P. Mehta and N. Andrei. Nonequilibrium transport in quantum impurity models: The bethe ansatz for open systems. *Phys. Rev. Lett.*, 96(21):216802, Jun 2006.

[119] Y. Meir and N. S. Wingreen. Landauer formula for the current through an interacting electron region. *Phys. Rev. Lett.*, 68(16):2512–2515, Apr 1992.

[120] N. Metropolis, A. W. Rosenbluth, M. N. Rosenbluth, A. H. Teller, and E. Teller. Equation of state calculations by fast computing machines. *J. Chem. Phys*, 21:120603, 1953.

[121] A. N. Michael Galperin, Mark A. Ratner. Hysteresis, switching, and negative differential resistance in molecular junctions: A polaron model. *Nano Letters*, 5, 2005.

[122] A. Mitra, I. Aleiner, and A. J. Millis. Phonon effects in molecular transistors: Quantal and classical treatment. *Phys. Rev. B*, 69(24):245302, Jun 2004.

[123] A. Mitra, I. Aleiner, and A. J. Millis. Semiclassical analysis of the nonequilibrium local polaron. *Physical Review Letters*, 94:076404, 2005.

[124] M. Moeckel. Real-time evolution of quenched quantum systems. *PhD Thesis*, 2009.

[125] M. Moeckel and S. Kehrein. Interaction quench in the Hubbard model. *Phys. Rev. Lett.*, 100:175702, 2008.

[126] M. Moeckel and S. Kehrein. Real-time evolution for weak interaction quenches in quantum systems. *Annals of Physics*, 324(10):2146 – 2178, 2009.

[127] L. Mühlbacher and E. Rabani. Real-time path integral approach to nonequilibrium many-body quantum systems. *Phys. Rev. Lett.*, 100:176403, 2008.

[128] K. A. Muller and B. G. J. The discovery of a class of high-temperature superconductors. *Science*, 237:1133–1139, 1987.

[129] Y. Nazarov and Y. Blanter. *Quantum Transport: Introduction to Nanoscience*. Cambridge University Press, 2009.

[130] A. C. Neto, V. Kotov, J. Nilsson, V. Pereira, N. Peres, and B. Uchoa. Adatoms in graphene. *Solid State Comm.*, 149:1094 – 1100, 2009. Recent Progress in Graphene Studies.

[131] T. K. Ng and P. A. Lee. On-site coulomb repulsion and resonant tunneling. *Phys. Rev. Lett.*, 61(15):1768–1771, Oct 1988.

[132] P. Nordlander, M. Pustilnik, Y. Meir, N. S. Wingreen, and D. C. Langreth. How Long Does It Take for the Kondo Effect to Develop? *Phys. Rev. Lett.*, 83:808, 1999.

[133] P. Nozières. A "fermi-liquid" description of the Kondo problem at low temperatures. *Journal of Low Temperature Physics*, 17:31, 1974.

[134] P. Noziéres and C. T. De Domincis. Singularities in the x-ray absorption and emission of metals. iii. one-body theory exact solution. *Phys. Rev.*, 178:1097, 1969.

[135] A. Oguri. Fermi liquid theory for the nonequilibrium Kondo effect at low bias voltages. *J. Phys. Soc. Jpn.*, 74:117, 2005.

[136] A. Paramekanti, M. Randeria, and N. Trivedi. Projected wave functions and high temperature superconductivity. *Phys. Rev. Lett.*, 87(21):217002, Nov 2001.

[137] H. Park *et al.* Nanomechanical oscillations in a single-c60 transistor. *Nature*, 407:57, 2000.

[138] J. Park *et al.* Coulomb blockade and the Kondo effect in single-atom transistors. *Nature*, 417:722, 2002.

[139] A. N. Pasupathy, A. Pushp, K. K. Gomes, C. V. Parker, J. Wen, Z. Xu, G. Gu, S. Ono, Y. Ando, and A. Yazdani. Electronic Origin of the Inhomogeneous Pairing Interaction in the High-Tc Superconductor BiSCCO. *Science*, 320(5873):196–201, 2008.

[140] M. Paulsson, T. Frederiksen, H. Ueba, N. Lorente, and M. Brandbyge. Unified description of inelastic propensity rules for electron transport through nanoscale junctions. *Phys. Rev. Lett.*, 100(22):226604, 2008.

[141] L. Perfetti, P. A. Loukakos, M. Lisowski, U. Bovensiepen, H. Berger, S. Biermann, P. S. Cornaglia, A. Georges, and M. Wolf. Time Evolution of the Electronic Structure of 1T-TaS2 through the Insulator-Metal Transition. *Phy. Rev. Lett.*, 97:067402, 2006.

[142] B. Persson. Inelastic vacuum tunneling. *Phys. Scr.*, 38(2):282, 1988.

[143] M. Pletyukhov, D. Schuricht, and H. Schoeller. Relaxation versus decoherence: Spin and current dynamics in the anisotropic Kondo model at finite bias and magnetic field. *Phys. Rev. Lett.*, 104(10):106801, Mar 2010.

[144] A. I. Poteryaev, M. Ferrero, A. Georges, and O. Parcollet. Effect of crystal-field splitting and interband hybridization on the metal-insulator transitions of strongly correlated systems. *Phys. Rev. B*, 78:045115, 2008.

[145] N. Prokof'ev and B. Svistunov. Bold diagrammatic monte carlo technique: When the sign problem is welcome. *Phys. Rev. Lett.*, 99:250201, 2007.

[146] N. V. Prokof'ev and B. V. Svistunov. Polaron problem by diagrammatic quantum monte carlo. *Phys. Rev. Lett.*, 81:2514, 1998.

[147] J. Rammer. *Quantum Field Theory of Nonequilibrium States*. Cambridge University Press, 2007.

[148] M. Rigol. Breakdown of thermalization in finite one-dimensional systems. *Phys. Rev. Lett.*, 103(10):100403, Sep 2009.

[149] M. Rigol, V. Dunjko, and M. Olshanii. Thermalization and its mechanism for generic isolated quantum systems. *Nature*, 452, 2008.

[150] M. Rigol, V. Dunjko, V. Yurovsky, and M. Olshanii. Relaxation in a completely integrable many-body quantum system: An ab initio study of the dynamics of the highly excited states of 1d lattice hard-core bosons. *Phys. Rev. Lett.*, 98(5):050405, Feb 2007.

[151] R.-P. Riwar and T. L. Schmidt. Transient dynamics of a molecular quantum dot with a vibrational degree of freedom. *Phys. Rev. B*, 80(12):125109, Sep 2009.

[152] N. Roch, S. Florens, V. Bouchiat, W. Wernsdorfer, and F. Balestro. Quantum phase transition in a single-molecule quantum dot. *Nature*, 453, 2008.

[153] A. Rosch, J. Kroha, and P. Wölfle. Kondo effect in quantum dots at high voltage: Universality and scaling. *Phys. Rev. Lett.*, 87(15):156802, Sep 2001.

[154] A. Rosch, J. Paaske, J. Kroha, and P. Wölfle. Nonequilibrium transport through a Kondo dot in a magnetic field: Perturbation theory and poor man's scaling. *Phys. Rev. Lett.*, 90(7):076804, Feb 2003.

[155] A. Rosch, D. Rasch, B. Binz, and M. Vojta. Metastable superfluidity of repulsive fermionic atoms in optical lattices. *Phys. Rev. Lett.*, 101:265301, 2008.

[156] D. Rossini, A. Silva, G. Mussardo, and G. E. Santoro. Effective thermal dynamics following a quantum quench in a spin chain. *Phys. Rev. Lett.*, 102:127204, 2009.

[157] D. Rossini, A. Silva, G. Mussardo, and G. E. Santoro. Long time dynamics following a quench in an integrable quantum spin chain: local versus non-local operators and effective thermal behavior. *arXiv:1002.2842*, 2010.

[158] G. Roux. Quenches in quantum many-body systems: One-dimensional Bose-Hubbard model reexamined. *Phys. Rev. A*, 79(2):021608, Feb 2009.

[159] A. N. Rubtsov, V. V. Savkin, and A. I. Lichtenstein. Continuous-time quantum monte carlo method for fermions. *Phys. Rev. B*, 72:035122, 2005.

[160] A. Rüegg, S. D. Huber, and M. Sigrist. Z2-slave-spin theory for strongly correlated fermions. *Phys. Rev. B*, 81:155118, 2010.

[161] M. Schiró. Real-time dynamics in quantum impurity models with diagrammatic monte carlo. *Phys. Rev. B*, 81(8):085126, Feb 2010.

[162] M. Schiró and M. Fabrizio. Real-time diagrammatic monte carlo for nonequilibrium quantum transport. *Phys. Rev. B*, 79:153302, 2009.

[163] M. Schirò and M. Fabrizio. *in preparation*, 2010.

[164] M. Schiro' and M. Fabrizio. Time dependent mean field theory for quench dynamics in correlated electron systems. *arXiv:1005.0992*, 2010.

[165] R. Schleser, E. Ruh, T. Ihn, K. Ensslin, D. C. Driscoll, and A. C. Gossard. Time-resolved detection of individual electrons in a quantum dot. *Applied Physics Letters*, 85:2005–2007, 2004.

[166] T. L. Schmidt and A. Komnik. Charge transfer statistics of a molecular quantum dot with a vibrational degree of freedom. *Phys. Rev. B*, 80(4):041307, Jul 2009.

[167] U. Schneider, L. Hackermuller, S. Will, T. Best, I. Bloch, T. A. Costi, R. W. Helmes, D. Rasch, and A. Rosch. Metallic and Insulating Phases of Repulsively Interacting Fermions in a 3D Optical Lattice. *Science*, 322(5907):1520–1525, 2008.

[168] H. Schoeller and F. Reininghaus. Real-time renormalization group in frequency space: A two-loop analysis of the nonequilibrium anisotropic Kondo model at finite magnetic field. *Phys. Rev. B*, 80(4):045117, Jul 2009.

[169] F. Schreck, L. Khaykovich, K. L. Corwin, G. Ferrari, T. Bourdel, J. Cubizolles, and C. Salomon. Quasipure Bose-Einstein Condensate Immersed in a Fermi Sea. *Phys. Rev. Lett.*, 87(8):080403, Aug 2001.

[170] J. Schwinger. Brownian motion of a quantum oscillator. *Journal of Mathematical Physics*, 2(3):407–432, 1961.

[171] A. Silva. Statistics of the work done on a quantum critical system by quenching a control parameter. *Phys. Rev. Lett.*, 101:120603, 2008.

[172] R. H. M. Smit, Y. Noat, C. Untiedt, N. D. Lang, M. C. van Hemert, and J. M. van Ruitenbeeck. Measurement of the conductance of a hydrogen molecule. *Nature*, 419, 2002.

[173] S. Sorella. Generalized Lanczos algorithm for variational quantum Monte Carlo. *Phys. Rev. B*, 64(2):024512, Jun 2001.

[174] S. Sorella. Wave function optimization in the variational Monte Carlo method. *Phys. Rev. B*, 71(24):241103, Jun 2005.

[175] S. Sorella, G. B. Martins, F. Becca, C. Gazza, L. Capriotti, A. Parola, and E. Dagotto. Superconductivity in the Two-Dimensional t-J Model. *Phys. Rev. Lett.*, 88(11):117002, Feb 2002.

[176] M. Srednicki. Chaos and quantum thermalization. *Phys. Rev. E*, 50(2):888–901, Aug 1994.

[177] N. Strohmaier *et al.* Observation of Elastic Doublon Decay in the Fermi-Hubbard Model. *Phys. Rev. Lett.*, 104:080401, 2010.

[178] O. Tal, M. Krieger, B. Leerink, and J. M. van Ruitenbeek. Electron-vibration interaction in single-molecule junctions: From contact to tunneling regimes. *Phys. Rev. Lett.*, 100(19):196804, 2008.

[179] N. J. Tao. Electron transport in molecular junctions. *Nature Nanotechnology*, 1, 2006.

[180] A. G. Truscott, K. E. Strecker, W. I. McAlexander, G. B. Partridge, and R. G. Hulet. Observation of Fermi Pressure in a Gas of Trapped Atoms. *Science*, 291(5513):2570–2572, 2001.

[181] H. E. Türeci, M. Hanl, M. Claassen, A. Weichselbaum, T. Hecht, B. Braunecker, A. Govorov, L. Glazman, J. von Delft, and A. Imamoglu. Shedding light on non-equilibrium dynamics of a spin coupled to fermionic reservoir. *arXiv:0907.3854*, 2009.

[182] W. G. van der Wiel, S. D. Franceschi, T. Fujisawa, J. M. Elzerman, S. Tarucha, and L. P. Kouwenhoven. The Kondo Effect in the Unitary Limit. *Science*, 289(5487):2105–2108, 2000.

[183] K. Van Houcke, E. Kozik, N. Prokof'ev, and B. Svistunov. Diagrammatic monte carlo, 2008.

[184] L. M. K. Vandersypen, J. M. Elzerman, R. N. Schouten, L. H. W. van Beveren, R. Hanson, and L. P. Kouwenhoven. Real-time detection of single-electron tunneling using a quantum point contact. *Applied Physics Letters*, 85:4394–4396, 2004.

[185] M. Wagner. Expansions of nonequilibrium green's functions. *Phys. Rev. B*, 44, 1991.

[186] S. Weiss, J. Eckel, M. Thorwart, and R. Egger. Iterative real-time path integral approach to nonequilibrium quantum transport. *Phys. Rev. B*, 77:195316, 2008.

[187] P. Werner, A. Comanac, L. de' Medici, M. Troyer, and A. J. Millis. Continuous-time solver for quantum impurity models. *Phys. Rev. Lett.*, 97:076405, 2006.

[188] P. Werner and A. J. Millis. Hybridization expansion impurity solver: General formulation and application to Kondo lattice and two-orbital models. *Phys. Rev. B*, 74:155107, 2006.

[189] P. Werner and A. J. Millis. Efficient dynamical mean field simulation of the Holstein-Hubbard model. *Phys. Rev. Lett.*, 99(14):146404, 2007.

[190] P. Werner, T. Oka, M. Eckstein, and A. J. Millis. Weak-coupling quantum monte carlo calculations on the keldysh contour: Theory and application to the current-voltage characteristics of the anderson model. *Phys. Rev. B*, 81(3):035108, Jan 2010.

[191] P. Werner, T. Oka, and A. J. Millis. Diagrammatic monte carlo simulation of nonequilibrium systems. *Phys. Rev. B*, 79:035320, 2009.

[192] K. G. Wilson. The renormalization group: Critical phenomena and the kondo problem. *Rev. Mod. Phys.*, 47:773, 1975.

[193] N. S. Wingreen, K. W. Jacobsen, and J. W. Wilkins. Resonant tunneling with electron-phonon interaction: An exactly solvable model. *Phys. Rev. Lett.*, 61(12):1396–1399, Sep 1988.

[194] D. Withoff and E. Fradkin. Phase transitions in gapless fermi systems with magnetic impurities. *Phys. Rev. Lett.*, 64:1835, 1990.

[195] G. Yuval and P. W. Anderson. Exact Results for the Kondo Problem: One-Body Theory and Extension to Finite Temperature. *Phys. Rev. B*, 1:1522, 1970.

[196] A. H. Zewail. Femtochemistry: Atomic-scale dynamics of the chemical bond. *The Journal of Physical Chemistry A*, 104, 2000.

[197] W. Zwerger. Mott-Hubbard transition of cold atoms in optical lattices. *J. Opt. B: Quantum Semiclass. Opt.*, 5, 2003.